University of Southern Queensland

Faculty of Health, Engineering and Sciences

Battery SMART charge controller / combined co-gen grid connected inverter Design and Simulation

A dissertation submitted by

C. Morgan Smith

Student ID: 0050098383

Supervisors: Dr Narottam Das & Mr. Andreas Helwig

in fulfilment of the requirements of

ENG4111 and 4112 Research Project

towards the degree of

Bachelor of Engineering (Honours) (Power)

Submitted: October, 2016

University of Southern Queensland

Faculty of Health, Engineering and Sciences

ENG4111 & ENG4112 Research Project

Limitations of Use

The Council of the University of Southern Queensland, its Faculty of Health, Engineering and Sciences, and the staff of the University of Southern Queensland, do not accept any responsibility for the truth, accuracy or completeness of material contained within or associated with this dissertation.

Persons using all or any part of this material do so at their own risk, and not at the risk of the Council of the University of Southern Queensland, its Faculty of Health, Engineering and Sciences, or the staff of the University of Southern Queensland.

This dissertation reports an educational exercise and has no purpose or validity beyond this exercise. The sole purpose of the course pair entitled "Research Project" is to contribute to the overall education within the student's chosen degree program. This document, the associated hardware, software, drawings, and any other material set out in the associated appendices should not be used for any other purpose: if they are so used, it is entirely at the risk of the user.

Certification

I certify that the ideas, designs and experimental work, results, analyses and conclusions set out in this dissertation are entirely my own effort, except where otherwise indicated and acknowledged.

I further certify that the work is original and has not been previously submitted for assessment in any other course or institution, except where specifically stated.

Clive Morgan Smith

Student Number: 0050098383

Abstract

Electricity generation and distribution is undergoing significant change under the influences of energy security, climate change, technological development, and economics. Technologies that have introduced two-way power flow onto a distribution grid that was designed for one-way power flow are creating challenges and opportunities for innovation in the electricity distribution sector. These technologies include solar photovoltaics (PV), wind turbines, and battery energy storage systems (BESS). As the newest technology, BESS present opportunities to both the electricity distribution network service provider (DNSP) and the consumer. This dissertation focused primarily on the consumer side of the switchboard, modelling and analysing the economics and some of the technical issues for an economic-mediated battery controller as part of a grid-tied residential hybrid renewable energy system (HRES) that consists of a BESS, 1 kW wind turbine, and 10 kW PV array.

The geographical context of this project is Nambour, Queensland; PV and wind power calculations were based on Nambour's meteorological history. Residential energy consumption was modelled as a 'typical' Nambour residential customer. The technological context was such that costs and choices applied at mid-2016. The tariff context used was the recently introduced TOU tariff 12, which played a significant role in the timing and logic development of the battery charge controller algorithm.

From a technical standpoint, the charge controller algorithm was a major achievement of the present work. In developing the algorithm, it was found that the use of data from individual system components could be used to formulate the optimum mix of power sourced from or sunk to both the grid and the BESS. The output of this formulation was then demonstrated as a data input used for the control of the switching patterns of the BESS power electronics, a two-quadrant DC-DC converter (chopper).

The other major achievement of the current work was the finding that although BESS economics continue to improve, they generally still need to achieve further cost reductions in order to realise economic feasibility for the modelled context. It was also found that economic feasibility is more likely to be reached more quickly under conditions of high energy consumption, high inflation, high peak TOU tariff, and low discount rate.

Acknowledgements

I acknowledge the Traditional Owners of the land on which I study and write, the Kabi Kabi / Gubbi Gubbi people.

I acknowledge the Traditional Owners of the land on which the School of Mechanical and Electrical Engineering of the University of Southern Queensland is situated, the Giabal and Jarowair people.

I acknowledge the guidance, advice, and support of my project advisors, Dr. Narottam Das and Mr. Andreas Helwig.

I acknowledge the support of the USQ Library staff that have assisted me with the acquisition of numerous resources that have been invaluable to my learning and this project.

I acknowledge the CEO of the Australian Power Institute, Mike Griffin, for the Institute's contribution to the betterment of the power engineering profession, and the specific acknowledgement of the API's provision of financial contributions to my study and of opportunities for industrial experience.

I acknowledge Energex Limited for its contribution and commitment to the development of student engineers such as myself; specifically, I would like to acknowledge the following people from Energex:

- Colin Lee, Network Systems Development Manager
- Stephen Fairless, Senior Asset Manager
- Steven Lynch, Asset Manager North
- Ana Smith de Perez, Engineering Standards and Grid Modernisation Manager
- Terese Milford, Senior Future Technologies Implementation Engineer
- Aidan Roberts, Senior Future Technologies Implementation Engineer

I acknowledge Dr. Wayne Troyahn, Principal of Nambour State College, Education Queensland, for his commitment to the education of children and teachers.

Finally, I acknowledge my family Tabitha, Finn, and Freya for their steadfast encouragement, unwavering support, and *raison d'être*, and my extended family and friends across the planet as we travel along the journey of life together.

Morgan Smith

Woombye, Australia

2016

Table of Contents

List of figures

List of tables

Glossary of terms

Abbreviation, acronym, or initialism	Full term
AC	alternating current
Ah	ampere-hours
AFLC	audio frequency line communications
AMDT	amendment
AS/NZS	Australian Standard / New Zealand Standard
BESS	battery energy storage system
BOM	Bureau of Meteorology
BOS	balance-of-system
BLDC	brushless direct current (rotating machine)
CAPEX	capital expenditures
C/D	charge / discharge
CPI	Consumer Price Index
CSIRO	Commonwealth Scientific and Industrial Research Organisation
DC	direct current
DG	distributed generation
DNSP	distribution network service provider
DTI	discrete time interval
EA	Engineers Australia
EMS	energy management system
EV	electric vehicle
FiT	feed-in tariff
GST	goods and services tax
HIL	hardware in the loop
HOMER	Hybrid Optimisation Model for Electric Renewables
HRES	hybrid renewable energy system
Hz	Hertz

Abbreviation, acronym, or initialism	Full term
IEEE	Institute of Electrical and Electronics Engineers
IGBT	insulated gate bipolar transistor
IPCC	International Panel on Climate Change
ISO	International Standards Organisation
JADE	Java agent development framework
kW	Kilowatt (power quantity)
kWh	Kilowatt-hour (energy quantity)
LC	local controller
Li-ion	lithium ion (type of BESS)
LV	low voltage
MAS	multi-agent system
mH	milliHenries
MILP	multiple integer linear programming
MPC	model predictive control
MPPT	maximum power point tracking
NEM	National Energy Market
NPC	net present cost
NPV	net present value
OPEX	operating expenditures
p.a.	per annum
PI(D)	proportional-integral-derivative (controller)
PLC	power line communications
P&O	perturb and observe (MPPT type)
PQ	power quality
PWM	pulse width modulation
PS	peak shaving
PV	(solar) photovoltaic
RHO	receding horizon optimisation

Abbreviation, acronym, or initialism	Full term
RMS	root mean squared
RTP	real-time pricing (tariff)
SEQ	south-east Queensland
SOC	state of charge
STC	standard test conditions
TMY	typical model year
TOU	time of use (tariff)
UPS	uninterruptible power supply
VR	voltage regulation
VSI	voltage source inverter

Chapter 1: Introduction

The technology involved in the production, distribution, and transmission of electricity is evolving at an unprecedented pace. The drivers of this evolution are both ecological and economic. Ecological drivers include climate change and environmental degradation. The economic drivers include increasing prices of electricity, fossil fuel depletion, "green" marketing and politically-or-otherwise motivated tariff, subsidy, and rebate schemes; and the continuing decline in cost of producing and connecting renewable energy.

It is beyond the project scope to establish the relationship between burning fossil fuels and climate change, but the science suggests that human activity is the primary driver of climate change in the current epoch (IPCC 2014); 97% of publishing climate scientists agree with this view based on the overwhelming body of peer-reviewed scientific evidence (Kokic *et al.* 2014). There is growing evidence that humans need to keep the vast majority of provable fossil-fuel reserves in the ground, in order to have a reasonable chance of limiting global temperature rises to two degrees Celsius in this century (McGlade & Ekins 2015).

If the developed world wants to maintain its current standard of living whilst addressing the climate change problem, then low-carbon energy production needs to accelerate concomitantly with a deceleration in fossil fuel combustion to minimise carbon dioxide emissions over the next few critical decades. Renewable energy, such as wind and solar, has the potential reduce fossil fuel emissions (IPCC 2014; Keyhani 2011), and eventually phase them out altogether (Bose 2014). Some evidence suggests that PV electricity generation produces 15 to 30 times less, and 25 to 50 times less carbon dioxide than coal and gas, respectively, per kilowatt-hour (kWh) of electricity produced over their lifespan (Olson *et al.* 2014). Finally, modelling done in several countries, including Australia, demonstrates that existing renewable technologies can replace existing fossil fuel technologies to provide year-round baseload power (Elliston *et al.* 2013).

To achieve the exceptionally lofty, but rather urgently required goal of the elimination of fossil fuel combustion will require the mobilisation of a wide range of resources and ideas. Hence, part of the rationale for undertaking this project is to contribute in some small way to the aforementioned mobilisation. However, these sought after goals cannot exist outside of economic reality. Hence, another rationale for undertaking this project is

to make a specific economic case for a BESS controller and to the economic case for BESS in a more general way.

The macroeconomic arguments that exist in favour of increased penetration of renewable energy include:

- mitigation of the risk of waning liquid fossil fuel energy supplies, particularly in countries that are net importers of petroleum, such as Australia; and
- peak demand shaving – the size and operational requirements of the reticulated energy system, which in Queensland are government-owned corporations (i.e. originally funded by taxpayers but now operated as a Government Owned Enterprise which pays dividends to Queensland Treasury) is strongly related to peak demand forecasts (Energex Limited 2015). Distributed generation (DG) reduces demand when the sun is shining or the wind is blowing. Battery and grid optimisation technology, for example, virtual power plants (Asmus 2010), and the smart power grid (Keyhani 2011), can theoretically shave demand at any point in time.

One key microeconomic argument exists in favour of the increased penetration of distributed renewable energy: it is rapidly becoming cheaper, at least for the individual system. However, this must be balanced with evidence that suggests that some network costs are rising as a consequence of renewable energy penetration, including customer complaints related to over-voltage (Energex 2015). It is hypothesised that it may be cheaper in some individual customer circumstances to run a hybrid renewables / battery energy storage system (BESS) system than one that relies purely on grid power, even without subsidies. This hypothesis, and the assumptions that underlie it, are explored in this dissertation. The impact on network costs is outside the project's scope.

1.1 Problem and task statement

The idea for this project is the design of a "Battery SMART charge controller / combined co-gen grid connected inverter design and simulation design confirmation for domestic sustainable energy production 5 - 10 kW PV and 0.5 - 1 kW wind generator." The idea originated from the supervisors of the project, Dr. Narottam Das and Mr. Andreas Helwig. However, the project touched several areas that warranted investigation, including renewable energy resources, microgrids, batteries, and controllers. The project specification outlined or implied some clear design requirements:

- a BESS;

- PV system within a specific range of power generation capacity;
- a wind turbine system within a specific range of power generation capacity;
- inverter(s) of particular specifications to handle the proposed power transactions among the BESS, wind turbine, PV system, and the main distribution grid;
- a charge controller to direct switching among the battery, residence, and grid; and
- software – communications, data, and memory system between the BESS and charge controller.

Beyond these, the design requirements were not specified. Other variations on the design specification may include:

- BESS size;
- BESS chemistry;
- system communications;
- type of connection – single-phase versus three-phase;
- reactive power compensation capability;
- internal modularity – the extent to which elements may be added to the controller/inverter at a later time if the system is under capacity; and
- external modularity – the extent to which systems may be strung together to permit the design/implementation of larger systems and/or microgrids.

There were also testing requirements, to occur within simulation environments:

- general analysis and economic modelling on the HOMER software; and
- transient analysis and performance simulation in the Matlab / Simulink environment. This was largely carried out with the assistance of the Sim Power Systems application, an add-on to the Simulink environment.

1.2 Project aims

Although there has been increasing discussion in the media about batteries and renewable energy, and their influence on the power grid (ABC 2016; Kelly-Detwiler 2013; Nelder 2013; Simpson 2016), batteries are not widely used purely for grid-tied economic purposes. They are currently of importance, for example, in electric vehicles, off-grid and uninterruptible power supply installations (UPS), and critical load applications. To bring BESS into mainstream application, they need to prove their economic value. Economics play a key role in technology acquisition; Energex estimates that a 50% $/kW reduction needs to be achieved before the technology reaches wide uptake (Energex 2015). The

economic analysis in this project aimed to contribute to the knowledge base that might be used to make future such estimates.

This project aims to contribute to the technology acquisition decision-making process, either by proof-of-concept at the design stage (evidence supports the hypothesis), or, conversely, by demonstrating the need for something different (evidence does not support the hypothesis). It also aims to provide a framework for future work, including the implementation and testing of a hardware-based system.

The project also aimed to conduct its work with the principles of sustainability and ethics in mind. These principles and their application to the project are summarised in Appendix B.

1.3 Problem context

The context describes the parameters outside of the physical system model that influence the outcome of the results that test the hypothesis. The types of parameters, and their specific characteristics used in the present work, are listed in Table 1.1. It is useful to note that these parameters can be varied in the proposed system model as per ordinary sensitivity analysis techniques in the HOMER software application.

Table 1.1. Context factors

Parameter type	**Proposed parameter in the current context**
Electricity tariffs	Residential, southeast Queensland
Weather conditions	Nambour, Queensland
Load profile	Residential
Cost of technology	Determined at point in time of May 2016
Discount rate	3% to 6.5%
Inflation rate	2% to 5.5%

1.4 Objectives

1.4.1 Primary objectives

- Development of an economic supervisory battery charging control algorithm that maximises economic benefit to the owner of a grid-tied HRES in a specific context;
- Design of a residential HRES/BESS system;
- Quantification of a specific meteorological and residential load context;
- Determine if the controller and system is capable of meeting applicable regulations and standards for power, voltage, and frequency in the transient state; and
- Determination of the optimal size of the selected BESS for the modelled system, load, tariff, and meteorological conditions.

1.4.2 Justification of primary objectives

The justification of meeting primary objective 1 is that a review of the literature indicated that economic supervisory control is a knowledge gap that required additional research. This also provided a platform for the design's BESS capacity performance to be tested in HOMER software as described in the project abstract of offer.

The justification of meeting primary objectives 2 and 3 stems from the basic requirements of the project – this must be done in order to provide a platform for the economic and transient analyses.

The justification of meeting primary objective 4 stems from the project brief and from a review of the literature that suggested that the impact of power fluctuations from renewable power sources in grid-tied systems required more research and that BESS may assist in voltage and frequency regulation in renewable systems.

The justification of meeting primary objective 3 stemmed from the presence in the literature of different mathematical techniques used to optimise BESS size. It is worth noting that the HOMER software, in and of itself, provided the facility to optimise BESS sizing based on the parameters modelled and specified in the course of the project.

1.4.3 Secondary objectives

- Design the system to the forthcoming Australian Standard AS/NZS 5139, originally scheduled for release in February of 2016 (Standards Australia 2016a), but unreleased as of 26 September 2016;

- Build-in and/or develop the model's capacity for sensitivity analysis of:
    - BESS type;
    - inverter specification;
    - generation plant size and type;
    - tariffs;
    - weather conditions; and
    - load profiles.

1.4.4 Justification of secondary objectives

The justification of meeting secondary objective 1 stemmed from interest in the new Standard AS/NZS 5139 and was viewed as a learning opportunity for the application of the project to emerging knowledge. Unfortunately, development of the Standard did not adhere to its original timeline, and was not explored further in the project.

The justification of meeting secondary objective 2 stemmed from interest in economic optimisation and scenario-based simulation; it was hoped that the model developed herein may be more broadly applied to a wider range of technical, tariff, meteorological, and consumer behaviour factors.

Chapter 2: Literature Review

2.1 Potential benefits of grid-tied BESS

In the suite of technologies in hybrid energy systems, energy storage (ES) including BESS is furthest behind in its development (Fathima & Palanisamy 2015). Maintenance, cost, and life-cycle issues render BESS as the weak link in the hybrid system (Mahesh & Sandhu 2015). Although these concerns were considered, BESS can potentially deliver several benefits as described in sections 2.1.1 to 2.1.3.

2.1.1 Short-term system stability

Power flows, voltage regulation, frequency regulation, spinning reserve (or operating reserve as it is referred to in the HOMER software), and load balancing are identified as stability issues that BESS may be able to beneficially influence. As renewables contribute to voltage and frequency fluctuations, BESS can assist in the smoothing of these fluctuations to deliver power to the grid within acceptable limits (Caruana *et al.* 2015; Daud *et al.* 2013; Fathima & Palanisamy 2015; Koohi-Kamali *et al.* 2013). BESS can provide frequency regulation in the timeframe of milliseconds; however, this function is usually provided by adjusting non-renewable power generation, on a scale of minutes to hours (Lucas & Chondrogiannis 2016). To highlight the importance of frequency regulation, frequency regulation services are identified as the most important ancillary grid management function that can be provided by energy technologies in the European electricity market (Lucas & Chondrogiannis 2016).

In the event of grid events that result in islanding (Fathima & Palanisamy 2015), voltage peaks, dips, or flicker (Koohi-Kamali *et al.* 2013), or during the regular event of power fluctuations from a hybrid system's PV or wind (Koohi- Kamali *et al.* 2013; Caruana *et al.* 2015), a properly designed circuit will allow for the BESS to immediately meet the short-term (or longer, depending on BESS sizing) voltage correction and/or load balancing requirements. The current project did not incorporate any modelling of islanding, nor was it the intent of the project to examine how aggregated BESS might contribute to wider grid stability; however, this may be an avenue for future research.

2.1.2 Demand shifting and economic dispatch

Grid demand shifting (Fathima & Palanisamy 2015; Caruana *et al.* 2015; Zheng *et al.* 2014) is the process of moving demand from times when demand is highest to when demand is lower; and economic dispatch, where batteries are controlled according to the state of tariffs (Yoon & Kim; Caruana *et al.* 2015; Dieulot *et al.* 2015). Tariffs are an economic response to technical issues that includes the matching of forecast demand with planned generation. BESS can act as a power sink when demand is low, for example, when the grid needs to shed excess PV power production (King 2014) as seen recently in Germany. In fact, in SEQ, there are times of the day and year where up to 250 11 kV feeders experience reverse power flow (Energex 2015). Conversely, BESS can act as a power source when demand is high (Fathima & Palanisamy 2015). In either case, BESS can support the grid, but the control of battery charging, and the proper design of tariff schemes should ensure that overall grid demand peaks and troughs are mitigated, not exacerbated (Jargstorf *et al.* 2015).

An example of such control is noted in California, where companies are making aggregated energy storage bids into the real-time market (Walton 2015). On the other hand, a Spanish energy market study suggests that the economic benefits of a residential BESS system on its own, used in a market-pool-based hypothetical real-time pricing (RTP) tariff structure, does not outweigh its costs (Dufo-Lopez 2015). Furthermore, Dufo-Lopez (2015) estimated that battery costs would need to halve (an estimate similar to the aforementioned Energex estimate), or the peak tariff : off-peak tariff ratio would need to nearly double to realise an economically feasible BESS system.

Consideration of tariffs was relevant to this project because tariffs were one of the parameters used in the BESS control scheme. Although it is not a RTP, a TOU tariff exists in SEQ. This project contributes to the knowledge about the relationship between tariffs and demand shifting by demonstrating a power-flow schedule for the BESS in the project context. It also demonstrates the economic benefits, or lack thereof, of the demand-shifting strategy to the consumer in the project context. While the project only addressed load-balancing at the residential level, this might also contribute to load-balancing benefits at the DNSP level. This expectation could be examined in future research. Additionally, it is beyond the scope of this project to look at the potential benefits to DNSPs of either the possible interaction of audio frequency line communications (AFLC) or power line communications (PLC) with the local residential BESS control scheme; or of tariff-mediated BESS aggregation. These are proposed as possible bases for further research.

2.1.3 Peak demand growth

BESS reduces the need for grid hardware upgrades and generation expansion (Koohi-Kamali *et al.* 2013), although it may increase expense in protection and other requirements. Energex is planning for a modest reduction in peak demand as battery storage increases (Energex 2015) (see Figure 2-1). Although peak demand has been reduced in SEQ over the past 5 years, its increase is still possible if society undergoes an increased electrification of (private) transportation. The economic success of Tesla's recent Model 3 pre-manufacture subscription registration (Parkinson 2016), along with the Queensland Government's vision for electric vehicle (EV) charging outlets along the Bruce Highway (Queensland Government 2015) suggest that the rate of private vehicle electrification may rise sooner rather than later. For the time being, Energex is watching EV but it is considered to be a small factor at this point (Energex 2015) (see Figure 2-1).

The project does not aim to examine the influence of BESS on peak demand growth at the distribution level, but could be a point of future research.

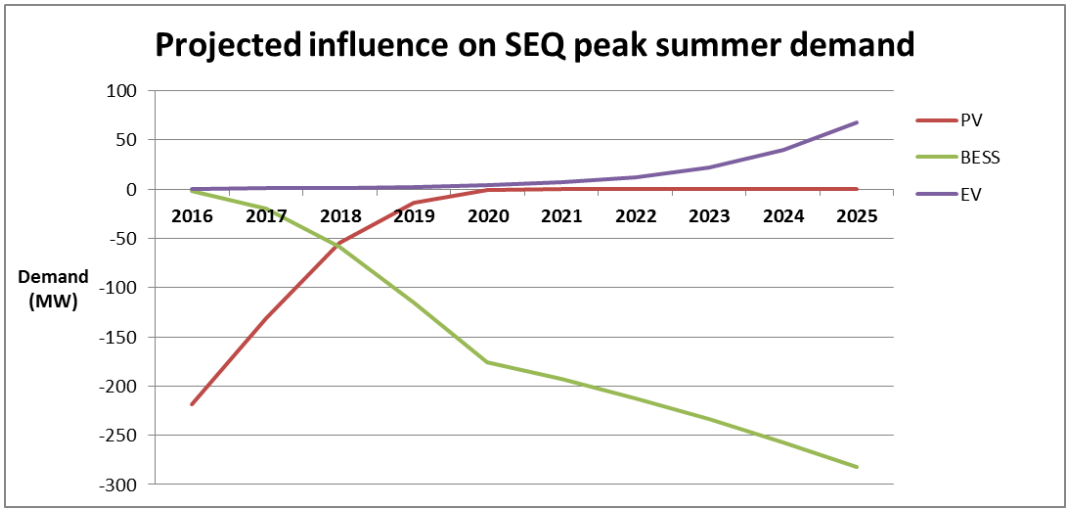

Figure 2-1. Projected influences on SEQ peak summer demand (adapted from Energex 2015).

2.2 Batteries and BESS

Many types of batteries exist; the choice of battery influenced both the economic and the transient modelling. A wide variety of batteries are commercially available or at varying stages of research and development (Koohi-Kamali *et al.* 2013; Daud *et al.* 2013). A comparison of ESS technologies in Figure 2-2 shows some of the possible benefits of these technologies. With the scale of this dissertation in mind (single-dwelling residential on the scale of 0.01 MW or 10 kW), this figure shows that only two technologies best apply to this dissertation: lithium-ion (Li-ion) and vanadium redox flow batteries.

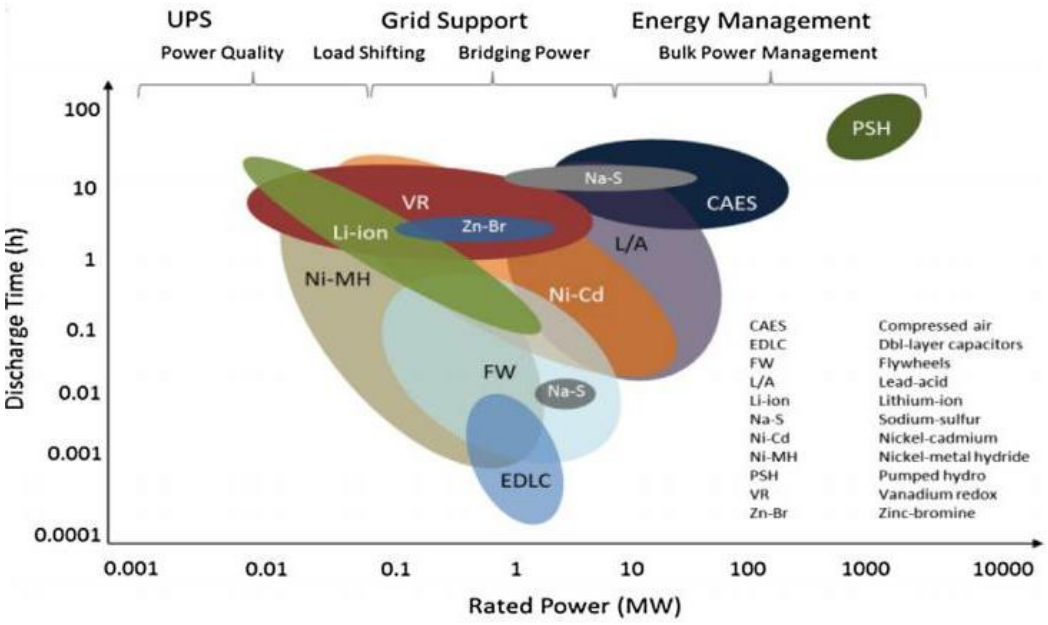

Figure 2-2. Applications of ESS technologies (Lucas & Chondrogiannis 2016).

Notably, lead-acid batteries appear on the scale at 1 to 100 MW of power. In spite of this, from a domestic use standpoint, lead-acid batteries have the greatest share of installed capacity, due mainly to their low cost, reasonable life-span and cycling characteristics, and their technological maturity (Daud *et al.* 2013; Zheng *et al.* 2014). Li-ion batteries are working their way into the market, notably in media reports about the Tesla Corporation (Simpson 2016) but are offered by many other producers. Research about this technology continues apace, but the technology is still relatively expensive (Daud *et al.* 2013). Recent examples of this were demonstrated in a study by Zheng *et al.* (2014) in which Li-ion batteries were deemed economically unviable for an ESS-only residential system; and less economically feasible compared to lead-acid batteries in a residential

hybrid grid-tied solar PV / BESS system (Khalilpour & Vassallo 2016). Conversely, other research points to a promising cost reduction probability of Li-ion batteries with respect to time (Dufo- López 2015; Mulder *et al.* 2013).

Other types of BESS, such as sodium sulphide, sodium nickel chloride, flow batteries, and metal-air are emerging technologies. One study found that optimally sized metal air, sodium nickel chloride, and zinc manganese dioxide flow battery systems without hybrid generation may be more economically optimal than more conventional batteries under certain tariff regimes (Zheng *et al.* 2014).

Regenerative fuel cells may be very economical for larger storage installations because of low additional cost per kWh capacity (200 kWh was given as an example), but perhaps not so for smaller ones because of high overhead cost (Koohi-Kamali *et al.* 2013) and voltage droop characteristics under loading.

The HOMER software is pre-loaded with the characteristics of several commercially available and generic types of batteries. However, other types of batteries can be modelled from available technical data. For this project, Li-ion batteries were selected as the first choice of BESS type to model for the following reasons:

- Disagreement in the literature about economic efficiency as described earlier in this section;
- Suitability for the project's scale of power requirements as outlined in Figure 2-2; and
- Modelling capabilities and quantitative characteristics available in HOMER and Simulink.

2.3 Battery characteristics

The specification of battery characteristics was a project requirement for two reasons. First, economic evaluation of the project required knowledge of charging and discharging rates, charging and discharging capacity, and expected life cycle. Second, evaluation of the system's transient performance depended on the correct parameter modelling.

Fundamental battery performance features include: charge and discharge voltage (Patel 2006); charge/discharge (C/D) ratio (Patel 2006); state of charge (SOC), output power, and charge/discharge rate, (Fathima & Palanisamy 2015; Mahesh & Sandhu 2015); round-trip energy efficiency (Patel 2006), charge efficiency (Patel 2006), internal impedance

(Patel 2006), temperature rise (Patel 2006), expected life (Gu *et al.* 2013; Mahesh & Sandhu 2015; Dufo-López 2015; Di Giorgio & Liberati 2014) which may be expressed in number of C/D cycles (Patel 2006); power (Mahesh & Sandhu 2015); and capacity (Keyhani 2011).

2.4 Mathematical modelling of batteries

The battery parameters outlined in section 2.3 were used to specify the inputs to mathematical models that existed in HOMER and Simulink. Mathematical modelling of the batteries was important because both the economic and transient evaluations depended on the simulation of these models with respect to time. The correct model for a given situation improves the validity of a simulation, but the correct choice is not always straightforward (Daud *et al.* 2013; Caruana *et al.* 2015). Examples of battery models can be found in Yoon & Kim (2016); Gu *et al.* (2013); Daud *et al.* (2013); Dieulot *et al.* (2015); Dufo-López (2015); and Di Giorgio & Liberati (2014). However, the choice of model was not examined in this project because the existing models within HOMER and Simulink were determined to be robust enough for the simulations.

Hardware in the loop (HIL) (Caruana *et al.* 2015; Dieulot *et al.* 2015) was proposed as a possible means of bypassing the need for choice, as well as offering the prospect of more realistic simulations (Caruana *et al.* 2015). However, HIL introduces additional expense for the hardware and interface, as well as additional health and safety risks and was deemed to be beyond the scope of this project, but could be an avenue for future research.

2.5 BESS sizing

In the particular case of grid-tied PV/BESS hybrid systems, significant variation exists in the literature about BESS sizing optimisation (Khalilpour & Vassallo 2016), including the analytical predictive model developed by Zheng *et al.* (2014), and the mixed integer linear programming algorithm detailed by Khalilpour and Vassallo (2016). Additional BESS sizing considerations are outlined by Keyhani (2011). Furthermore, review of the literature strongly suggests that BESS sizing must be considered in the economic optimisation of HRES (Zheng *et al.* 2014; Daud *et al.* 2013; Dufo-López 2015; Khalilpour & Vassallo 2016; Mulder *et al.* 2013). This is because BESS type and characteristics (Zheng *et al.* 2014), tariffs (Jargstorf *et al.* 2015), loads, and climate have an influence on BESS size. In this project, HOMER software was used for the project's

economic analysis. HOMER employs its own BESS optimisation strategy based on a host of factors including BESS type, tariffs, load, climate and electricity generation characteristics. Therefore, HOMER was used to determine the optimal BESS size for the scenario modelled.

At the project's outset, the optimum BESS size was not known. Whilst it is of primary importance for the economic modelling in HOMER, its influence on the transient case was also unknown. Practical consideration of BESS sizing might suggest that higher-capacity BESS would provide a higher magnitude and / or longer duration of support during high-load switching events or weather-related generation transients. A loss of grid power at full-load was originally considered to be of interest, but is suggested as an avenue of further research. For the transient modelling, the project simply modelled the economically optimal BESS size for the transient case. Changes to BESS size were not considered for the transient model, and are suggested as future research.

To conclude this section, it is worth noting that a BESS/HRES may have objectives other than economic ones. For example, an owner might specify a minimum emergency capacity for a specified time frame. Investigation of non-economic objectives is beyond the project scope and may be an avenue for future research.

2.6 Standards

Standards are important because they reflect best practice about system design and safety considerations. As mentioned in section 1.4.4, no Australian Standard exists in relation to batteries used in conjunction with grid-tied systems. AS/NZS 5139: "Electrical Installations – Safety of battery systems for use in inverter energy systems" is under development. Although the Standard was originally expected to be released in February of 2016, Standards Australia had released a consultation paper for the Standard in May 2016, requesting feedback from interested parties (Standards Australia 2016a). This suggests that the Standard is some time away from release.

No fewer than 18 other AS/NZS standards exist for batteries and battery chargers, some of these are listed in Appendix C.1. However, none warranted further investigation of their applicability to the project. One Standard, AS/NZS 4755.3.5:2016, was only introduced in July 2016 (Standards Australia 2016c), and was not investigated in the current project, although its subject matter would be of significance to any future work. It is recommended that future works in this area investigate the possible application of these

Standards to their specific requirements. Their application depends both on system design and choice of electrochemistry (Standards Australia 2016b).

Fire safety is another important issue in regards to energised Li-ion systems and is certainly a gap in the AS/NZS Standards. A report commissioned by the National Fire Protection Association in the USA is an example of filling this knowledge gap (Blum & Long Jr. 2016); some of its findings are described in Appendix C.2.

2.7 Characteristics of other system components

2.7.1 General characteristics of solar photovoltaic panels

For the purposes of this project, the solar PV panels and their installation were not investigated extensively. However, it was assumed that the modelled panels and installation will adhere to AS/NZS 5033-2012, AS/NZS 5033-2014, installation and safety requirements for PV arrays (Standards Australia 2014), as well as AS/NZS 5033-2005 AMDT 1 & 2, installation of PV arrays (Standards Australia 2015a). Some of the fundamental safety and protection requirements of such installations can be found in Appendix C.3.

Basic mathematical modelling of PV panel power and voltage output, and wind turbine power output, is summarised by Fathima & Palanisamy (2015), pp. 434-5. A PV array model that is based on five parameters, and that is commonly used in research, is highlighted by Wang *et al.* (2015). Other sources of modelling PV panels include Daud (2014), Keyhani (2011), Patel (2006), and Khaligh and Onar (2010).

Ambient temperature influences PV output (Keyhani 2011; Patel 2006). This applied to the current work because the PV output affected both economic and transient system modelling. Since HOMER has the capacity to consider the temperature effects on solar PV (and wind and BESS), a Nambour temperature model was used in the HOMER modelling; however, it was not considered in the transient model.

2.7.2 General characteristics of small wind turbines

This project did not extensively investigate wind turbines, but were selected with reference to AS 61400.21-2006 which "specifies a methodology for the measurement and assessment of the power quality characteristics of grid connected wind turbines" (Standards Australia 2015c). The model selected is a variable-speed brushless direct

current (DC) machine (BLDC) as described in Khaligh and Onar (2010), referred to as a permanent magnet alternator in Clark (2014).

The power output of wind turbines is inherently unpredictable, and is noted for susceptibility to harmonic distortion (Fathima & Palanisamy 2015). This feature needed to be considered in any model developed for simulation, particularly in the transient case. Mathematical modelling of wind power is presented extensively in the literature, for example in Ahfock (2014), and Caruana *et al.* (2015). Wind turbine power output is summarised by Fathima & Palanisamy (2015), p. 434-5. Other systems and mathematical modelling is provided Patel (2006), and Khaligh and Onar (2010).

Dynamic modelling of three-phase induction machines requires seven differential equations and a non-linear algebraic equation (Keyhani 2011). Because of the volume of work required to properly model the wind turbine, wind modelling of the transient case was not conducted and is suggested as future work.

2.7.3 General characteristics of power inverters

The following Australian Standards apply to grid inverters (Standards Australia 2015a):

1. AS/NZS Standard 4777.1-2005 "Grid connection of energy systems via inverters - Installation requirements";
2. AS/NZS 4777.2-2005 "Grid connection of energy systems via inverters - Part 2: Inverter requirements"; and
3. AS 4777.3-2005 "Grid connection of energy systems via inverters - Grid protection requirements".

Because many types of inverters exist, so too do their respective mathematical models. A Simulink-based model is available in (Wang *et al.* 2013), which was of relevance to the project because the dynamic modelling for this project was done in Simulink. A thorough review of specifications, topologies, and control strategies of multi-function grid connected inverters was also available (Zeng *et al.* 2013).

As the inverter was one of the key components of the design specification, existing models from the literature were reviewed. Numerous examples of inverter strategies used in hybrid renewable energy systems are present within the literature (Shivarama Krishna & Sathish Kumar 2015; Khadem *et al.* 2011; Quesada *et al.* 2014; Zeng *et al.* 2013; Keyhani 2011; Patel 2006; Khaligh & Onar 2010). A two-arm (single-phase), full bridge

configuration with insulated-gate bipolar transistor (IGBT) switches and anti-parallel diodes was ultimately selected for the system design (see section 3.5.4).

2.7.4 Other converters

The PV and battery converters were selected according to the configurations required, and available models in the literature.

Obtaining power from wind, solar, and battery sources to supply a residential alternating current (AC) load required several types of power conversions prior to delivery.

1. *Wind power*. As wind turbines are AC sources, wind power is first rectified to DC. This DC power is then inverted to AC to grid specifications. HOMER accommodates this type of architecture but does not explicitly model rectifiers. An alternative application of small wind turbines is direct battery charging via a full-bridge rectifier and charge controller, sparing the expense of additional conversion of the wind energy for direct use by a load (Clark 2014; Khaligh & Onar 2010). Direct economic modelling of this type of system architecture cannot be conducted in HOMER.
2. *Solar power to DC bus by DC/DC boost converter*. To obtain maximum power extraction from wind and solar PV sources, techniques based on the maximum power point concept (Ahfock 2014), such as maximum power point tracking (MPPT) were employed. A MATLAB-based mathematical model of this technique based on a 30 kW wind-PV system with BESS already exists (Sungwoo & Kwasinski 2012). However, a Simulink technique was found in Saharia *et al.* (2016) and applied to the transient model. MPPT can be by-passed in HOMER; furthermore, many commercial inverters incorporate MPPT.
3. *Battery power to DC bus by two-quadrant converter*. This converter is of particular importance to the project because it directs power flows to and from the BESS when charging and discharging, respectively. BESS are normally comprised of the storage itself and a multi-quadrant DC-DC converter (Caruana *et al.* 2015). The basic technique, circuit model, and equations are described in section 3.8 of Keyhani (2011), as well as by Ahfock (2014). A standalone solar PV to BESS charge / discharge converter is also described (Patel 2006; Khaligh & Onar 2010). An alternative hysteresis circuit model was described by Tyagi (2012), and ultimately selected for the transient model.

2.8 Control and optimisation

Many studies have been conducted on the control of grid-tied distributed energy. Several meta-reviews of these studies have also been conducted, focusing on operations and control (Rahman *et al.* 2015), optimisation (Fathima & Palanisamy 2015), energy storage operations (Koohi-Kamali *et al.* 2013; Subburaj *et al.* 2015), hybrid renewable systems (Mahesh & Sandhu 2015; Shivarama Krishna & Sathish Kumar 2015; Upadhyay & Sharma 2014), and load-frequency control (Pandey *et al.* 2013). These reviews were sought out for their perspective on gaps in the knowledge in the area, and on recommendations for further research, described further in the present section 2.8.

2.8.1 Control

Reviews of the literature indicate that further progress is required in a breadth of controller functions. These functions include fundamental control strategies (Rahman *et al.* 2015); controller design and battery state of charge control (Daud *et al.* 2013); and power management control, inverter control, and energy management control (Mahesh & Sandhu 2015). Specific examples of control strategies and how they may apply to the proposed system follow.

Control strategy applied to microgrids is "widely accepted" as applying at three basic levels (Meng *et al.* 2016):

1. *Primary*. Local level control; governs voltage, current, and power, on the time order of milliseconds;
2. *Secondary*. Power quality, voltage and frequency regulation, and harmonics; on the time order of up to a second; and
3. *Tertiary*. This is the 'intelligent' level, which deals with economics and efficiency on the time order of up to a few hours (Meng *et al.* 2016).

Meng *et al.* (2016) argue that these three layers can be implemented centrally (i.e. by a DNSP) or locally. The degree to which local control is implemented depends on the local controller (LC). Localised control has many advantages but its implementation is difficult. Key to localisation is the quality of the control scheme(s) employed by the LC. Multi-agent systems (MAS) are discussed as a way of accomplishing such local control. Model predictive control (MPC) is one such MAS (Meng *et al.* 2016). They propose that a system is composed of physical, control, and agent subsystems, where the control

system manages the physical components; the agent(s) act to modify the parameters of the control system to achieve the desired goals of the system.

Application of agents was described in a study that used a JAVA-based language, JAVA Agent Development Framework (JADE) to implement a three-layer four-state, grid-tied, PV/wind/BESS HRES MAS energy management system (EMS) (Jun *et al.* 2011). It proposes agents for each of the PV, wind, BESS, grid, and load, each with their own objective function and constraint(s). The outputs of the five agents are incorporated into a system level EMS objective function with only a single constraint. A token-ring facilitator arrangement is also used, whereby at any given time-step, any single of the four non-load agents becomes the 'main facilitator' of the system level EMS (Jun *et al.* 2011). Although simulated in JADE, the control and EMS techniques and analysis were investigated for their application in Simulink. What is of particular interest is the compartmentalisation of the agents, meaning that basic schemes may be designed for four agents, and a more complex (if warranted) scheme for BESS, the fifth agent, the SMART battery controller.

Another study used a four quadrant voltage-power control scheme for the BESS under the voltage source inverter (VSI) inversion technique (Lucas & Chondrogiannis 2016). This study was modelled in Simulink and provides some ideas on how one might implement a control scheme; however the BESS was linked to the grid as a distribution storage strategy rather than as a residential strategy. In particular, the proportional-integral (PI) current-control method of prevention of over-charge/discharge was explored for its application to the transient analysis, but this was not implemented. Another method, connecting the HRES/BESS directly to the grid, rather than directly to the prosumer loads, was explored. However, subsequent HOMER modelling indicated that this was not the best design for the system.

2.8.2 Optimisation

Reviews indicate that optimisation strategies still require further advancement in the areas of system performance (Rahman *et al.* 2015), power quality, system stability, energy management, demand tracking, ESS design configuration (Fathima & Palanisamy 2015), and system sizing (Mahesh & Sandhu 2015).

Optimisation of hybrid system problems involves a number of real-time variables that can make problem-solving difficult. Optimisation problems may be related to generation, control, distribution (Fathima & Palanisamy 2015) and/or BESS sizing (Khalilpour &

Vassallo 2016). Optimisation related to siting and sizing of generation, as well as that related to primary control (droop control) and secondary control (steady-state error) has been extensively studied (Fathima & Palanisamy 2015). However, tertiary control (power exchanges between the grid and microgrid), and "the major tasks of scheduling demand tracking and optimal energy management provide a significant area of research" (Fathima & Palanisamy 2015, p. 438), even though another study suggests that the technical and economic case for this demand shifting strategy has already been made (Koohi-Kamali *et al.* 2013). Other reviews suggest that the design of power converters, particularly in regard to the addressment of renewables' power fluctuations on the power grid, needs further research (Mahesh & Sandhu 2015; Koohi-Kamali *et al.* 2013).

Two optimisation strategies that warranted further investigation were the differential evolutionary algorithm used by (Basu *et al.* 2012) to evaluate resource and load schedules and costs, and the particle swarm method used for real and apparent power sharing between the grid and microgrids (Al-Saedi *et al.* 2013). However, neither strategy was employed in the final model.

Fathima and Palanisamy (2015) concluded their paper by suggesting that optimisation strategies involving power quality and stability require further investigation, because strategies involving economic and environmental objectives are more extensively researched at present. It is expected that ESS technologies will assist these strategies by quickly varying active power (for frequency correction) and reactive power (for voltage correction of loads) (Koohi-Kamali *et al.* 2013).

2.8.3 Project relevance

The author's specific area of interest is the economic control of BESS. Energy management control (Mahesh & Sandhu 2015) and optimisation (Fathima & Palanisamy 2015) are areas that require further research. This may have benefits for individual customers, and this was the context of the current work. A corollary to individual systems, that is, aggregated storage capacity, can provide economic benefits to electricity distributors (Di Giorgio & Liberati 2014; Jargstorf *et al.* 2015), and may help to continue an increase in the penetration of renewable energy systems (Lucas & Chondrogiannis 2016). Aggregated storage is suggested as an avenue for future work.

2.9 Economic control schemes for battery charge controllers

To develop the SMART charge controller central to this project, it was necessary to examine the current state of the discipline. The idea of a "SMART" charge controller may have different connotations. For the purpose of this dissertation, 'smart' will be taken in the context of AS/NZS 5711:2013, which refers to the smart grid as "an electricity system incorporating electricity and communications networks, that can intelligently integrate the actions of parties connected to it" (Standards Australia 2013). In the context of this project, the *electricity system* will be assumed to refer to a grid-tied HRES with BESS. The *electricity network* includes the customer, distributor, and baseload energy producers and transmitters. *The communications network* was an unknown entity at the project outset, and was not further explored, but could include for example, PLC, AFLC, Zigbee (Di Giorgio & Liberati 2014), IEEE 802.11, Ethernet, smart meters, microcontrollers, and/or P / PI / PID controllers. Design and modelling of the communications systems is suggested as future work. The *parties connected to it*, will physically include at a minimum, the owner/occupier and the electricity distributor; and virtually include at a minimum, electricity retailers but might also encompass data service providers. This project modelled the owner/occupier's load and the electricity retailer's tariff regime. It also attempted to model the distributor's poles and wires in the transient model but this proved to be too challenging within the project's time constraints and is suggested as future work.

In the course of reviewing the literature, economic controllers appeared in many forms, as discussed below. A theme emerged, whereby economic controllers exist as a system of intelligence that acts to influence the control system, which in turn manages the behaviour of the physical system. According to one set of authors, few power system controllers have been expressly developed with economic objectives (Dieulot *et al.* 2015). Contrary to this assertion, several examples are outlined below. The examples described below were selected for their relative similarities to this dissertation's context as outlined in section 1.3.

The authors who made the assertion of the limited development of economic controllers, Dieulot *et al.* (2015), designed a controller with a model predictive control (MPC) approach. This approach uses an economic optimisation layer that minimises a cost function. The optimisation layer sits on top of the control layer that manages the physical layer of the system; both control and optimisation were subject to the constraints of the physical system. Their particular study developed an economic control model for a hybrid

system based on a gas turbine, solar PV, and ESS (Dieulot *et al.* 2015). It employed tariff, fuel, ESS cycling costs and meteorological parameters within a control algorithm to compute reference power within a HIL simulation. Fundamental to the model is solution of "an optimisation problem that minimizes the cost function subjected to model and operational constraints" (Dieulot *et al.* 2015, p. 224).

A second method employed has some similarities to this project's context (Sichilalu & Xia 2015). Their use of mixed integer non-linear programming to design the economic control strategy for a grid-tied solar PV / BESS / heat-pump hybrid system under a South African solar PV feed-in tariff (FiT) and TOU tariff was detailed. It concluded that the economic benefits are likely to be substantial. The parallels of this study to the Queensland context is the recent introduction of the residential TOU tariff (tariff 12 for SEQ); however, the previously available 44c/kWh FiT is no longer available to new customers. A more modest FiT is available to customers but this varies by retailer.

A third method, described by Di Giorgio & Liberati (2014), is an economic controller based on "an event- driven model predictive control (MPC) approach" for a grid-tied solar PV / BESS / EV / smart- appliance system. It uses a discrete-time approach to model the battery SOC as a function of power flow, efficiency, and state of charge constraints, and includes life cycle costs in the controller objective function. An economic-based MPC algorithm is also employed in a hybrid PV / BESS system (Mégel *et al.* 2015). Notably, its objective function includes economic returns to the owner based on primary frequency control, a market mechanism that is not present in this project's market context.

The fourth method reviewed is a state- space control MPC method that simulated, under varying conditions: BESS three-phase balancing performed on a 10 kW / phase solar PV system; peak shaving; and load balancing under islanded conditions (Wang *et al.* 2013). The model was performed in Simulink and the MPC method was demonstrated to have satisfactory outcomes for the scenarios that were modelled.

The fifth method is a dynamic programming approach of ESS energy management control that accounts for TOU pricing, real-time pricing (RTP) and presence or absence of local energy production (Yoon & Kim 2016). The simulation software was not disclosed in the article. Of relevance to this dissertation is the fact that the method accounts for battery capacity, efficiency, and charge/discharge rates.

A sixth technique, using a simpler but elegant ESS control algorithm, is described by Dufo-López (2015). However, it is based on an ESS-only system. It amounts to supplying the load and charging batteries on a low tariff, and discharging the batteries to

the load during a high tariff. Of significance to this project, it accounts for BESS's lifetime cost by defining it as an average cost per charge cycle. This strategy was not directly specified to the present context, with solar PV feed-in tariffs, and direct charging/discharging strategies related to the wind and solar PV system components. However, HOMER did provide facilities for SOC limits and expected lifetime throughput, which in turn assigned a cost per charging cycle in the modelling.

A seventh technique, also based on an ESS-only system, modelled the battery control regime as a function of charge/discharge rate and state of charge (Zheng *et al.* 2014). The charge rate in turn was modelled on ESS capacity, storage and load supplied from the grid; the state of charge was modelled on battery depth of discharge, efficiency of ESS energy delivery to load, storage capacity, and quantity of electricity discharged over a given interval. Each of these characteristics were modelled in HOMER.

The eighth technique used a multiple integer linear programming (MILP) approach to optimise a solar / BESS system is found in Khalilpour & Vassallo (in press). A ninth technique used a different linear programming approach to the economic optimisation by applying a day-ahead ESS charge and discharge schedule for a residential PV / BESS system that does not require load or PV production forecast data (Ratnam *et al.* 2015). The value of these two studies is in the scheduling system, but it should be noted that load and production modelling were used in this dissertation; the day-ahead methods described were not explicitly used.

In each of the aforementioned economic controller studies, none were based on a residential grid-tied wind, solar PV, and ESS hybrid system. However, a tenth study developed a receding horizon optimisation (RHO), real-time economic control strategy for a diesel / wind / PV / BESS residential system, based in the MPC method (Wang *et al.* 2015). However, the system was not grid-tied, used diesel in the energy mix, had a system configuration of a 10 kW wind turbine with a 1.61 kW PV system, and used lead-acid batteries. It cursorily addressed battery SOC and its influence on life expectancy, and rightfully assumed that daily operational costs of the system are proportional to the energy produced and stored. Furthermore, a detailed bi-temporal demand response algorithm involving one-day advance load data and real-time load and immediate future weather data was proposed for the stand-alone system, a method that was not applied in this project because the demand response was based on the meteorological and load models described in detail in section 3.7. The authors (Wang *et al.* 2015) suggested that future work should investigate application of the system under grid-tied conditions.

The current work aimed to build on the work of Dieulot *et al.* (2015). A comparison of their studied system and the project specification can be found in Table 2.1.

Table 2.1. System configuration comparison: specification v. Dieulot et al. (2015).

System parameter	**Dieulot *et al.* (2015)**	**Project specification**
Solar PV	17 kW, 108 x 160 W British Petroleum panels	5 – 10 kW
ESS	307 Ah (maximum) supercapacitor system	Unspecified. A 6.4 kWh Lithium-ion (Li-ion) battery was specified
Gas micro-turbine	30 kW maximum	No
Wind turbine	No	0.5 – 1.0 kW
Carbon tax	Yes	No
Feed-in tariff	No	Yes

The systems are of the same order of magnitude in scale, but the gas turbine and ESS are obvious marked differences in the system arrangement. Furthermore, that study is primarily interested in short-term (1 to 5 days) time frames, in contrast to the current study that examines very long-term (decades) and very short-term (milliseconds) time frames.

Design of a system for the residential context was at the heart of this project. The design of the controller was focused on customer benefits. While it is important to keep possible benefits to DNSPs in mind, these were not the primary focus of the project. For example, it can be argued that there is a load-shifting (peak demand) benefit realised as a result of BESS application with the tariff schemes. On the other hand, other benefits (for example frequency regulation) might arise only coincidentally, because at present there are no economic incentive schemes for the residential owner to invest in so doing.

2.10 Meteorological modelling

The literature suggested that solar insolation patterns depend on geo-location, climate, month, and season (Yarhands 2013). A variety of statistical models were considered: beta distribution best fit data from Victoria, Australia (Caliao & Zahedi 2000) and the south-eastern United States (Rahman *et al.* 1988); a variety of statistical techniques were examined for Ghanaian insolation patterns (Yarhands 2013), including Weibull, lognormal geometric, geometric, gamma, and exponential distributions. It was found that the statistical distribution of best fit was dependent on the month of the year.

A more recent paper attempted to normalise raw data to fit a normal distribution, for the purpose of economic simulation over the longer-term (Sedić *et al.* 2015). Each month was normalised, modelled, and tested for its proximity to original raw data. Although the end result of this process is elegant, the process is time-consuming and beyond the scope of this dissertation.

Another paper attempted to derive a general model based on meteorological data from 83 weather stations in China. They noted that the general model did not perform as well as individual models that had been developed for each particular station, but that the general model would probably have value in terms of applying to a variety of climate zones in China (Li *et al.* 2013).

The problems with modelling insolation data can be seen in Figure 2-3. First, there is more variation in the maximum insolation from day to day in the warmer months than in the cooler months. This may be related to both the length of day, and the fact that summer in Nambour is characterised by hot and humid conditions, associated with a lot of cloud and storm formations. Second, the minimum daily value from day to day (each day is based on 10-13 years of data) has a lot more variation than the maximum value. Third, insolation on a given day has both a floor (zero) and a ceiling (as a function of length of the day). The statistical ramification of this observation suggests that a Beta model is relevant. A comparison of the plot area between the maxima and mean, with the plot area between the minima and mean, shows that this is probably a negative (left-skewed) distribution. One interpretation of this data is that insolation maxima are likely to be dependent on the length of day, but the minima are likely to be dependent on cloud cover, and can be driven close to the ultimate floor of zero. These cloudy days may reduce the mean to below that of the median.

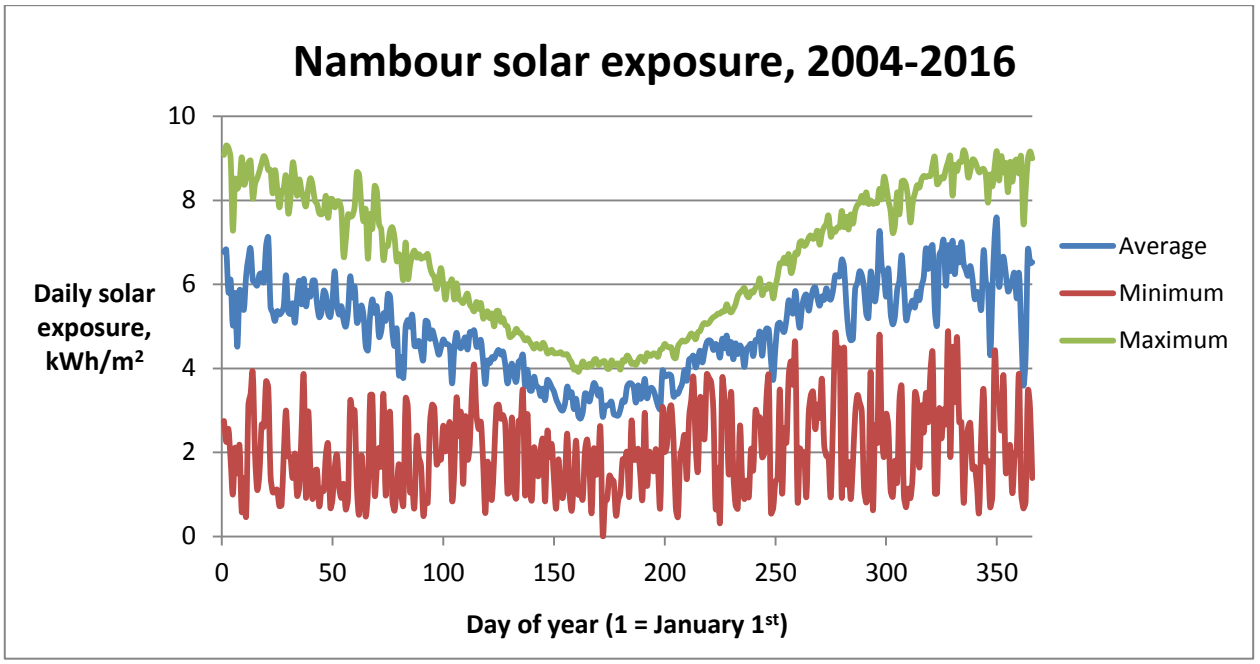

Figure 2-3. Nambour daily solar exposure, annual

Wind resource modelling depends on the availability of a wind resource data set or map (Keyhani 2011; Clark 2014). Wind data for Nambour was available from the Australian Bureau of Meteorology (2016b). If an average wind speed is known, a wind speed distribution can be constructed based on the Weibull or Rayleigh distributions (Patel 2006; Clark 2014). HOMER provided the facility for use of the Weibull distribution. The wind speed distribution can then be used to determine the output power for a given turbine based on that turbine's output power curve characteristics (Khaligh & Onar 2010; Clark 2014; Patel 2006).

Temperature affects battery (Patel 2006; Keyhani 2011), solar PV (Patel 2006; Keyhani 2011), and wind power (Khaligh & Onar 2010) performance. Modelling depends on the availability of a temperature data set, which was available from the Australian Bureau of Meteorology (2016b).

Chapter 3: Methodology

3.1 Project feasibility analysis

One outcome of modelling a grid-tied economic-mediated battery charge controller with wind and solar PV is the determination of its economic viability in the present context. The presence of federal installation rebates, state feed-in tariffs and favourable solar insolation profiles make SEQ one of the most deeply penetrated solar PV markets in the world. A specific example of the scale of this uptake for the location chosen for the modelling, Nambour, can be seen in Figure 3-1. TOU pricing (tariff 12) and off-peak pricing (tariff 31 and tariff 33) suggests that there is enough incentive to consider BESS load shifting strategies. Therefore, the project was initially deemed as having a reasonable chance of economic feasibility from the commercial perspective. Ultimately, this depended on a number of other factors, including the expected life and price of the BESS used in the system; these factors and their modelling are detailed later in section 3.7 of the present chapter.

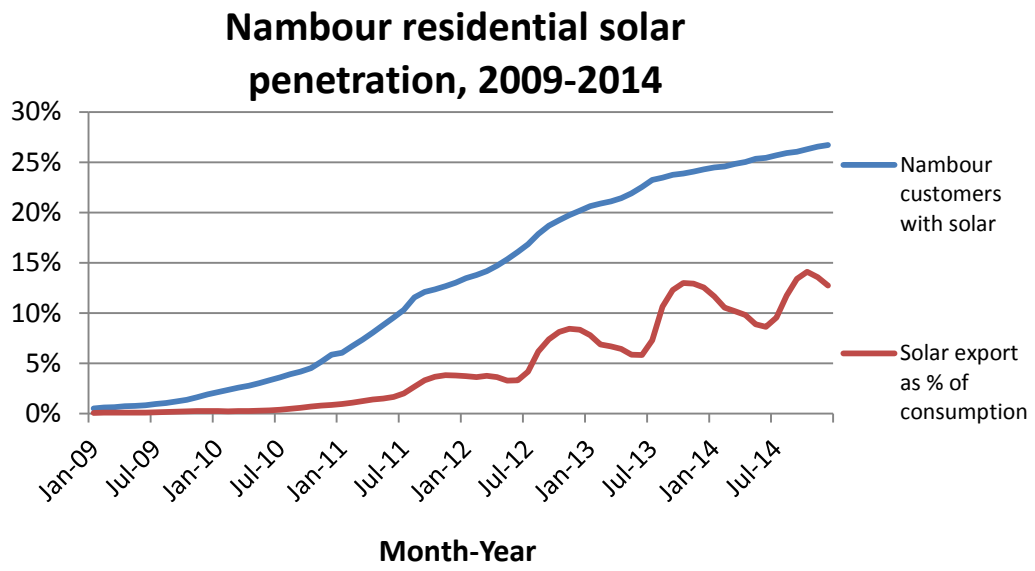

Figure 3-1. Uptake of solar PV in Nambour, Q, 2009-2014, adapted from Energex (2015).

Preliminary economic analysis was carried out in HOMER for some scenarios. The results are not reported here as the focus was on developing deeper skills with HOMER

beyond familiarity, rather than developing a dedicated economic feasibility study. It was clear that there were some factors within HOMER that required detailed examination, including integration of meteorological data construction of a load profile, choice of discount and inflation rates, estimation of fixed costs, and proper modelling of tariff regimes. These factors and their details are presented in section 3.7.

3.2 Expected outcomes and benefits

1. Confirmation or rejection of the hypothesised benefit of an economically-mediated grid-tied HRES battery charge controller in the context prescribed in section 1.3.
2. Determination of optimal BESS sizing in the context prescribed in section 1.3.

3.3 Outline of methodology

- Select and/or design the proposed physical system. This will need to account for "power flows of grid-to-load, PV-to-load, battery-to-load, battery-to-grid, grid-to-battery, PV-to-battery, PV-to-grid as well as battery state-of charge" Khalilpour & Vassallo 2016). Practical and economic considerations of power flows are detailed later in this chapter, in sections 3.4 and 3.5.
- Select the components of the physical system:
    - BESS type;
    - Converter types;
    - PV and wind generation; and
    - Controller type.
- Design the physical system.
- Select and/or develop the relevant mathematical models of physical system components.
- Select the economic controller design technique.
- Determine the objective function for the controller.
- Determine the parameters and constraints that influence the objective function.
- Incorporate physical system mathematical models into the controller algorithm.
- Acquire, design, or select load profiles for simulation purposes.
- Acquire meteorological data pertinent to the simulation including:
    - temperature

    - solar insolation
    - wind speed; and
    - atmospheric pressure.
- Design the economic controller.
- Acquire and/or simulate load and production data.
- Choose the simulation periods:
    - hourly
    - daily
    - annually; and / or
    - BESS and / or system life cycle.
- Establish a grid-only control case for comparison.
- Implement the steady-state system in HOMER.
- Model and test the transient state in SIMULINK, including:
    - power flow;
    - grid and consumer voltage level; and
    - grid and consumer voltage frequency.
- Conduct economic analysis of
    - Net present cost (NPC) of system over expected life; and
    - Electricity bills / refunds over a one year period.
- Report on how the testing and analysis meet the aims and objectives specified in sections 2 and 3.

3.4 Power flow modelling

Analysis of power flows is of fundamental importance to the project. Both the transient and economic models require a sound description and analysis of power flows. The primary difference between the two models is the time-scale, rather than the parameters.

3.4.1 Power flow conditions and options

- Supply feed-in power to the grid, to the benefit of the distributor and to the economic benefit of the owner, under certain conditions, either through BESS or through wind / PV.
- Supply power to the owner, under the condition of still being able to be supplied by the grid.

- Supply power to the owner, under the condition of isolation from the grid due to circumstances beyond the grid operator's control (e.g. blackout, storm, cyclone, etc.). This option was not considered further in the project but is suggested as future research.
- Supply power to charge the BESS, under certain conditions.

3.4.2 Possible modes of BESS operation

- Supply stored energy to the grid via the inverter.
- Supply stored energy to the residential load via power converters.
- Store energy supplied from the grid operator.
- Store energy supplied from wind / PV.

3.4.3 Desired modes of wind/PV operation

- Produce power for delivery to BESS.
- Produce power for delivery to residential load.
- Produce power for delivery to grid under general feed-in tariff regime.

3.4.4 Functions of controller operation

- Manage the flow of power among inverter, BESS, wind/PV, grid, and residential load in the most economically beneficial manner to the residential system owner.
- Monitor tariff signals to assist power flow management.
- Monitor BESS voltage, SOC, etc. to optimise power flow management.
- Act as a data storage and access device to assist in power flow optimisation. Technical methods to deliver this function were not further explored, but it was assumed that devices were available to permit such data storage and access.

3.4.5 Components absorbing and / or supplying power

To describe the power flows, it was necessary to first define the system components in terms of their capacity to supply power, absorb power, or both. This description is summarised in Table 3.1.

Table 3.1. Components supplying or absorbing power

Component	**Absorb or supply power**
Solar PV	Supply
Wind turbine	Supply
BESS	Supply and absorb
Load	Absorb
Grid	Supply and absorb
Power converters	Absorb (as losses)
Connections (wires etc.)	Absorb (as losses) – assumed to be negligible

3.4.6 Power balance equations

Assuming that the analysis was carried out in software, analysis was conducted in the discrete-time domain. The following equations, [3.1] to [3.6] summarise the power flows to balance during each discretization. Table 3.2 provides a summary of the symbols used in the power flow equations.

Solar PV power

$$P_{pv} = P_{pvb} + P_{pvl} + P_{pvg} \qquad [\,3.1]$$

Wind power

$$P_{w} = P_{wb} + P_{wl} + P_{wg} \qquad [\,3.2]$$

Load power

$$P_{l} = -(P_{pvl} + P_{wl} + P_{gl} + P_{bl}) \qquad [\,3.3]$$

Grid power

$$P_{g} = P_{gl} + P_{gb} - P_{pvg} - P_{wg} - P_{bg} \qquad [\,3.4]$$

BESS power

$$P_{b} = -[P_{pvb} + P_{wb} + P_{gb} - P_{bl} - P_{bg}] \qquad [\,3.5]$$

System balance of power

$$0 = P_{pv} + P_{w} + P_{l} + P_{g} + P_{b} \qquad [\,3.6]$$

Table 3.2. Symbols used for power flow equations and models

Symbol	Interpretation	Notes and conventions
P_b	BESS power	Positive (discharging) or negative (charging)
P_{bg}	Power supplied by BESS to grid	Provided for illustration; will be maintained at zero for economic reasons related to TOU tariff and feed-in tariff that are detailed in section 3.4.7
P_{bCmax}	Maximum BESS charge power	A negative value, by convention
P_{bDmax}	Maximum BESS discharge power	A positive value, by convention
P_{bl}	Power supplied by BESS to load	Positive
P_g	Grid power	Positive (supplying load) or negative (absorbing excess power generated)
P_{gb}	Power supplied by grid to BESS	Positive
P_{gl}	Power supplied by grid to load	Positive
P_l	Load power	Negative only (always absorbing power)
P_{pv}	PV power	Positive only
P_{pvb}	Power supplied by PV to BESS	Positive
P_{pvl}	Power supplied by PV to load	Positive
P_{pvg}	Power supplied by PV to grid	Positive
P_w	Wind power	Positive only
P_{wb}	Power supplied by wind to BESS	Positive
P_{wl}	Power supplied by wind to load	Positive
P_{wg}	Power supplied by wind to grid	Positive

Symbol	Interpretation	Notes and conventions
C	State of charge (SOC) of BESS	
C_{min}	Minimum SOC to be enforced by system	
C_{max}	Maximum SOC to be enforced by system	

3.4.7 Tariff influence on the planning of power flow control

The aim of the control scheme is to direct power flows to realise the greatest economic benefit. The tariff context of this study is the TOU tariff 12, as mentioned in section 1.3. The tariffs indicate that whenever possible, power produced by the HRES should feed the BESS or the load, depending on several factors including the BESS SOC, time of day (tariff) and load level. The FiT clearly economically disadvantages the export of power to the grid, that is, *the value of exported power is less than the value of power not imported from the grid*, even at the lowest TOU tariff offered by retailers. Therefore, system planning needed to accommodate the minimisation of power export to the grid. It was considered possible that the "overbuilding" of the PV system may have economic benefits if the capital cost of installed PV is low enough; this scenario was modelled and analysed in the economic modelling of the system inverter in section 5.8.

In terms of deriving the control strategy, it is worth noting that for all retailers, the following tariff relationships exist:

- The feed-in tariff is always less than the off-peak TOU tariff.
- The feed-in tariff is always less than the super-economy tariff.
- The super-economy tariff (tariff 31) is always less expensive than the off-peak TOU tariff.

3.4.8 Control of BESS power flows

The following control specifications were based on the TOU tariff 12 regime that was selected for the project, as well as on the works of Dufo-Lopez (2015) Ratnam (2015),

Sichilalu (2015), Wang (2013), Yoon & Kim (2016), Khalilpour & Vassallo (2016), and Fathima (2015).

- During TOU peak, discharge BESS to the load to C_{min}, at the maximum practical rate of discharge, which may or may not be P_{bDmax}. Discharge rate should not exceed the instantaneous power requirements of the load. Discharge should cease on reaching C_{min}.
- At C_{min}, but still at TOU peak, idle the BESS; any excess PV or wind power should be absorbed by any load that requires supply, rather than to the BESS. This will offset the lifetime cycling costs as well as reduce the minor losses due to extra power conversion processes.
- Ideally charge from the grid only on the TOU off-peak grade, at P_{bCmax}, until C_{max} is reached. The converter should be optimised for this purpose.
- Charging the BESS from PV and / or wind is acceptable at any time, if the following two conditions are met:
    - $C < C_{max}$; and
    - The instantaneous residential load has already been supplied by PV and wind power.
- Discharging to the load was *never* permitted to occur during the off-peak tariff. However, a case *could* exist for supplying the load during off-peak if $C = C_{max}$ at the start of the off-peak tariff. This would suggest either that load was small during the 1600h – 2200h time frame (reducing the need to discharge to load in the first place) and/or that wind/PV power was significant during the 1600h – 2200h time frame (to sufficiently supply load in preference to BESS for reasons stated in the second bullet point of this section) and/or that wind power was significant during the 2000 h – 2200 h time frame (enough to significantly charge BESS to C_{max}). It was hypothesized that the addition of such control elements would only have a minor to negligible economic impact on the project, in addition to introducing additional complexity to the control algorithm. Wind and PV resources are not normally significant during these time-frames, whereas load normally is significant. The planning, modelling, and incorporation of these control elements was beyond the scope of this dissertation.
- If predictive models were used, discharging during the weekday TOU shoulder period could occur if and only if the load was predicted to be low during the next TOU peak period, and / or if it was expected that PV / wind power would be sufficient later during the shoulder period to adequately recharge the BESS. This considered that PV

and wind power would be directed to the load as first priority during the shoulder period. For the purpose of this dissertation, however, such predictive measures were not designed to account for this possibility. This would require the incorporation of a near-future predictive algorithm based on meteorological forecasts and real-time weather data, and was beyond the scope of this dissertation, suggested as an avenue for future work.

- BESS discharging to the load during weekdays will only be scheduled for TOU peak periods.
- Given that weekends comprise $\frac{2}{7}$ of possible days, weekend BESS discharging to load was permitted to occur at any time during the TOU shoulder rate period. This was subject to the determination that PV and/or wind power production could not supply the instantaneous load requirements. This suggests that discharging to load was most likely to occur during times of low wind and sun resources.
- Weekend BESS charging from wind / PV could occur at any time provided that $C < C_{max}$ AND that the load had already been supplied by PV and wind power.
- BESS discharging to the grid *never* occurred; the feed-in tariff is very low when compared to the potential benefit of supplying the load during peak periods. Such a discharge may be feasible in the future if DNSPs determine that there is sufficient value to be realised by supporting the network during peak time with a peak time feed-in tariff that sufficiently exceeds the value of the TOU peak supply tariff.
- During the peak tariff period, PV and wind power produced in excess of load requirements should directly feed the grid to earn FiT revenue, rather than charge the BESS.
- Based on the previous points in this section and in the next sections, the parameters of BESS rated capacity, $P_{bCmax}, P_{bDmax}, C_{max}$, and C_{min} had a significant impact on the framing of the economic case, and on the behaviour of the transient case.

3.4.9 Control of PV power flow

It is possible to direct PV power flow to any of BESS, load, or the grid. The planned control of PV power flow follows.

1. During shoulder and off-peak times (occasionally the sun will shine before 0700 hrs), PV power is used to supply the load, and charge the BESS if $C < C_{max}$. If $C = C_{max}$, then the PV power (and wind) should supply the load. If additional PV

power is available after serving the instantaneous load requirements, this should feed the grid for FiT revenue.

2. During peak periods, the BESS will normally be discharged to the load. However, any PV produced during the peak period should supply the load before the BESS supplies the load, for two reasons. First, there are additional small extra life-cycle costs incurred to charge the BESS later on (during shoulder/off-peak) as a result of peak discharging. Second, supplying the load at peak time saves approximately 35c/kWh compared to earning approximately 6c/kWh by feeding in to the grid. If the PV power meets the instantaneous load requirements by itself, then excess PV power *could* charge the BESS if $C < C_{max}$. However, given that this is likely to be a rare occurrence because of typical load and PV power during peak times, and because the greatest payback opportunity for BESS exists during peak times, and because the system may encounter delays to safely switch from charging to discharging mode, excess PV power will always supply the load first, then the grid, and never BESS during the peak period.

3.4.10 Control of wind power flow

The flow of wind power should be controlled similarly to PV power, with the notable caveat that sometimes wind blows at night, during any of the TOU grades.

- During shoulder and off-peak times, wind power is used to supply the load, and charge the BESS if $C < C_{max}$. If $C = C_{max}$, then the wind power (and PV) should supply the load. If additional wind (and PV) power is available after serving the instantaneous load requirements, this should feed the grid to earn FiT revenue.
- During peak periods, the BESS is normally discharged or idled. If wind occurs at peak TOU, it should be directed to the load to reduce or to stop BESS discharging, or feed the grid to earn FiT revenue. As described above for PV, wind power will not be directed to BESS charging during the peak tariff.

3.4.11 Control of grid power flows

In this project, the grid was considered to be an infinite bus, capable of supplying any residential load on its own. Islanding was not considered.

- Supply power to the load when locally produced power is insufficient to meet demand by making up the difference as per equation *[3.3]* for load, above.

- Supply power to charge the BESS only during the TOU off-peak times, or during the shoulder period on weekends.
- Absorb excess power from wind and / or PV, provided that the instantaneous load has already been supplied by the wind / PV.
- Never absorb BESS power. There may be scope for its absorption in emergent conditions or as a protective requirement, but this is beyond the scope of this project. For example, if C_{max} is attained, but a catastrophic failure leads to overcharging combined with a protection failure, and no load exists for discharging, discharging to the grid might be advised. However, it will be assumed in this project that the grid will not normally accept BESS power.

3.4.12 Control of load power flows

This is essentially a summary of the previous four sections as each section pertains to load. No new ideas are presented here; however, it is useful to consider their collective influences on the residential load.

- Load is composed of non-DNSP-controllable elements, i.e. there is no economy or super-economy load. Even if some loads were to be DNSP-controllable, the off-peak TOU tariff exceeds the economy tariffs 33 and 31; it would not be advisable from an economic standpoint to supply BESS or PV power to controlled loads when greater benefits could be realised by supplying the uncontrolled load.
- Load is supplied first by wind and PV power, at any time such power is produced.
- Load is supplied by BESS during the TOU peak period only on weekdays, and to a degree during the shoulder tariff on weekends, but only after wind and PV power is insufficient to supply the load. This has a high probability of occurring during peak times, given the specified wind power of this project, and the time of day of TOU peak period which coincides with low to zero PV power production. If BESS supplies the load it does so at the maximum possible rate, i.e. at the rated BESS $C_{max,}$ or less if a lower rate is sufficient to make up the remaining instantaneous load requirements.
- Load is supplied by grid power at any time when wind, PV, and BESS power is insufficient to power the load on its own as mandated by the control scheme or the instantaneous weather conditions. The grid power makes up the difference between the load requirements and the locally available power.

3.4.13 Other power flow considerations

- It will be assumed that the project will always operate under grid-tied conditions. No technical or economic provisions will be made for islanding.
- The controller will need to monitor tariff signals (or the time depending on technology choice, which is not modelled in the project) to control switching.
- The controller will need to monitor C to control switching.
- The controller will need to monitor instantaneous load to control switching.
- The MAS approach detailed in an earlier section is one method of monitoring the system elements that feed in to the controller.
- It is proposed that a real-time system be designed to enact control of the power flows in the system, and that the real-time system controller behave in a purely deterministic fashion. A deterministic system must:

> "predict how a system will behave under all possible conditions, which includes all system states and event combinations. Assuming that a real-time system operates with bounded inputs and a finite number of system states, it should be possible to predict all system responses and any resulting change in system state. "(Zhou 2016) p. 7

- To be a perfectly deterministic system, it is necessary to define all system states, bounded inputs, and event combinations. For the dissertation purposes, the system states were considered to be the timing relationships to the TOU tariffs. These states are specific with respect to time and were assumed to be 100% predictable. For each state, a set of values for the power of each element defined in sections 3.4.8 to 3.4.12, the control of flow of these elements as defined in sections 3.4.8 to 3.4.12 (as Boolean logic), the BESS parameters of C, C_{max}, $C_{min,}$ P_{bCmax}, P_{bDmax}, and the balance of power detailed in section 3.4.6, are all known. With reference to this set of values, the controller was to calculate the amount of power to be supplied or absorbed by the battery, and subsequently the quantity of power to be supplied or absorbed by the grid. The essence of the algorithm in the power flow control problem is to send a reference power to the BESS controller that will in turn provide switching signals to the BESS two-quadrant converter for the appropriate level of charging or discharging current. The current is in turn subject to the voltage of the battery, which was also assumed to be known and measureable at any point in time.
- Real-time system design was outside of the project scope, but is an avenue for future work. However, the next three sections provide details of constructing a logical

flowchart that could be converted to programming language, followed by the set of flowcharts for each state in section 3.4.17.

3.4.14 States

- State 1 – TOU Peak period
- State 2 – TOU Off-peak period
- State 3 – TOU shoulder weekday period
- State 4 – TOU shoulder weekend

3.4.15 Variable inputs at time t, or sample k

- Load, in W
- PV power, in W
- Wind power, in W
- BESS SOC, in kWh or Ah
- BESS voltage, in V
- DC bus voltage, in V

3.4.16 Constants required at all times

- BESS maximum charge rate
- BESS maximum discharge rate
- BESS maximum SOC
- BESS minimum SOC
- Converter efficiency ratios

3.4.17 Decision making procedure for states

In each state, at each time, the optimum battery power flow reference is derived as a function of the data from sections 3.4.15 and 3.4.16 and the equations specified in section 3.4.6. The grid power reference is then derived from the battery power flow reference. Given this data at each sampling time, the controller should exert control over the switches of the two-quadrant converter connected to the battery to provide the optimum battery power flow. The decision-making process for each TOU tariff state is detailed in the flow charts of Figure 3-2, Figure 3-3, Figure 3-4, and Figure 3-5.

In each of the four flow charts, the BESS power reference, P_b, and the grid power reference, P_g, must be defined prior to reaching the end of the algorithm. At the end of the algorithm, the algorithm is directed to return to the start of the algorithm at the beginning of the new sample time.

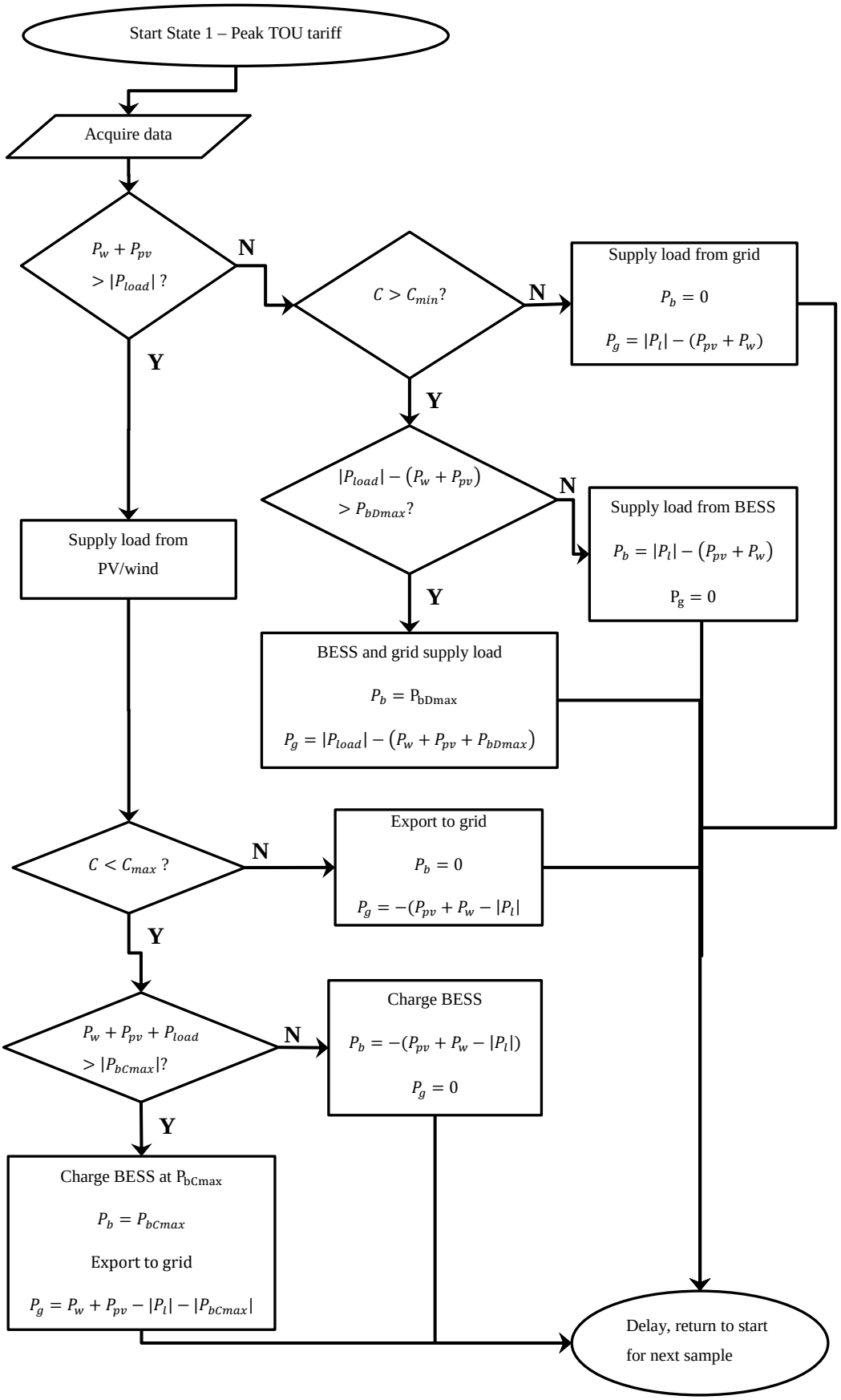

Figure 3-2. BESS power flow decision tree for peak TOU tariff (state 1).

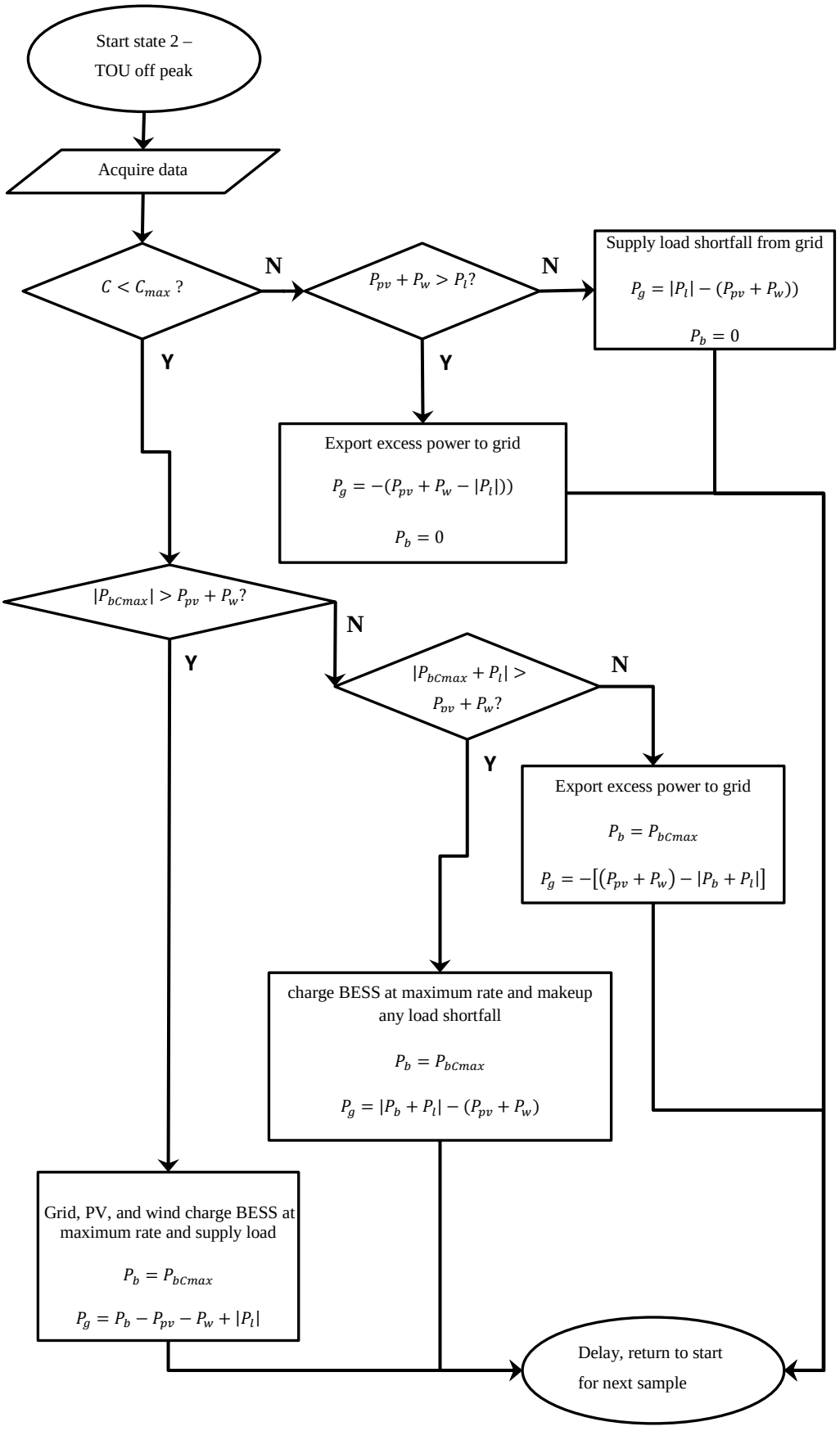

Figure 3-3. BESS power flow decision tree for off-peak TOU tariff (state 2).

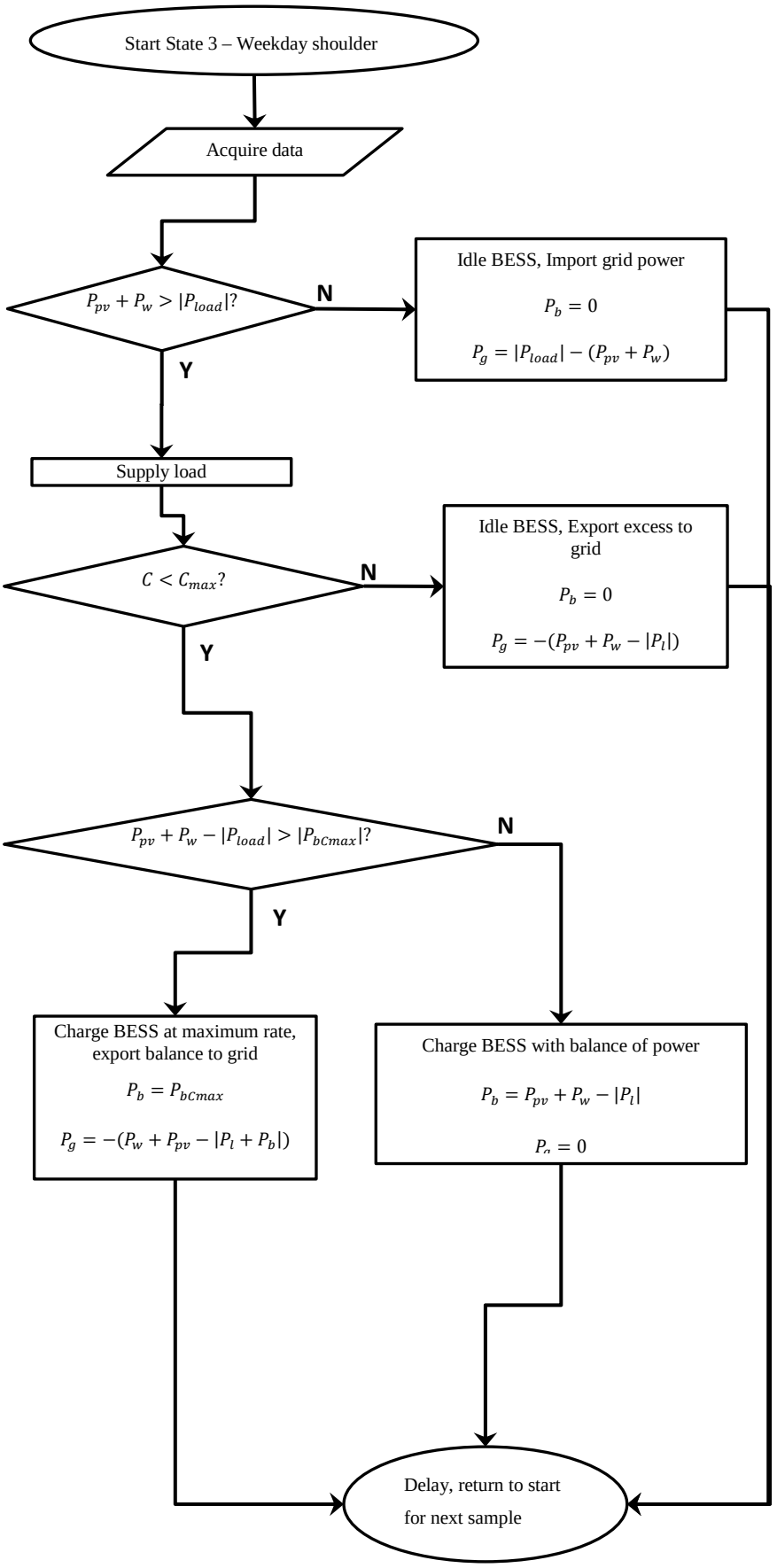

Figure 3-4. BESS power flow decision tree for weekday shoulder TOU tariff (state 3).

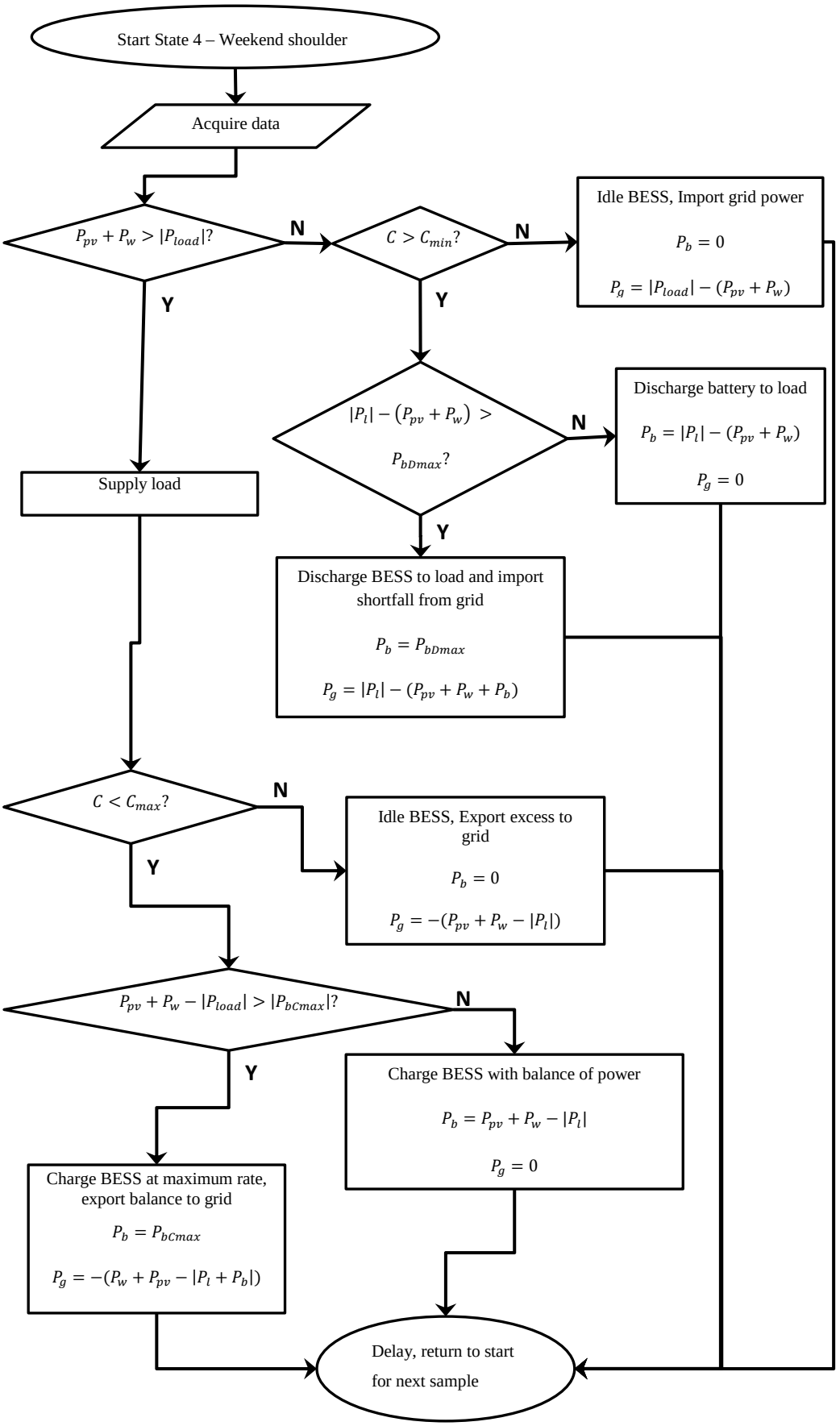

Figure 3-5. BESS power flow decision tree for weekend shoulder TOU tariff (state 4).

3.5 Transient modelling

3.5.1 Power electronics interface

Several options for the system were possible. In this case the choice was made to design the circuit based on work by Khaligh and Onar (2010). In this design, specifications were provided for a PV / BESS system linked in parallel at the DC bus. This interfaced with the residential load and the AC grid via a bidirectional single phase full-bridge converter. The model uses a boost converter as an MPPT controller to extract maximum power from the PV system; the boost inverter also provides the advantage of boosting the PV DC voltage to a suitable level for the DC / AC inverter that supplies power to the AC load and AC grid. This particular DC voltage is referred to hereafter as the DC link voltage, symbolised as V_{DCl}, the voltage across the inverter's DC input. Khaligh and Onar (2010) employed a suite of inter-connected control modules to maintain V_{DCl} and inverter output current, however, Simulink modelling of these aspects was deferred as future work.

3.5.2 Bus topology

Two primary topologies exist for a HRES of this project. The first is a common DC bus, the second is a common AC bus (Al Badwawi *et al.* 2015). There are advantages and disadvantages to both topologies.

In a common DC bus, individual converters supply the three power sources (BESS, PV, and wind) to the DC bus, and the grid inverter controls the voltage of the DC bus; the BESS, PV, and wind act as current sources. MPPT control is possible for each source, and control is possible with modern communications. In a common AC bus, there is a grid inverter for each power source as well as a rectifier to condition the variable AC wind output to DC. Advantages in this case include:

1. "Standardized off-the-shelf components for grid connection;
2. Cost reduction due to simplified design, installation, operation and maintenance
3. Connection of off-grid systems to the utility network is possible
4. Parallel operation allows unlimited extension of the system and increases reliability
5. The power on AC-side adds together from all components, the inverter is not a bottle neck in the system
6. Productive use due to AC network structure" (Wollny & Hermes 2007).

Some of the literature indicates a preference for a common DC bus as seen in Khaligh and Onar (2010), and Keyhani (2011).

Interestingly, much of the literature on economic control schemes seemed to prefer a common AC bus: Dieulot (2015), DiGiorgio and Liberati (2014), Khalilpour (2016), Ratnam (2015) (possibly), Sichilalu (2015), Wang (2013). No indication of bus preference was detailed by Yoon and Kim (2016), nor Fathima (2015).

Further investigation showed Simulink modelling of HRES/BESS systems under a common DC bus configuration (Fei *et al.* 2010; Saib & Gherbi 2015).

It could be argued that as the project specified a battery controller / combined co-gen grid connected inverter design, a common DC bus architecture is implicitly specified, as a common AC bus configuration would require three separate grid connected inverters, one each for the wind, PV, and BESS elements. Additionally, there appeared to be an emphasis on a common AC bus in the economic control scheme literature as mentioned above, which may suggest a gap in the literature; however this was not explicitly explored during review of the literature. For the reasons of the project specification, and of the apparent gap in the economic control literature, the choice was made to design a system with a common DC bus.

3.5.3 DC bus voltage control

In this dissertation, the DC link voltage is of primary importance to the problem of inverter design and configuration, because this voltage input needs to be high enough to allow the inverter to deliver a 240 V root mean squared (RMS) AC output to the AC side without over-modulation. The PV and MPPT system design plays a significant role in the determination of this value, and is detailed in sections 3.5.4 and 3.5.5. The DC link voltage is also important in terms of the control of the charge and discharge current of the BESS. Because the BESS current depends on the *power reference* calculated as per section 3.4.17, the power reference must be subsequently modified into a *current reference* before its use in the BESS switching control:

$$I_B = \frac{P_B}{V_{DCl}} \qquad [3.7]$$

where I_B is the battery current (A)

V_{DCl} is the DC link voltage (V)

This is a simple arithmetic calculation; although the arithmetic is simple, the fact that V_{DCl} is dependent on three inputs (wind, solar and BESS power), two of which are directly dependent on weather conditions, suggests that there is likely to be some variation of V_{DCl} during system operation. It is therefore necessary to consider that the BESS current reference depends on both V_{DCl} and P_B. DC bus voltage control is deferred as future work; in the system's modelling, it will be assumed to be held at a constant value, although the modelling was able to simulate a pseudo-randomly varying voltage as an input to the BESS controller.

3.5.4 AC inverter design specification

Using the methodology outlined in Keyhani (2011) the preliminary grid-tied inverter plus PV system design without consideration of wind, BESS, or PV buck / boost DC/DC converter follows:

$$V_{grid} = 240\ V$$

$$f_{grid} = 50\ Hz$$

$$M_a = 0.82$$

$$V_{DCl} = \sqrt{2} * \frac{V_{grid}}{M_a} \qquad [3.8]$$

$$V_{DCl} = 413.9\ V$$

$$V_{MPP} = 30.9\ V$$

$$N_M = \frac{V_{DCl}}{V_{MPP}} \qquad [3.9]$$

$$N_M = 13\ modules\ per\ string$$

$$V_{pv} = V_{MPP} * N_M \qquad [3.10]$$

$$V_{pv} = 401.7\ V$$

$$P_{module} = 255\ W$$

$$P_{MPP} = N_M * P_{module} \qquad [3.11]$$

$$P_{MPP} = 3315\ W$$

$$P_{max} = 10\ 000\ W$$

$$N_S = round\ down\left(\frac{P_{max}}{P_{MPP}}\right) \quad [3.12]$$

$$N_s = 3\ strings$$

$$P_{system} = P_{MPP} * N_S \quad [3.13]$$

$$P_{system} = 9\ 945\ W$$

$$M_a = \sqrt{2} * \frac{V_{grid}}{V_{dc}} \quad [3.14]$$

$$M_a = 0.82$$

$$f_{inverter} = 5\ 000\ Hz$$

$$N_M = \frac{V_{dc}}{V_{MPP}} \quad [3.15]$$

$$M_f = \frac{f_{inverter}}{f_{grid}} = 100$$

To reduce switching harmonics, an odd frequency modulation index was chosen:

$$M_f = 101$$

Based on this design framework, the specification of the inverter and the solar PV system was determined.

Simulink provides a variety of methods for modelling inverters. A universal bridge was selected for the modelling, using a full bridge two-arm (single phase) configuration with IGBT / anti-parallel diode switches.

3.5.5 10 kW PV system

Using the methodology outlined in Keyhani (2011), the preliminary PV system design without consideration of wind, BESS, or PV buck/boost DC/DC converter is outlined in Table 3.3.

Table 3.3. Inverter design parameters

Parameter	**Value**
Module power at MPPT	255 W
Modules per string	13
Number of parallel strings	3
String voltage at MPPT	401.7 V
DC bus voltage	413.9 V
System power at MPPT	9945 W + 0-3%
AM index of inverter	0.82
FM index of inverter	101

The voltage-current and voltage-power characteristics of the Trina solar PV modules are displayed in Figure 3-6.

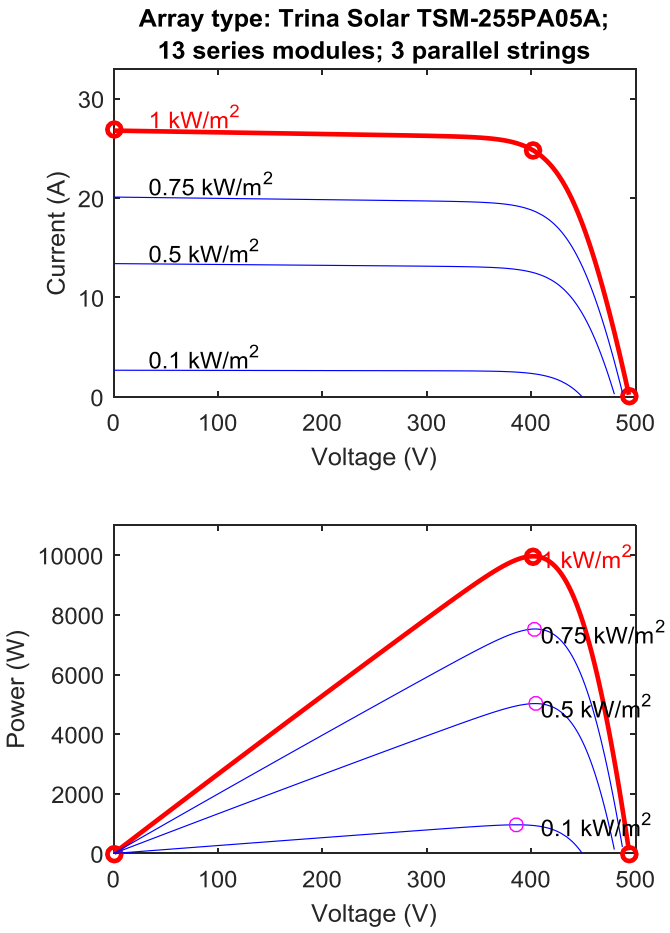

Figure 3-6. PV array with MPPT - output characteristics for various irradiances

3.5.6 PV boost MPPT converter specification

Using the methodology outlined in Keyhani (2011), it was necessary to determine the MPPT boost converter design.

$$D_{boost} = 1 - \frac{V_{pv}}{V_{dc}} \qquad [3.16]$$

$$D_{boost} = 1 - \frac{401.7}{413.9} \qquad [3.17]$$

$$D_{boost} = 0.02948$$

$$f_{boost} = 10\ kHz$$

Using the methodology outlined in (Sulthan & Devaraj 2014), initial specification of the boost converter inductor follows:

$$I_{pvmppt} = \frac{P_{pv}}{V_{pv}} \qquad [3.18]$$

$$I_{pvmppt} = 24.76\ A$$

Ideally, the power output at the DC link will equal the power input to the inverter:

$$\eta_{boost} = 1$$

$$P_{dclink} = P_{pv} * \eta_{boost} \qquad [3.19]$$

$$P_{dclink} = 9\ 945\ W$$

The corresponding DC link current can be obtained:

$$I_{dclink} = \frac{P_{dclink}}{V_{DCl}} = 24.027\ A \qquad [3.20]$$

Assuming an inductor ripple of approximately 5%:

$$k_{Lripple} = 0.05$$

$$\Delta I_L = I_{dclink} * K_{Lripple} \qquad [3.21]$$

$$\Delta I_L = 1.201\ A$$

Inductor size:

$$L_{boost} = V_{dc} \frac{D_{boost}}{f_{boost} *\ \Delta I_L} \qquad [3.22]$$

$$L_{boost} = 1.017\ mH$$

The choice was made to use and inductor size of $1\ mH$.

Using the methodology outlined in (Sulthan & Devaraj 2014), the initial specification of the capacitor used for the boost converter is as follows:

Assuming a capacitor voltage ripple of no more than 2% of output voltage:

$$\Delta V_C = 0.02 V_{DCl} \qquad [3.23]$$

$$\Delta V_C = 8.728\ V$$

$$C_{boost} = I_{dc} * \frac{D_{boost}}{f_{boost} * \Delta V_C} \qquad [3.24]$$

$$C_{boost} = 8.566\ \mu F$$

The capacitor chosen was a 10 μF capacitor.

To test the solar PV system with the boost converter under full insolation at steady-state of 1000 W/m^2, the boost converter was connected to a test resistance located at the position of the expected DC link. The test resistance was computed as follows:

$$R_{test} = \frac{P_{dclink}}{I_{dc}^2} \qquad [3.25]$$

$$R_{test} = 17.227\ \Omega.$$

3.5.7 PV MPPT algorithm

The primary purpose of MPPT control is maximization of power production of the solar PV array; it is also a significant input to V_{DCl}. PV cell voltage and current behaviour is affected by both insolation and ambient temperature. In this model, the output terminals of the PV array are interfaced with the DC bus by a boost DC chopper as modelled by a Simulink SimPower Systems block. The DC chopper receives an input voltage and delivers an output voltage as a function of the "on" and "off" time of the chopper's IGBT switch for a switching cycle (note the switching frequency is designed at 10 kHz). The on and off times are regulated by the phase-width-modulation (PWM) technique, and controlled by a duty cycle signal, which dictates the proportions of switch on and off times. It is this duty cycle value which is controlled by the MPPT controller.

Several methods of MPPT control are possible, including fuzzy logic, neural network, and perturb and observe (P&O) (Saharia *et al.* 2016; Khaligh & Onar 2010); as well as linearized functions, fractional open circuit, fractional short-circuit, incremental conductance, ripple correlation, current sweep, and DC link capacitor droop control voltage (Khaligh & Onar 2010). P&O is a commonly used control, is relatively easy to implement, and is relatively robust (Khaligh & Onar 2010; Saharia *et al.* 2016). In Simulink, the P&O algorithm was simulated with a switching-based subsystem based on the work of Saharia et al. (2016), seen in Figure 3-7.

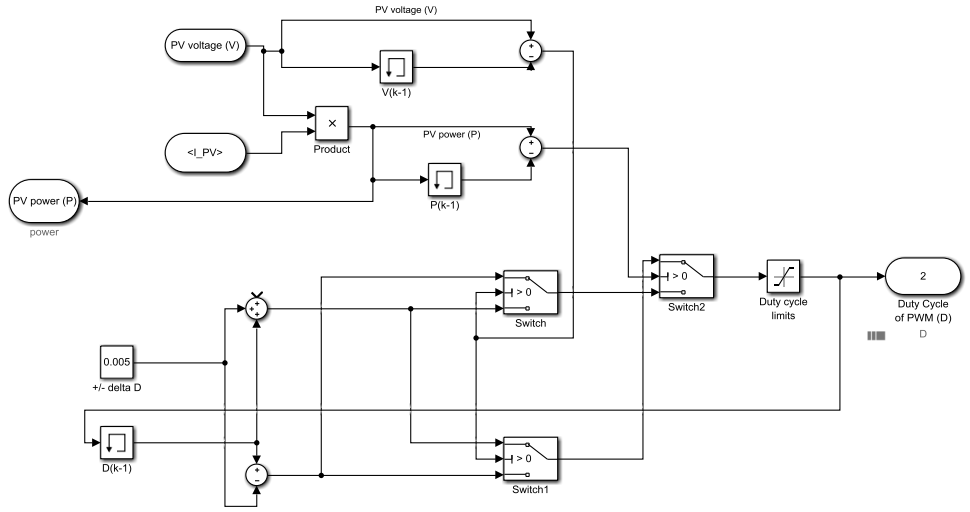

Figure 3-7. MPPT perturb and observe Simulink algorithm

3.5.8 Solar block scenario

Using a relatively simple methodology based on spherical geometry outlined in Appendices A and B of (Badescu 1997), a Matlab script for solar insolation as a function of day of the year and time of day was derived for Nambour, Queensland. No accounting was made for atmospheric conditions, nor for the elliptical pattern of Earth's orbit around the sun. As the scope for transient testing is a short time period, the first step in model development was to develop a clear-sky profile for 25 September at the resolution of 1 s intervals as a data-table to be accessed by the Simulink model. Shorter time resolution is possible.

This Matlab script was of no consequence to the dynamic modelling of the system, because the dynamic modelling took place in the space of seconds, rather than hours, days, or years. The script is found in Appendix J.1 for reference.

The transient case considered insolation in the context of minutes and seconds, rather than days and years. A Guadeloupe-based study used Dirichlet distributions to determine that four different types of days existed through the year, and would impact on transient behaviour (Soubdhan *et al.* 2008). The application of their work to this work's transient modelling is best summed up by the following passage, i.e. that transient solar power could vary by

> "700 W/m² and occur within a short time interval, from few seconds to few minutes (*sic*) according to the geographical location. These variations depend on the clouds (*sic*) size, speed and number." (Soubdhan *et al.* 2008).

The implications of this transient power information were of importance for the transient case. Such transients can cause power system instability in some instances (Soubdhan *et al.* 2008). However, these are inconsequential on the long-term steady state case, which is modelled in HOMER, unless of course, the system instability leads to blackouts, which are not assumed. The type of distribution used for the economic modelling, on the other hand, is of significance. Appropriate Monte Carlo modelling of a reasonable statistical distribution can help to determine the probabilities that a particular location may have a string of cloudier years, for example, and the influence that this might have on the economic viability of the project. However, this introduces scope creep and was a discretionary part of this dissertation that was deferred to future work.

The solar PV array block model in Simulink facilitates solar irradiance and temperature inputs to the block. This can be accomplished with a script, dataset, or other Simulink source blocks. The irradiance source block was designed to model a clouding transient that resulted in a decrease or increase of 700 W/m^2 over a few seconds as described by Soubdhan *et al*. (2008). Modelling of full-insolation at steady-state was accomplished with the use of a constant block of value 1000 W/m^2. The clouding transient was designed with sequential ramp and saturation blocks. The ramp block provided the rate of shading or un-shading; the saturation block provided the desired limits of irradiance. Temperature modelling was not considered for the transient model.

The PV model is seen in Figure 3-8.

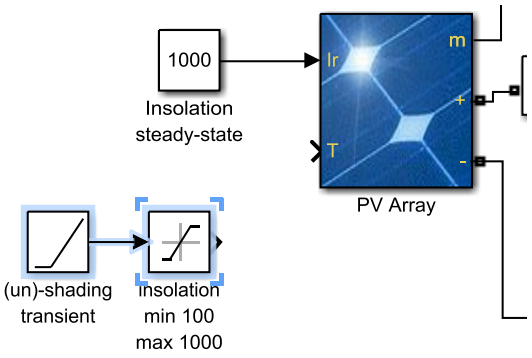

Figure 3-8. Modelling of solar insolation values.

3.5.9 Final solar model

The final solar PV model is in Figure 3-9.

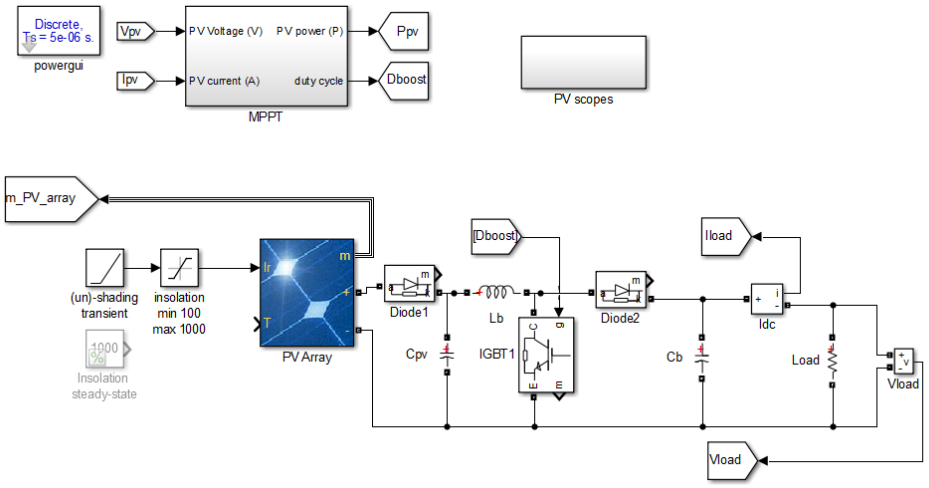

Figure 3-9. Final solar model.

3.5.10 Building the wind block scenario

An analysis of wind speed for Nambour for the month of September showed that the mean average (that is, the average of the averages) wind speed at half-hourly intervals did not reach the minimum specified start-up speed for the given turbine, only peaking at 1.61 m/s. However, the maximum average wind speed was 7 m/s. From the BOM data, the highest wind gust recorded in September between 2004 and 2015 was 54 km/h or

15 m/s. For the purposes of the transient simulation, a choice was made to make a crude simulation of the wind speed with a sine curve fluctuating between 0 and 7 m/s, representing a fairly windy day by Nambour standards. A separate block should be constructed for a short wind gust that fluctuates from 7 to 15 m/s and back to 7.

Incorporation of the wind block and the wind turbine physical model is deferred as future work.

3.5.11 Building the load block

A block should be constructed for a load transient that simulates, the instantaneous draw and release of a 2.2 kW air conditioner, or some other reasonable load transient during a five minute period.

Development and incorporation of the transient load block model is deferred as future work.

3.6 Transient model: BESS, power electronics, and control

3.6.1 Battery model

The battery selected for the project design is the LG Chem Resu, a 6.4 kWh lithium-ion battery capable of 5 kW peak power at a maximum current of 110 A. Nominal operating currents are 42 A charging when in constant current / constant voltage charging mode, and 42 A discharging when in constant current mode.

Simulink provided a battery modelling block to design the system. The block allows for specified parameters to be entered. These parameters and their values were obtained from the LG data sheet, as applicable, and were entered into a Simulink SimPower battery model for Li-ion type batteries. These parameters are detailed in Table 3.4.

Table 3.4. LG Chem Resu battery specifications

Parameter	Value
Nominal voltage	51.8 V
Rated capacity	126 Ah
Initial state of charge	Specified per simulation
Battery response time	Unknown
Maximum capacity	126 Ah
Cut-off voltage	45.2 V
Fully charged voltage	58.1 V
Nominal discharge current	42 A
Nominal charge current	42 A
Internal resistance	0.00411 (determined by Simulink)
Capacity at nominal voltage	126 Ah
Exponential zone of voltage	55.964 V (determined by Simulink)
Exponential zone of capacity	6.19043 Ah (determined by Simulink)

3.6.2 Battery charge controller and converter introduction

The proposed DC-DC two-quadrant converter battery charge controller does not use the conventional duty cycle control technique described in Ahfock (2014), but rather the hysteresis feedback technique described in Tyagi (2012), which does not prescribe a set switching frequency. This technique uses the power reference, battery voltage, and battery current measurements to generate gate pulses to the IGBT gates.

A constant DC source of 413.9 V was used to model the DC link voltage (i.e. the designed voltage input to the system inverter as described in section 3.5.4). To simulate DC link voltage variation, a random number generator was connected to the DC source input, initially set to zero variation. A voltage measurement block was incorporated to use for further control requirements. A 50 mH inductor was selected to smooth the output current. Switches were modelled as ideal IGBTs with antiparallel diodes.

3.6.3 Choice of power electronic switching device

A choice between power MOSFET and IGBT was required. Power MOSFETS typically have higher switching speed capability, but lower power handling capabilities as compared to IGBTs. A higher switch speed improves the current output waveform ripple, reducing the converter's inductor size requirements, which in turn improves the response time to changes in current requirements dictated by the power reference signal.

This system must deliver up to 110 A in discharge mode for the LG battery. It also has the requirement to handle the potential difference between the DC link voltage of 414 V (+/- depending on system conditions) and battery voltage of 42-58 V. Although Batarseh (2011) suggests that it is possible to obtain power MOSFETs up to 1000 V and current ratings up to 300 A (Batarseh 2011), it was difficult to find such a unit within a reasonable time. For example, Fairchild Semiconductor (2016) did not have any MOSFETs meeting this requirement; Infineon (2016) had a unit rated at 600 V but 109 A, still insufficient to meet the system design. It was decided to use IGBT switches without comparing to MOSFETs. A Littelfuse IGBT rated at 600 V and 200 A was selected. This unit has a sum of 600 ns required for on-delay, rise time, off-delay, and fall time (Littelfuse 2016), indicating possible switching speeds of up to 150 kHz. A switching speed of 100 kHz was selected for the Simulink model, using the discrete Powergui block with period T = 10 microseconds. The circuit modelled in Simulink can be viewed in Figure 3-10.

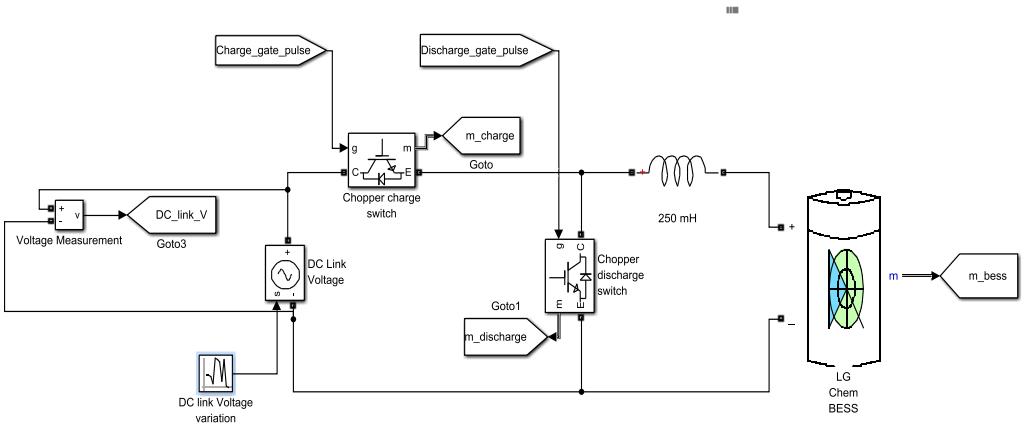

Figure 3-10. Simulink circuit model for DC-DC two-quadrant (positive voltage) converter.

To perform as a typical charge controller, the unit needed to charge or discharge the battery as warranted by the conditions of the power reference. This depends in turn on

the behaviour of the solar PV, wind, load, and the battery SOC. It also needs to perform under conditions of varying voltage of the DC link, i.e. the DC voltage at the inverter input, and adapt to changes in the DC voltage of the battery.

The controller circuit shown in Figure 3-10 is composed of six circuit elements, described in Table 3.5, and three control parameters, described in Table 3.6.

Table 3.5. Charge controller circuit elements.

Element	**Description**
DC Link Voltage	Used to simulate the DC link voltage at the input of the system inverter. Variation of this voltage is simulated with the random distribution block described below.
Chopper charge IGBT switch	Used to manage the input current to the battery during charging, under the charging gate pulse, described further below.
Chopper discharge IGBT switch	Used to manage the battery output current during discharging, controlled by the discharging gate pulse, described further below.
Anti-parallel diodes	Provides a path for current flow during switch-off periods.
5 mH inductor	Provides a more consistent output current by reducing the current ripple. The lower ripple afforded by this large inductor is traded off by slower response time to changes in the power reference, plus additional costs.
Battery	As described earlier, a model of an LG Chem battery.

Table 3.6. Charge controller control elements

Control parameter	**Description**
Charge gate pulse	Activates / deactivates the gate of the IGBT responsible for battery charging. The signal is developed according to the power reference and circuit element parameters
Discharge gate pulse	Activates / deactivates the gate of the IGBT responsible for battery discharging. The signal is developed according to the power reference and circuit element parameters
DC link voltage variation	This block simulates random variation in the DC link voltage that might be encountered in a fully developed system

3.6.4 IGBT switch gate control

To regulate the charge or discharge current, it was necessary to establish control over the gate pulses of the switches, as seen as the charge_gate_pulse and discharge_gate_pulse tags in the Simulink model in Figure 3-10 and Figure 3-11. The gate pulse control block was set up with the inputs of the power reference (value to be obtained with reference to section 3.4.17), as well as the BESS voltage and the BESS current, which were obtained from the measurement output signal of the battery model block. The control block mask is in Figure 3-11.

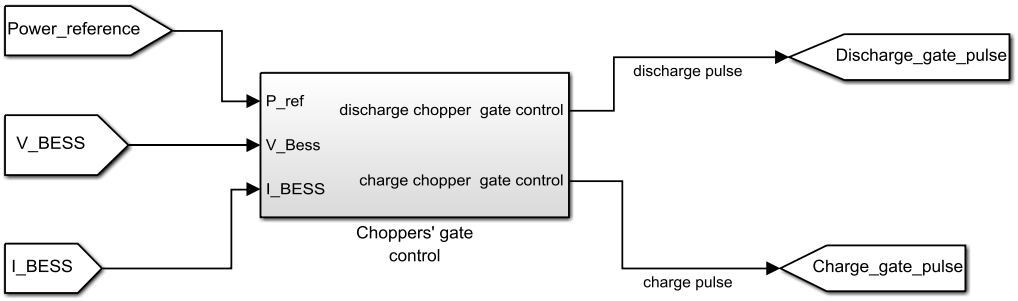

Figure 3-11. DC-DC chopper gate control mask

The internal architecture of the control block is seen in detail in Figure 3-12, Figure 3-13, and Figure 3-16. The block can be viewed as a complete block in Appendix D.

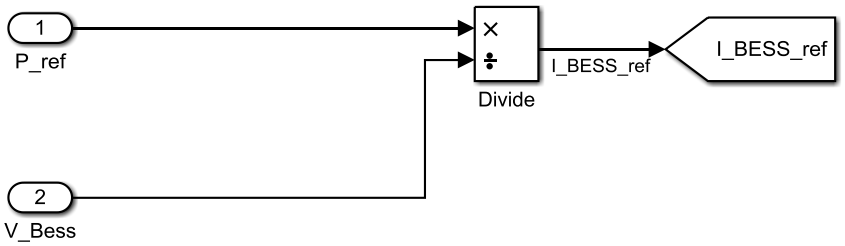

Figure 3-12. Controller sub-block 1: BESS reference current

The first function of the control block is the BESS reference current block, as displayed in Figure 3-12. Using a simple arithmetic function, the BESS reference current is derived from the power reference and the BESS voltage as follows:

$$I_{BESSref} = \frac{P_{ref}}{V_{BESS}} \qquad [\ 3.26]$$

Where $I_{BESSref}$ is the battery reference current,

P_{ref} is the power reference generated by the system conditions, and

V_{BESS} is the instantaneous voltage of the battery obtained by a voltage sensor, which is modelled as a signal from the Simulink battery block.

The second function of the control block is the PID controller block, in Figure 3-13. The BESS reference current obtained from the first function block as per equation [3.26] was processed with a PID controller to provide a faster response of the BESS current to the BESS reference current. The values of the PID block were set using the controller tuning function in Simulink, using the Simulink Control Design application according to the following expression:

$$P + \frac{I}{s} + \frac{ND}{1 + \frac{N}{s}} \qquad [\ 3.27]$$

where P is the proportional constant,

I is the integral constant,

D is the derivative constant,

N is the filter coefficient, and

s is the frequency domain variable.

The values for the PID obtained from the controller tuner are in Table 3.7. This was then multiplied by the DC-DC inverter plant transfer function as in Figure 3-13.

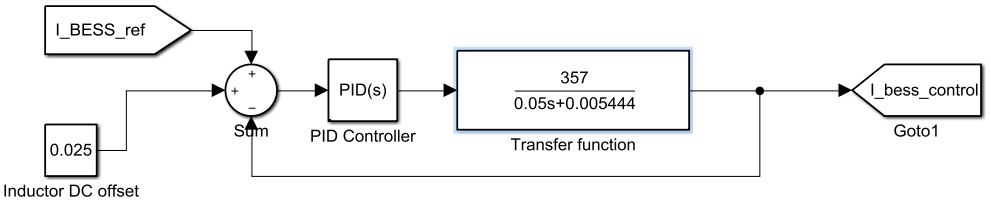

Figure 3-13. Controller sub-block 2: PID controller

Table 3.7. PID controller parameters.

Parameter	Value
Proportional (P)	1.929
Integral (I)	985
Derivative (D)	-279 x 10^{-6}
Filter coefficient (N)	3284

The plant transfer function was initially modelled for the battery charging state of the converter circuit model (negative power reference, or sinking current), with the IGBT switch in the ON state. The equivalent circuit model is in Figure 3-14.

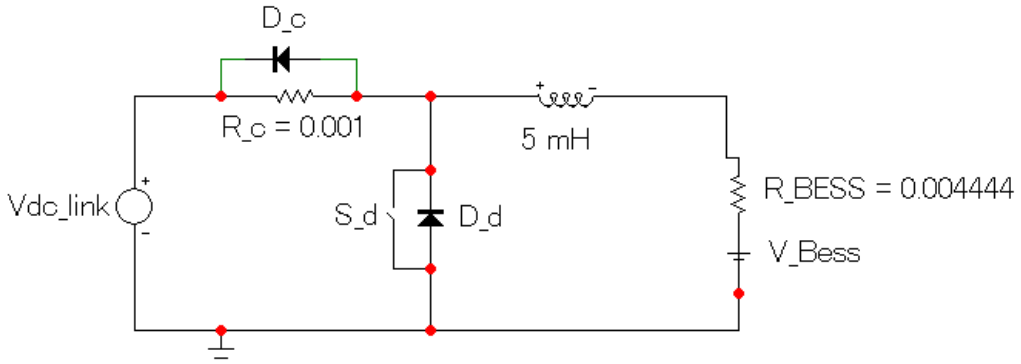

Figure 3-14. Battery charging IGBT switch "ON" equivalent circuit

In the initial derivation of the plant transfer function, assumptions were made about the value of the DC link voltage and the battery voltage at a particular point in time. Ideally, these values would be obtained in real time as the battery and DC link voltages change, and passed to the plant transfer function. However, the following values were assumed:

$$V_{DCl} = 414\,V$$

$$V_{BESS} = 57\,V$$

By KVL:

$$V_{DCl} = iR_c + L\frac{di}{dt} + iR_{BESS} + V_{BESS} \qquad [\,3.28]$$

Where i is the instantaneous current,

R_c is the IGBT charging switch-on resistance, and

R_{BESS} is the internal battery resistance.

For zero initial conditions, where

$$R = R_c + R_{BESS} \qquad [\,3.29]$$

then converting to the frequency domain, the following is obtained:

$$V_{DCl}(s) - RI(s) - LsI(s) - V_{BESS}(s) = 0 \qquad [\,3.30]$$

Subsequent rearrangement results in:

$$I(s) = \frac{V_{DCl}(s) - V_{BESS}(s)}{Ls + R} \qquad [\,3.31]$$

Substitution for the values of $V_{DCl}, V_{BESS}, L,$ and R in equation [3.31], the following transfer function was obtained:

$$I(s) = \frac{357}{0.05s + 0.005444} \qquad [\,3.32]$$

The result of [3.32] would also be the case for the *discharging* situation when the discharge IGBT is in the "off" position, but with current flow in the opposite direction.

Processing of the BESS reference current with the PID controller and plant transfer function resulted in the BESS controller current, which was used as an input to stage 3 of the controller (Figure 3-16). Note that an inductor DC offset is included in the controller summer. This addition was included after noticing during several trial simulations that the actual battery current only exceeded the reference current for a brief period, which caused the relevant IGBT switch to reverse state immediately. The result of this was that the average current was always less than the reference current by approximately 50 mA. To permit the average current to be nearer to the reference current, half of this value, or 25 mA, was added to the control current. As seen in Chapter 4, this appeared to be a reasonable measure, as the BESS current more closely followed the reference current.

An equivalent circuit was also drawn for a positive power reference, i.e. a discharging situation. The equivalent circuit for this situation, when the discharging IGBT switch is in the "on" position, is in Figure 3-15.

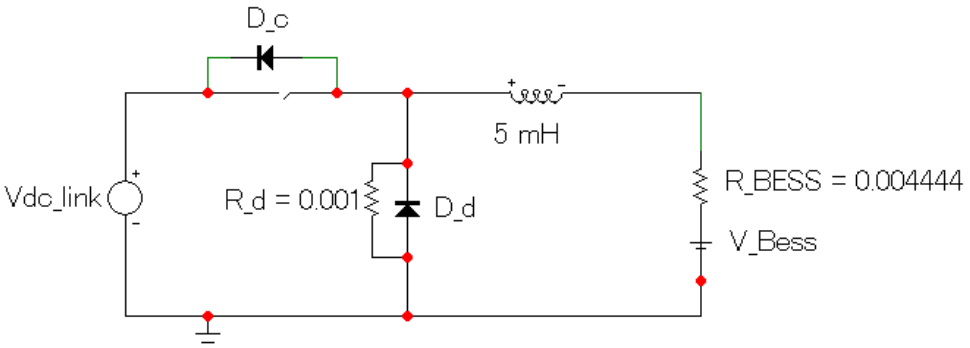

Figure 3-15. Equivalent circuit for discharging situation, discharging IGBT is "on".

For this equivalent circuit, the following values were assumed:

$$V_{DCl} = 414\,V$$

$$V_{BESS} = 57\,V$$

By KVL on the left-hand side of the circuit diagram:

$$V_{DCl} + V_{Cd} + V_{ds} = 0 \qquad [\,3.33]$$

where V_{Cd} is the voltage across the charging diode

V_{ds} is the voltage across the discharge IGBT switch.

Assuming negligible voltage drop across the discharge IGBT switch, i.e. $V_{ds} = 0$, the voltage across the diode is equal and opposite that of that across the DC link voltage, i.e.

$$V_{Cd} = -V_{DCl} \qquad [\ 3.34]$$

Subsequently, by KVL on the right-hand side of the circuit:

$$V_{ds} + V_L + V_{BESS} + i(R_d + R_{BESS}) = 0 \qquad [\ 3.35]$$

where R_d is the resistance of the discharge IGBT switch when switched on.

Substitution of [3.34] in [3.35], obtained the following:

$$0 + L\frac{di}{dt} + V_{BESS} + i(R_d + R_{BESS}) = 0 \qquad [\ 3.36]$$

If the voltage drops across the resistances are assumed to be near zero, then the voltage across the inductor is approximately equal and opposite to that of V_{BESS}, or approximately -57 V.

For zero initial conditions, where

$$R = R_d + R_{BESS}, \qquad [\ 3.37]$$

substitution of [3.37] in [3.36] followed by conversion to the frequency domain, obtained the following:

$$RI(s) + LsI(s) = -V_{BESS}(s) \qquad [\ 3.38]$$

Subsequent rearrangement of [3.38] and substitution of assumed values results in:

$$I(s) = \frac{-V_{BESS}(s)}{Ls + R} \qquad [\ 3.39]$$

$$I(s) = \frac{-57}{0.05s + 0.005444} \qquad [\ 3.40]$$

This is a different result than for the on-state of the charging IGBT switch as per [3.31]. A similar result would be obtained for the *charging* scenario with the IGBT switch in the "off" position; the current flow would, however, be opposite.

The result of two different transfer functions applied to different equivalent circuit configurations indicates that possible benefits may be realised by the implementation of switching between two different controllers, or by dynamically switching different parameters to the plant transfer function as required. However, the design and application of this is deferred to future work.

The third stage of the controller can be further divided into 3 stages, as viewed in Figure 3-16.

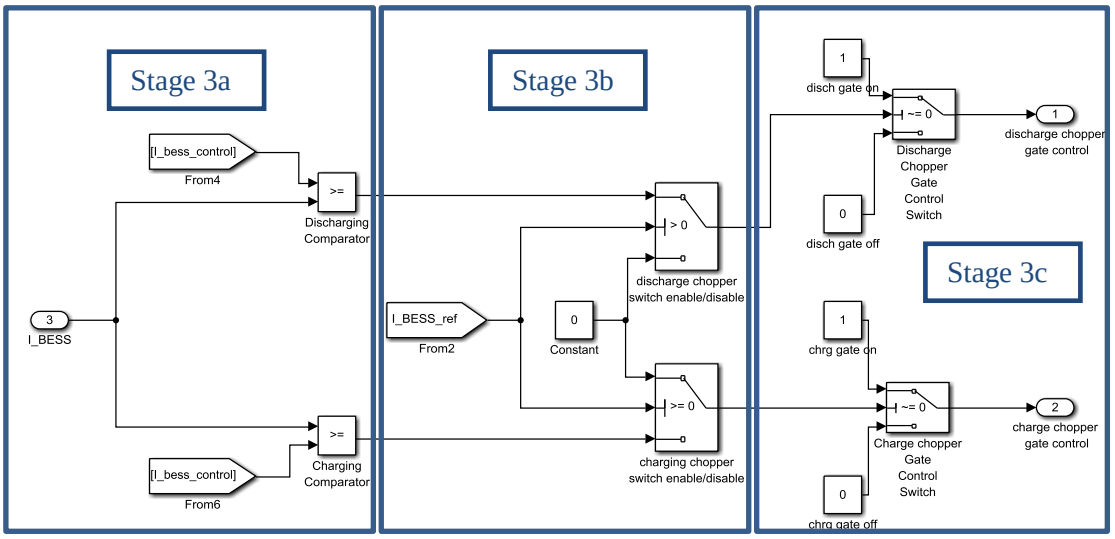

Figure 3-16. Controller sub-block 3: IGBT chopper gate logic

Each of stages 3a, 3b, and 3c has simultaneous parallel control logic for each of the two IGBT switches. To describe stage 3, it will be assumed that the power reference, and

hence current reference, is negative, indicating a state of battery charging (the same assumption used to describe stage 2). Recalling that only one IGBT switch may be on at any point in time, Stage 3a determines if an enabled IGBT (by Stage 3b) should be active or inactive. It uses comparators to compare the actual battery current to the BESS control current derived from the second stage (PID control). The discharging comparator compares the reference current to the battery current; if the control current exceeds the actual current, logic 1 is returned to stage 3b. The charging comparator compares the reference current to the control current; in this case, if the control current is less than the actual current, logic 1 is returned to stage 3b, activating the charging switch, which is desirable if the battery needs to sink more current to reach the reference current. The opposite cases occur if the control current is less than the battery current.

Stage 3b is used to ensure that only one switch is active at a time to prevent short-circuiting of the DC-DC converter. If the reference current (not the control reference current from stage 2) is negative, as is the case for a charging situation, the charging chopper IGBT switch is enabled, allowing the signal from Stage 3a to pass through to stage 3c. At the same time, the discharging chopper switch is disabled, passing logic zero to stage 3c, regardless of the Stage 3a signal. In the event of a positive reference current, i.e. discharging, the opposite logic occurs.

Stage 3c is used to pass the logic from the previous two stages to determine the actual gate logic passed to the IGBT switches. To continue the negative current reference example, consider first the discharging IGBT. Because Stage 3b returned a logic zero, this in turn produces a zero signal, keeping the discharge IGBT off. Second, considering the charging IGBT, the gate signal sent to the switch may be zero or one, depending on the logic sent from Stage 3a, as the Stage 3b logic allows the Stage 3a logic to pass through to Stage 3c.

The stage 3 logic is summarised in Table 3.8.

Table 3.8. IGBTs' gate control logic summary

Reference current	Control current reference	Battery current	Stage 3b, 3c charging switch logic	Stage 3b, 3c discharging switch logic	Charging switch	Discharging switch
Negative	Negative, charging	Less than reference	1, 0	0, 0	Enabled, off	Disabled
Negative	Negative, charging	Greater than reference	1, 1	0, 0	Enabled, on	Disabled
Positive	Positive, discharging	Greater than reference	0, 0	1, 0	Disabled	Enabled, off
Positive	Positive, discharging	Less than reference	0, 0	1, 1	Disabled	Enabled, on
Zero			0, 0	0, 0	Disabled	Disabled

3.6.5 Simulation of power reference

The power reference should ultimately be derived from the overall system conditions, but during the controller design phase, was selected from a block step, ramp, or random conditions, as seen in the block of Figure 3-17. The step, ramp and random power reference block conditions can be individually specified but are not shown here.

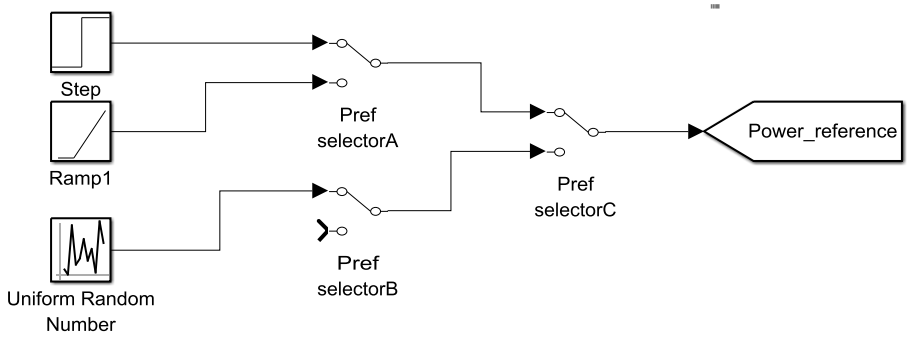

Figure 3-17. Power reference modelling for controller testing.

3.6.6 Suggested controller improvements:

- A delay block to account for the settling of battery chemistry dynamics when the power reference changes sign within a single discretisation. As described before, the third stage is a pair of parallel chopper switch enable/disable switches. This stage is designed to prevent simultaneous operation of the two IGBT switches, which would result in a short circuit of the dc link voltage. Practical switches have longer off times than on times (Czarkowski 2011), for example, 400 ns v 180 ns for the Littelfuse model described earlier (Littelfuse 2016). This overlap means that if on and off gate signals are simultaneously delivered to opposite switches, the on-switch would arrive at full current at 180 ns, prior to the start of the fall time of the other switch, which starts at 340 ns after arrival of the pulse in the Littelfuse model, for example. To eliminate this occurrence, a blanking time is required (Czarkowski 2011). For this model, a blanking time of at least 400 ns plus a safety factor would be required to ensure the first switch returns to zero current prior to activation of the other switch. However, the Simulink model design assumes perfect switches with no on/off time, so no blanking time has been considered in the model. This could be implemented by a comparator that compared a previously sampled power reference to the presently sampled power reference; if their signs are different, then the blanking time delay must be applied to the switches. The application of a dynamic saturation block and/or protection switch that may help to limit or cut off current flow if currents fall outside of the battery specifications.
- A zero-current reference disconnector control used to disconnect the BESS circuit when the power reference is zero, to prevent parasitic current losses.
- A state of charge limiter that disconnects the BESS circuit when the battery reaches its prescribed lower or upper limit of state of charge.

3.7 Economic modelling

3.7.1 Time modelling

The model was designed to analyse a given system's configuration net present cost (NPC) over a 25-year time frame.

3.7.2 Meteorological modelling

The project required meteorological data on wind speed, solar insolation, and temperature (Mahesh & Sandhu 2015), as well as pressure. Such data might assist in hybrid BESS systems that employ a predictive control technique, for example in (Di Giorgio & Liberati 2014; Dieulot *et al.* 2015; Mégel *et al.* 2015; Wang *et al.* 2015), or in a MILP approach (Khalilpour & Vassallo 2016). Climate data for the aforementioned parameters was acquired from the Australian Bureau of Meteorology for the Nambour monitoring station for a fee (Australian Bureau of Meteorology 2016).

3.7.3 Solar insolation modelling

Solar insolation data was necessary to estimate of the timing and magnitude of PV output. Analysis of Nambour's solar insolation data suggests that solar insolation does not conform to a normal distribution. Because the system design specification meant that solar insolation provided a significant quantity of the system's energy over the model lifetime, a statistical model of the insolation was required to design a realistic scenario.

After consideration of the literature (see section 2.10), there appears to be a lack of consensus on choice of statistical technique, as well as evidence that season, month, climate, and geospatial position, will influence the choice of best model. Indeed, selection and construction of the best insolation model appeared to have enough potential scope to be a dissertation in and of itself. It was arbitrarily decided to choose a simple daily mean model, rather than to determine the best model from the literature. The modelling software, HOMER, also uses a default insolation model that is attributable to monthly means. This method is a "typical model year" (TMY), which is an inferior, but less time-consuming method than the determination of a statistical distribution (Caliao & Zahedi 2000).

Although the HOMER application can provide default insolation values, they are based on 1983-2005 values, at a geo-spatial resolution of one degree of latitude by one degree of longitude, or more than 175 km by 175 km. In the Nambour region of the Sunshine Coast and Brisbane, there is considerable hourly, seasonal, and long-term meteorological variation, so a more localised model was deemed appropriate for the resulting model. This is discussed in the next section.

3.7.4 Solar energy resource model

The solar resource model was constructed from the Australian BOM Climate Data Online site for daily solar exposure at the Nambour Daff – Hillside site. (Meteorology 2016). A daily average insolation was constructed from 2004-2016 data, and converted to a monthly average. It is possible for an hourly data model to be input to HOMER, but hourly data resolution is not available from the BOM for the Nambour site.

The HOMER application utilizes a method known as the Graham algorithm to develop "a data sequence that has realistic day-to-day and hour-to-hour variability and autocorrelation" based on the monthly averages provided (HOMER 2015).

The BOM data was selected for the simulation and is summarised in Figure 3-18. For comparison, the HOMER data based on the NASA surface meteorology and solar energy database from 1983-2005 at a spatial resolution of 1 degree latitude by 1 degree longitude, is also provided in Appendix F:. Note that clearness indices are also provided and are required for the HOMER model. The clearness index figures are based on the HOMER acquired NASA data for the years 1983-2005, and are unlikely to be exactly representative of the 2004-2016 figures, which cannot be easily derived from the BOM data .

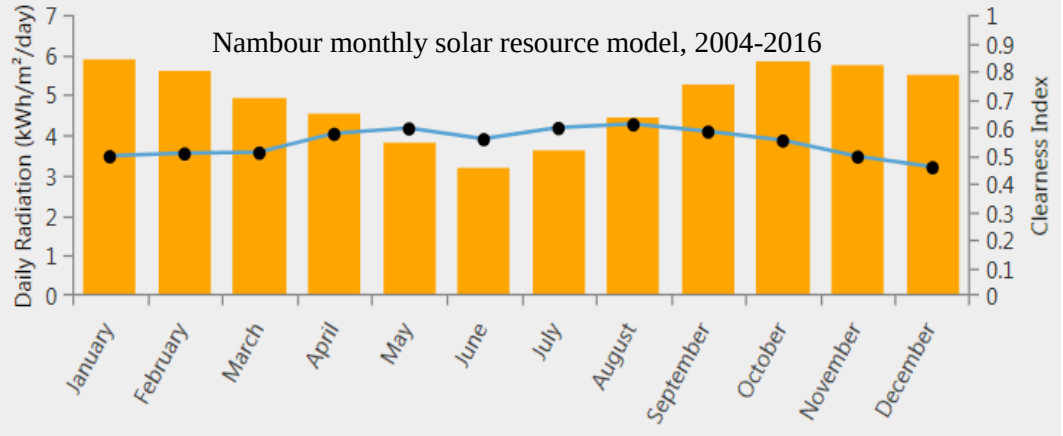

Figure 3-18. Nambour average monthly solar resource (2004-2016), adapted from the Australian Bureau of Meteorology (2016a).

3.7.5 Wind modelling

To properly model the economic influence of the wind turbine, it was necessary to create a local wind profile for the Nambour area. This was done with data purchased from the BOM (Australian Bureau of Meteorology 2016b). This covered the period of January 2008 – April 2016. The model was constructed as an hourly (8760 point) annual time series. Each hourly point was derived as an average from the historical BOM data. Blank data was excluded from the calculation of each point's average. February 29 data from 2008, 2012, and 2016 was excluded. The annual profile was created with the assistance of simple filtering and pivot table tools available in MS Excel.

To facilitate the inclusion of the model in HOMER, the data was converted to a single column vector in a text file and imported into HOMER, which interprets the data as a yearly time series of evenly-spaced intervals, of interval length 1/n years where n is the vector length, in this case, 8760. A summary of the wind profile is seen in Figure 3-19. The average hourly wind speed over one year is included with the DVD appended to the dissertation as the dataset is too large to accommodate in an Appendix.

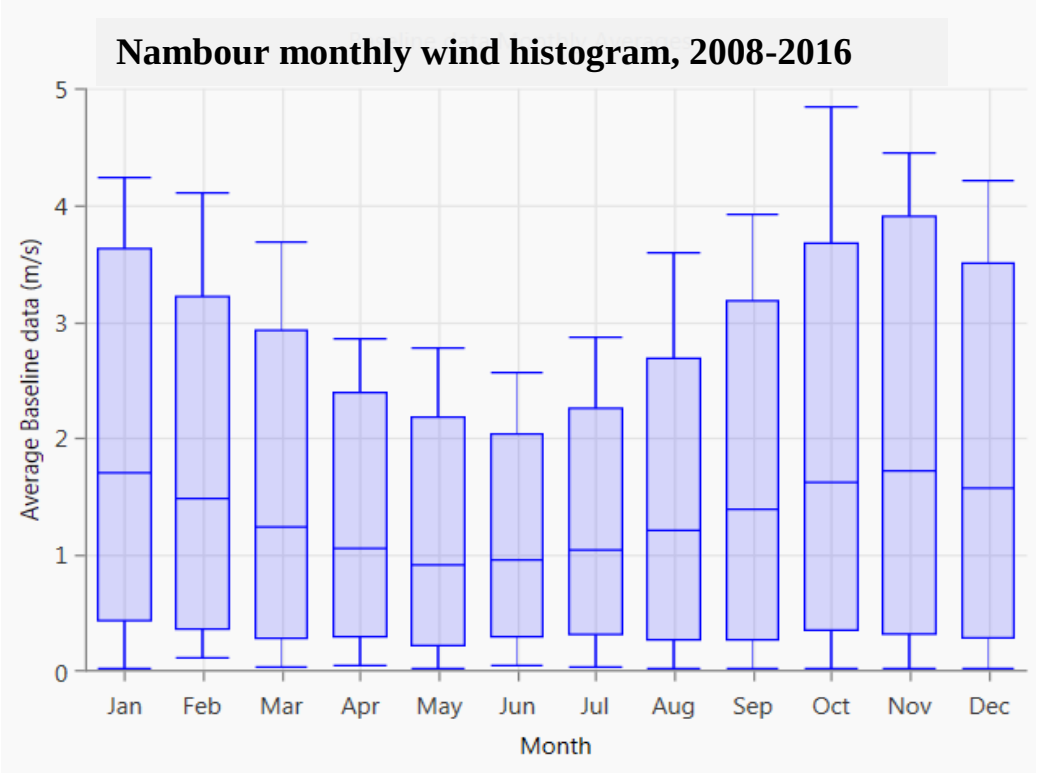

Figure 3-19. Nambour monthly wind histogram, 2008-2016.

3.7.6 Temperature resource model

Several aspects of the model are influenced by ambient temperature. These include the PV array output, effective battery capacity, wind power, and effective battery life. An hourly annual model was constructed from the 9-year recent Australian BOM data for Nambour. Data for each hour of the year was extracted from the data set by using a pivot table and filtering in Microsoft Excel. The temperature for each hour of the year over the 9 years was averaged to create an "average temperature year". The temperature profile can be seen in Figure 3-20. The average hourly temperature over one year is included with the DVD appended to the dissertation as the dataset is too large to accommodate in an Appendix.

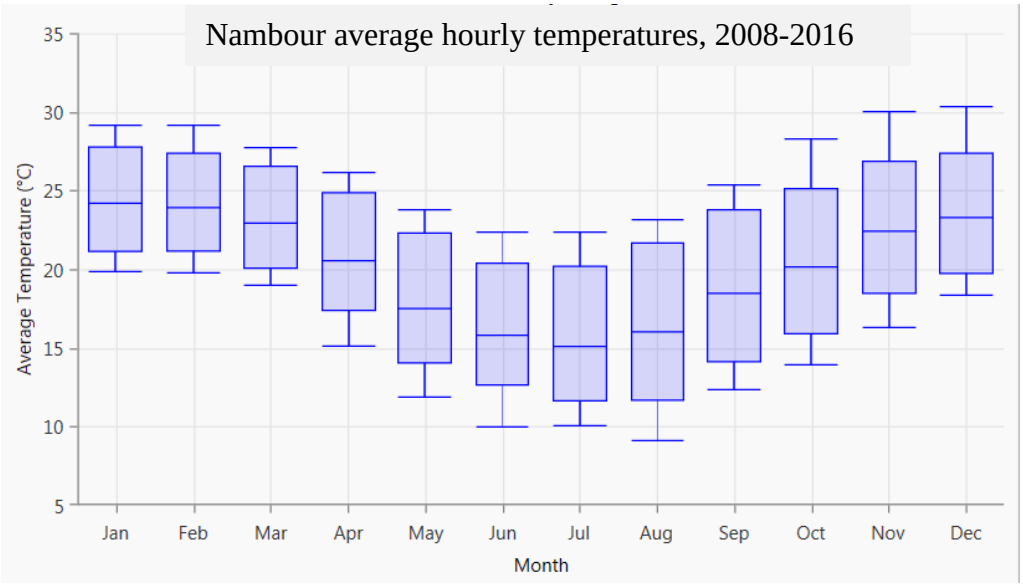

Figure 3-20. Nambour hourly temperature profile, by month (2008-2016)

3.7.7 Load modelling

Proper evaluation of daily and seasonal residential load profiles was important because it had a high impact on the economic evaluation of the project, as well as an influence on optimal ESS sizing. The load model required a broad set of assumptions. Household load is affected by individual residents' tolerances for temperature comfort, local thermal effects due to housing aspect, proximity to wind cooling, housing insulation, residents' lifestyle, household size, types of appliances, thermostat settings, use of gas appliances,

seasonal and weekly patterns, and more. 'Typical' energy savings that might result from the application of a particular loading strategy are not typical at all, and vary widely depending on a number of factors (Zheng *et al.* 2014). An Energex-commissioned study by the CSIRO for Energex (Berry *et al.* 2015) provided some insight into the caution that should be applied in the development of 'typical' load profiles. Although it is possible to develop an *average* load profile, Berry et al. (2015) observed that load profiles could not be attributed to household demographics, including household income, household members, and dwelling type, and ownership. The reality is that significant variability can be found among these individual characteristics. It is beyond the scope of this project to develop an ideal profile, or even to test multiple load profiles for the same technological and meteorological context. This is suggested as future work.

Time and device resolution of the load modelling could also be performed and evaluated. Smaller time increments offer more realistic simulations but increases computational overhead. Similarly, profiles can be constructed at the switchboard or at the appliance level (Zheng *et al.* 2014; Di Giorgio & Liberati 2014). Development of appliance level profiles is considered to be outside the scope of this project but is an avenue for future work.

A "typical" annual load profile can be constructed from energy bills, online load data, or from publicly available Energex data. Zheng *et al.* (2014) make reference to Pecan Street (Pecan Street 2015), which provides free energy data to university researchers on registration. HOMER provides a series of basic load profiles and provides the facility for input of custom load profiles. Ultimately, it was decided to develop the load profile from two sets of Energex data as described below. These data allowed for the modelling of:

- the load to incorporate monthly bulk energy consumption,
- daily variations in seasonal consumption that could be attributed to climate control, water temperature, and other requirements, and
- weekday vs. weekend consumption patterns.

The first set of data was derived from publicly available consumption data by month, by post code. It was decided to model a load for a detached residential home, of size 3 to 4 people, from the Nambour or adjacent areas. Nambour experiences relatively warm winters, combined with relatively hot, humid summers. Examination of Nambour energy data from 2009-2014 suggests that residential energy consumption is highest in the winter (Energex 2016). Exploration of the reasons for this are beyond the scope of this project,

but may include additional hot water requirements, climate control requirements, and food and drink consumption patterns.

To simplify the load model, it was assumed that the residence utilized electric hot water but does not subscribe to an economy rate. This may seem to be a questionable assumption; however, if one considers that the system design is to include solar PV, then the economic rationale for this simplification is sound. Hot water heated on a super economy rate (Tariff 31) is about 0.1244 $/kWh. However, the energy export rate to the grid is typically 0.06 $/kWh. Therefore it makes economic sense, even on the super economy tariff, for any excess energy produced locally (mostly PV) to be delivered to the hot water system rather than to the grid for export, provided that the desired water temperature has not been reached. Therefore, the simplification of the load model is based on the assumption that a significant proportion of, if not most hot water heating will occur during times of excess solar PV power generation. Such an assumption negates the requirement for application of a super-economy tariff. The control of such hot water heating could be accomplished by measures as simple as a timer.

The specific allocation of the load to hot water heating is not considered in the model, rather, it is considered as part of the aggregate load. The optimisation and control of hot water thermostats for excess PV to delivery to the hot water system is suggested as an avenue for future research.

The Energex (2016) data was consulted to design a baseline profile of monthly residential energy consumption over time by Nambour residential connection. Nambour is a town with a significant proportion of units and townhouses, i.e. non-detached residential dwellings, but the project concerns itself with a detached dwelling because of the requirement to erect a wind turbine and PV panels. It was decided to utilise consumption data from Woombye, a town adjacent to Nambour on the southern border that has a much larger proportion of large-block, single-family detached dwellings. Figure 3-21 summarises the values of monthly consumption between 2009-2014 for Nambour and Woombye based on the Energex data (Energex 2016). Note that these values do not consider the possible impact of solar PV, and only reflect net consumption at the meter.

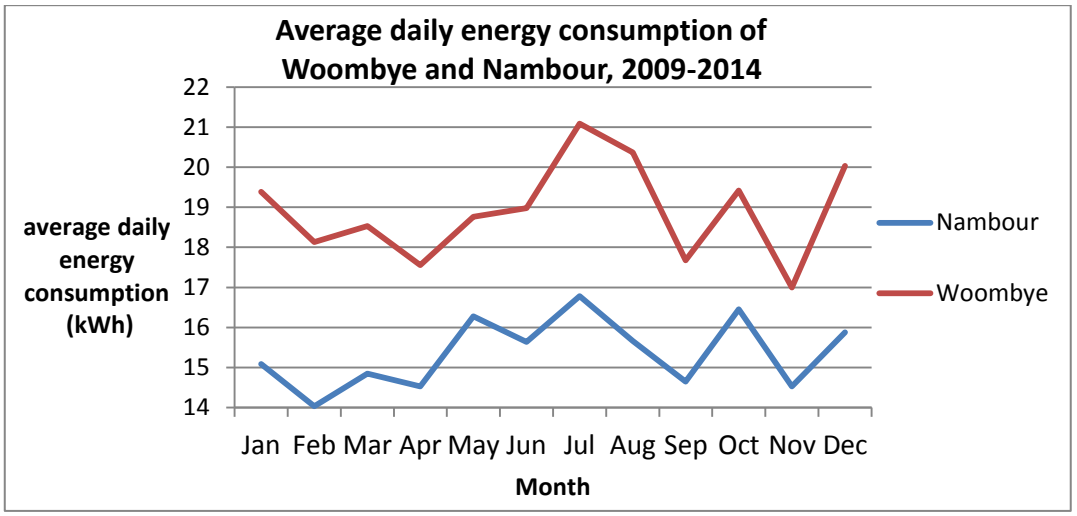

Figure 3-21. Comparison of Nambour and Woombye average daily energy consumption

It could be argued that an additional seasonal factor should be added to these figures to account for self-consumption of energy ascribed to PV, noting that the ratio of solar export to residential consumption has markedly climbed since 2009 (see Figure 3-1). However, no such factor was incorporated in the current work and is left to future research.

The second input to the load model was to derive a reflection of the typical patterns of seasonal energy consumption. This input was derived from a CSIRO report commissioned by Energex (Berry *et al.* 2015). First, each monthly consumption datum derived from the 2009-2014 Energex data was synthesised into an hourly use pattern for the month that aimed to reflect typical usage suggested by the CSIRO data (Berry *et al.* 2015), that is, higher consumption from 6:00 a.m. to 8:00 a.m., an evening peak from 4 p.m. to 9 p.m., and little consumption overnight. This assumed that hot water demand was mostly satisfied during the 6:00 a.m. to 10:00 p.m. period, requiring only maintenance charging overnight. Seasonal variation was also input to the load data, including lower overnight values in the summer (less energy to heat hot water), higher peak evening values in the summer and winter, and higher peak winter morning values as a proportion of daily load, reflecting additional heating and cooling requirements in these months.

The third input to the load model was variation between weekdays and weekends variation. Weekend variation was accounted for by examining the median values in Figure 3-21 (Berry et al. 2015). As an aggregate, weekend loads typically have later (by

about 1.5 hours) and flatter (by about 10%) a.m. peaks, similar p.m. peaks, higher mid-day loads (10-30% greater between 8 a.m. to 4 p.m.), and a longer taper into the late evening, when compared to weekdays (Berry et al. 2015).

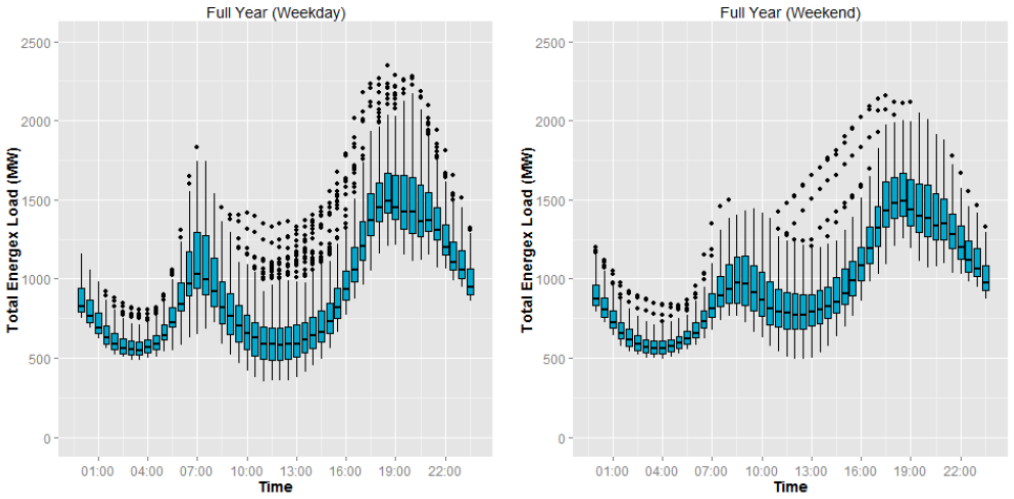

Figure 3-22. Energex weekday v weekend load comparison, 05/2012 - 04/2013 (CSIRO 2015).

From Figure 3-22, based on the CSIRO report, a set of Energex-wide weekday and weekend demand tables were derived. This tabular derivation is found in Appendix G.1.

The hourly values are very different at times, with different peak times and magnitudes. The key value from this derivation (Appendix G.1) is the fact that total weekend demand, or energy use, E_{we}, is on average 6.9% greater than weekday energy use, E_{wd}:

$$E_{we} = 1.069 * E_{wd} \qquad [\ 3.41]$$

The average daily consumption, E_{avg}, for any given month irrespective of the day of the week (as derived above and summarised in Figure 3-21) was then modelled as:

$$E_{avg} = \frac{5 * E_{wd} + 2 * E_{we}}{7} \qquad [\ 3.42]$$

Substitution of [3.41] in [3.42] obtained the following:

$$E_{avg} = \frac{[5 * E_{wd} + 2 * (1.069 * E_{wd})]}{7} \qquad [\ 3.43]$$

$$E_{avg} = \frac{7.138 E_{wd}}{7}$$

The weekday consumption could then be modelled in terms of the average monthly values derived earlier:

$$E_{wd} = \frac{7}{7.138} * E_{avg} \quad [\ 3.44]$$

$$E_{wd} = 0.981 * E_{avg} \quad [\ 3.45]$$

Weekend values were then modelled by substituting [3.41] in a rearranged [3.45]:

$$E_{we} = 1.069 * \frac{7}{7.138} * E_{avg} \quad [\ 3.46]$$

$$E_{we} = 1.0483 * E_{avg} \quad [\ 3.47]$$

Based on this scaling method, the values were obtained as displayed in Table 3.9.

Table 3.9. Energy consumption scaled for weekdays vs. weekends

Month	average (kWh)	weekday (kWh)	weekend (kWh)
Jan	19.39	19.02	20.33
Feb	18.13	17.78	19.00
Mar	18.53	18.17	19.42
Apr	17.56	17.23	18.41
May	18.76	18.40	19.67
Jun	18.98	18.61	19.90
Jul	21.09	20.68	22.11
Aug	20.37	19.98	21.36
Sep	17.68	17.34	18.53
Oct	19.42	19.04	20.36
Nov	17.00	16.67	17.82
Dec	20.03	19.64	21.00

A weekday and weekend half-hourly load profile, expressed as a percentage of total daily consumption, was constructed from these figures, as well as the half-hourly median use

figures derived from the CSIRO graphs. This was then modified to account for a significant proportion of the overnight load to be transferred to the daytime load, i.e. water heating. The model assumed that half of the load between midnight and 5:30 a.m. on weekdays, half of the load between midnight and 6:30 a.m. on weekends, and 25% of the load between 11:00 p.m. and midnight would be shifted to the daytime load. It was assumed that the use of simple switching would enable daytime water heating, increasing load by 25% from 8:30 a.m. to 9:30 a.m., and by 50% between 9:30 a.m. and 2:30 p.m., and by 25% from 2:30 p.m. to 4:00 p.m. to correspond to the plan to source water heating power from the system's solar PV generation. Performing this scaling resulted in total consumption very nearly equal to that without scaling (within 0.3%). Finally, the half-hourly load profiles were converted to an hourly profile to plan for the HOMER model requirements.

From the weekday and weekend hourly percentage profiles, 12 weekday and 12 weekend profiles were generated, one for each month. The hourly energy consumption profiles by month are provided in Appendix G.2 and Appendix G.3 for the weekday and weekend variations, respectively.

These 24 profiles, combined with the original monthly energy consumption data for Woombye (Figure 3-21) were combined to develop an hourly (8760 point) load profile for one year. For modelling purposes, HOMER treats each year as if January 1st falls on a Sunday.

A degree of randomness was introduced into the profile by using the RANDBETWEEN function in MS Excel, allowing any hourly value to fall between +/- 30% of the modelled value. This step required a few iterations until the 8760 randomized hourly figures for the year summed to be within 0.2% of the original non-randomised yearly load based on the Woombye monthly consumption data. The results of this procedure are summarised graphically in Figure 3-23 and Figure 3-24.

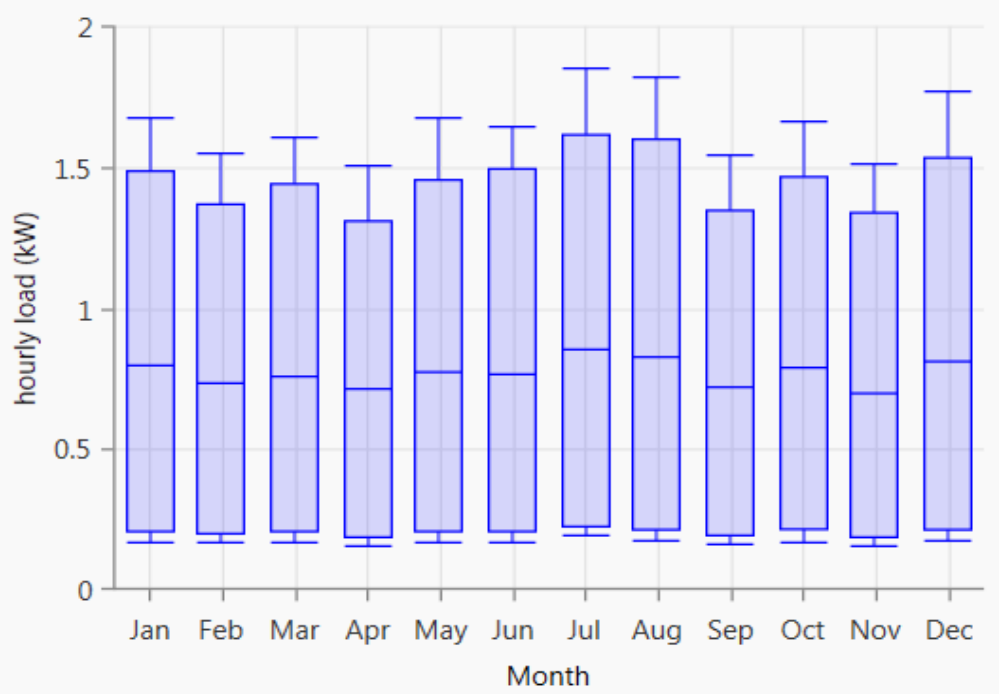

Figure 3-23. Distribution of hourly loads by month.

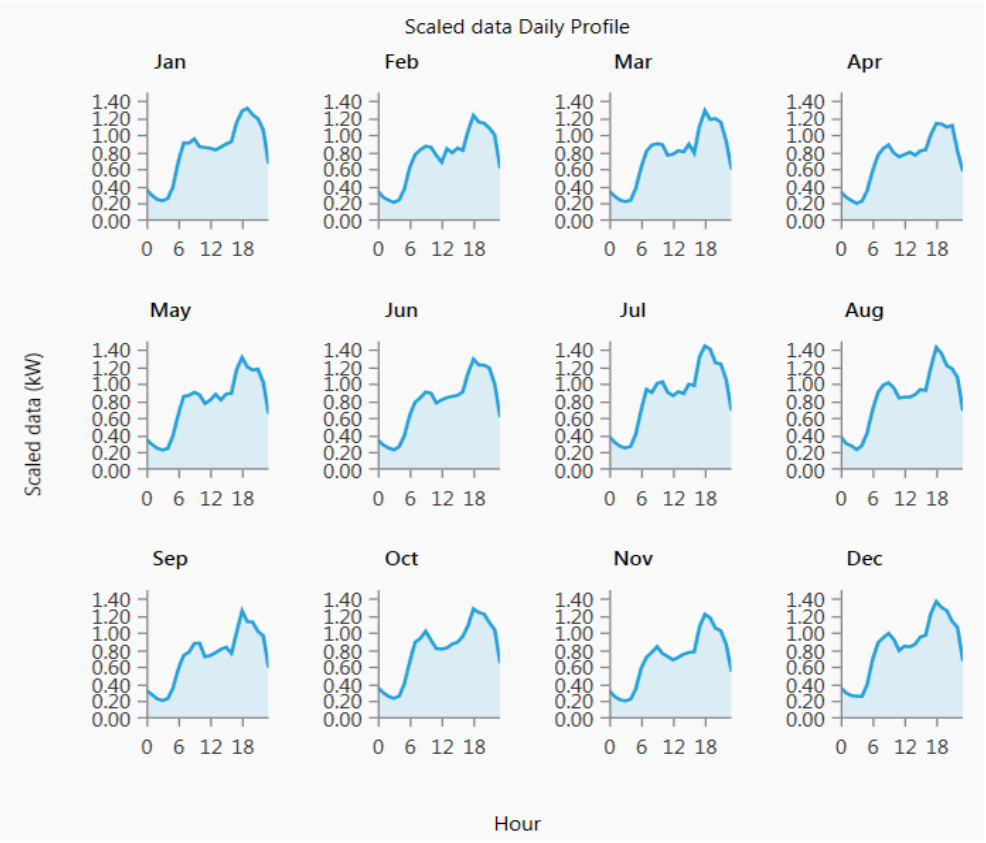

Figure 3-24. Monthly load profile (weekend vs. weekday variation not shown)

3.7.8 Tariff modelling

Residential tariffs present in the SEQ context include the conventional bulk supply tariff 11, economy (tariff 33), super economy (tariff 31), and TOU tariff 12. Demand charges, reactive power, and frequency support exist as tariffs in other jurisdictions, but do not exist in the Queensland residential context and were not explored.

Economic control of the grid-tied system meant that tariffs had a significant influence on many aspects of the system design, as described in Jargstorf *et al.* (2015) and Mulder *et al.* (2013), and therefore the tariffs needed to be modelled accurately. These aspects included the control algorithm design (Di Giorgio & Liberati 2014), and BESS sizing optimisation (Zheng *et al.* 2014).

Solar PV FiTs exist in Queensland, but differ depending on when the solar PV system was installed. The dissertation will examine the FIT influence on system design and simulation, but will only model the tariff that is available to new installations. A more generous FIT was available to new customers until 2013. An MPC model that accounts for feed-in tariffs was found in Mégel *et al.* (2015) and to some extent in Dieulot *et al.* (2015). In any case, HOMER had the capacity to vary tariffs from the grid with respect to time, and can model the economic impact of feed-in tariffs.

Tariff 12 was introduced recently to provide incentive to users to shift their energy use away from the peak demand times of the evening peak from 4 to 8 p.m. BESSs are certainly capable of performing this task, by providing an additional energy source to supply the load at these times. For this reason, Tariff 12 was selected as the modelling choice. Table 3.10 provides tariff and supply charges for a variety of retailers; prices are inclusive of GST. This information is based on figures available from the Australian Energy Regulator in July of 2016 (Australian Energy Regulator 2016b).

Table 3.10. Tariffs and supply charges for time of use (TOU) tariff 12.

Tariff (c/kWh unless noted)	AGL	Dodo 1	Energy Australia	Dodo 2	Urth 10	Sanctuary
12 - Peak	35.871	34.54	35.20	32.8295	40.81	32.8295
12 - Off Peak	21.065	18.865	17.897	17.8882	20.24	17.8882
12 - Shoulder	25.85	24.53	24.53	23.2375	28.27	23.2375
P-OP gap	14.221	15.675	17.303	14.9413	20.57	14.9413
12 - Supply charge (c/day)	115.236	129.80	128.70	131.225	128.15	128.04
Feed in tariff	6	4	6	4	10	0

Table 3.11 provides the time frames for the application of each of the three TOU tariffs. Green sections display the off-peak tariff. Yellow sections denote the shoulder tariff. Red sections specify the peak tariff times.

Table 3.11. TOU tariff timetable.

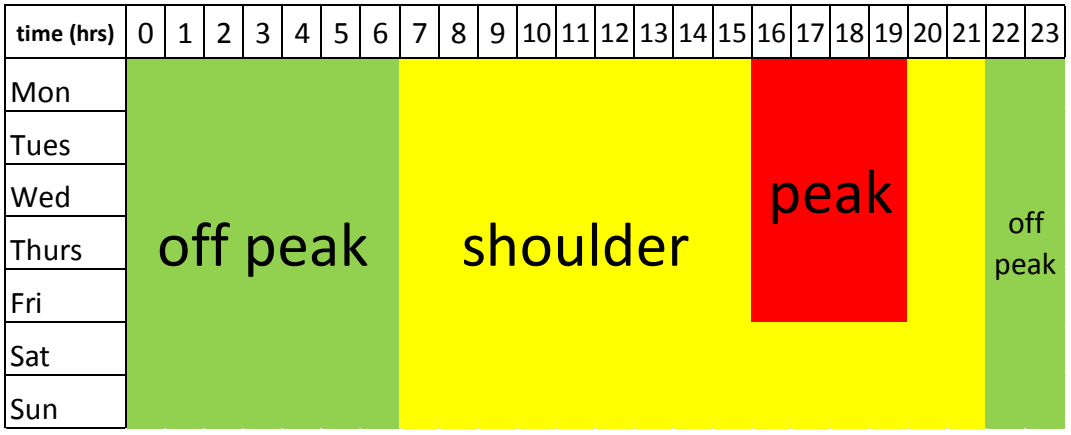

It is beyond the scope of the project to work with a controlled load on an economy or super-economy tariff, but this is suggested as further possible work. It is also beyond the scope of the project to work with the now discontinued Queensland FiT of 44c/kWh, but again, is suggested as further possible work, because a significant proportion of

Queensland residences can still access the tariff until 2028. Preliminary analysis with HOMER suggested that BESSs are not currently economically feasible when installed in a residence that benefits from the 44c/kWh tariff, but this will not be explored further.

The tariff model was developed according to a TOU structure employed by a large retailer (AGL 2016). The tariff's three divisions are off-peak (OP) rate of 0.21065$/kWh, shoulder (S) rate of 0.2585 $/kWh, and peak (P) rate of 0.35871 $/kWh; all prices are inclusive of GST. Additional factors include 1.15236$/day supply charge. This is factored into HOMER as an annual "standby charge". This amounts to $420.61 per annum (p.a.).

A feed-in tariff of 0.06 $/kWh applies at all times of the day. A 13% online account / pay-on-time discount package offered by the company does not apply to solar customers.

It is the experience of the author that scheduled interruptions to service occur from time to time, on average about once per year for about four hours. This normally occurs on a weekday and it will be assumed to occur in the month of April. HOMER only simulates monthly normal outages; four weekly outages of one hour in April at 1300 hrs are used to approximate scheduled interruption frequency. Random failures are rare but do occur from time-to-time. Notably, ex-cyclone Oswald resulted in loss of power for more than two days in 2013. This was simulated as a random event lasting 36 hours +/- 50% once every four years on average. HOMER cannot institute pseudo-randomness, i.e. a cyclonic event is not expected in July, although a winter-time East Coast low could provide the impetus for such an outage.

3.7.9 Economic framework model

Inflation

The Australian Consumer Price Index (CPI) has varied between 1.0 and 5.0% for all categories since 2008 (Australian Bureau of Statistics 2016a). It stands at the 1.0% as at June 2016, which is, historically, very low (Australian Bureau of Statistics 2016b). The simulation covers 25 years, so a range of inflation values between 2.0% and 5.5%, in 0.5% increments, were run for the various scenarios.

Fixed capital costs

Fixed costs were assumed to be $1250 for system design. Other fixed capital costs such as installation and wiring are included in the fixed cost of individual components, as described below in sections 3.7.10 to 3.7.14.

Fixed annual costs

Annual costs are assumed to be $55 p.a. for the extra value of a home and contents insurance premium, based on the author's own insurance affairs, but this would vary depending on insurance retailer and resident's insurance history. Other fixed annual costs, including operating and maintenance expenses are described per component in sections 3.7.10 to 3.7.14. Access charges associated with the grid are included in the grid model as per section 3.7.8.

Nominal discount rate

At an absolute minimum, for a zero-risk investment, the nominal discount rate should reflect the time value of money, commonly interpreted as the government bond rate for a time-length similar to the time length of a project (The New Zealand Treasury 2002). This project is modelled over a 25 year time-frame; the government bond with the closest time-length is an Australian Government 23 year bond. This bond has a coupon rate of 3.25% with estimated yield of 2.57% (Australian Stock Exchange 2016).

It is proposed that the system as modelled is a below average risk investment – it is assumed that the resident will need electricity for a variety of domestic requirements over the next 25 years, regardless of the origin of that electricity. Therefore, it is reasonable to assume that the investment will always be paying a dividend of some value directly to the resident. It is also reasonable to assume that the greatest debt carried by the project is at its inception. Once commissioned, it begins to pay itself back.

Risks to the project include wind and solar resources below those forecast by the model, loss to force majeure, loss to environmental event covered by insurance (which covers assets but not dividends derived from daily operation), early system component failure not covered by product warranties, and the risk that rate of return on the project is lower than a possible investment somewhere else, for example, in stocks.

In light of the above factors, a discount rate of between 3% and 6.5%, in 0.5% increments, was selected for sensitivity analysis in the modelling.

3.7.10 Solar PV hardware economic model

The panels used in this simulation are the Trina Honey panels of 255 W. After some research, it was found that panels could be obtained from an online distributor via Alibaba.com for $0.45/W provided that at least 10 kW of panels are purchased (Alibaba.com 2016). Shipping costs for a 1.5 t pallet from a Shanghai warehouse to

Queensland address was estimated at $1000 inclusive of GST, customs, currency conversion, terminal fees and local transport (Australian Trade and Shipping 2016)., leading to a total panel price of $5500. To estimate installation costs, several solar PV package installers were consulted. The ecoelectric Web site was able to provide the best breakdown of figures attributed to installation costs (ecoelectric 2016). Analysis of a typical package suggests that installation costs are approximately $1700, which includes inverter and grid connection installation, plus $60 per panel for wiring, connectors, and mounting on a rail and tilt kit, of approximately $1200.

A Chiko brand rail and tilt kit for 40 panels can be acquired from the Integra Energy Group via ebay.com for approximately $1400 (Integra Energy Group Pty Limited 2016). The total price of the panels, including panels, mounting kit, shipping, connection, and installation is therefore estimated at a total cost of $9800 installed or deferring $400 of installation costs to the inverter to $9400. This does not include any deductions that may have been realised as part of the small scale renewable energy scheme (SRES), which will not be considered in the costings.

In the HOMER model, additional parameters that were applied included ambient temperature derating coefficient, output power efficiency de-rating, efficiency at standard test conditions (STC), nominal cell operating temperature, and explicitly modelled MPPT (as provided by the inverter). These figures were derived from the Trina Honey technical data sheet (see Appendix E.4). Panel tilt of 26.6 degrees as per Nambour latitude was assumed in the HOMER model, as was a fixed north azimuth. Future research may consider additional trials of a westerly azimuth to see if a PV production shortfall in the early a.m. is off-set by benefits realised by higher thermal efficiencies and peak period tariffs in the weekday peak period time. Operating and maintenance expenses are estimated to be $20 p.a. for cleaning and inspection. Life expectancy was modelled as 25 years, with a derating to 80% efficiency at 25 years.

3.7.11 Wind turbine economic model

As suggested in the wind resource model, Nambour has marginal wind resources. Preliminary modelling of the project suggested that because of the marginal wind resources, a wind turbine would be marginally economically justifiable at best. To improve economics, it was a goal to try to obtain a wind turbine for a reasonable price. However, to provide a reasonable estimation of power output, it was also necessary to acquire that wind turbine's power curve. The power curve describes the output power

delivery for a set of given wind speeds; it is typically a non-linear curve. Another factor considered was that the HOMER software platform only handles iterations of 1 kW, so it was decided to avoid turbines in the 0.5 to 0.999 kW range (as possibly specified by the design brief).

The initial search included a search engine survey of Australian suppliers; ebay; Alibaba.com; and some USA and UK suppliers. Two interesting trends were noticed during this search. First of all, cut-in, cut-out, and rated wind speeds were normally provided, but it was uncommon to see a power curve provided in the specification sheet. Second, the price of turbines seems to be relatively high when compared to solar PV systems; $3000 to $7000 for a turbine alone was a fairly typical price for a machine rated at 1 kW.

AliExpress, an Alibaba.com company, was able to provide more reasonably priced turbines, all sold without a tower. Of the 25 products viewed, only two provided power curves. One of these was selected, a 1 kW turbine, delivered to Australia for about $1650 (Guangzhou HY Energy Technology Limited Corp 2016). When pricing individual wind systems, the turbine, mast, and installation costs must be factored in. A 9 m mast capable of handling a small turbine of this size can be purchased for about $850 (Oz Wind Engineering 2016). Installation was estimated at $400. The total price of the installed wind turbine system used in the HOMER modelling was therefore estimated at $2900. This turbine has a DC output of 48 or 110 V. It will be assumed that the turbine will deliver its rectified DC power to the grid via the single inverter profiled below.

The power curve of the PSHY-1000 can be seen in Figure 3-25. Values derived from the power curve were put into the wind turbine model in HOMER at 1 m/s intervals to obtain an accurate profile. Although the curve is not visible past 18 m/s, speeds of this level are rare (only occurring once during ex-tropical cyclone Oswald in 2013) in Nambour; speeds of 18 to 25 m/s were estimated to decrease linearly by 0.1 kW per m/s, and cut-off at 25 m/s for modelling purposes. Operations and maintenance expenses were estimated at $25 per year for a biennial inspection. Other parameters used in the modelling included a lifetime of 15 years as specified, a hub height of 9 m, and accounting for temperature effects. Efficiency and loss parameters were not specified in the technical specifications; losses were estimated as 0.3% for down-time (about 1 day per annum) and 2% ‘other’.

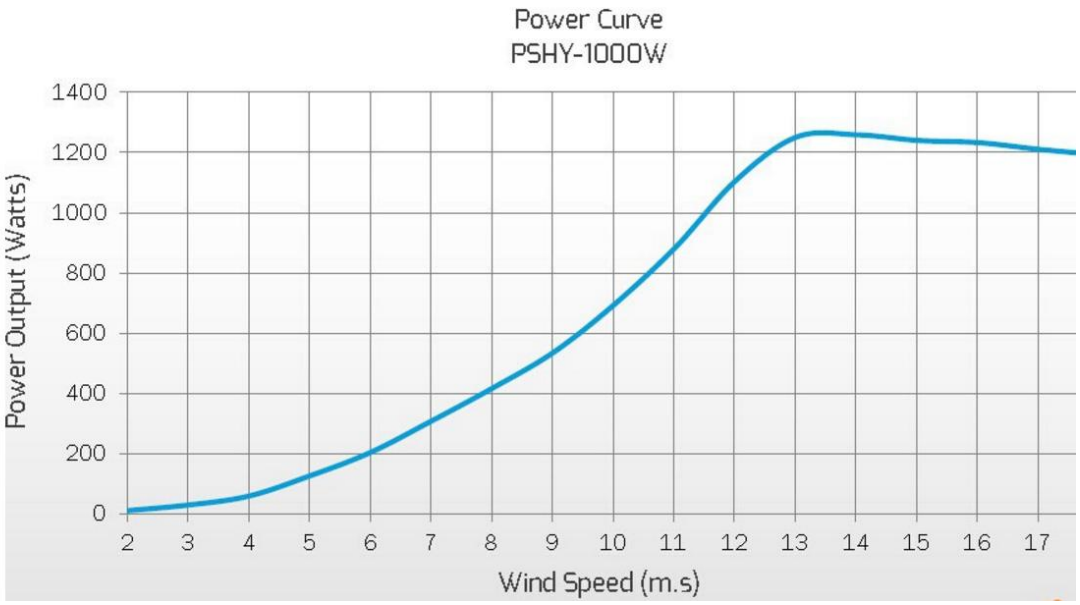

Figure 3-25. Power curve of wind turbine model

3.7.12 BESS hardware economic model

The 6.4 kWh, 5 kW LG Chem RESU lithium-ion battery can be obtained on ebay for $6100 including shipping (Prime Solar Power Systems 2016). Installation was estimated at $400 for the battery including system connection. Since the battery charge controller cannot be entered as a specific component in HOMER, a value of $1500 was added to the BESS cost (see additional notes in section 3.7.13). Operating and maintenance expenses were estimated as $20 p.a.

Since the battery was not available from the HOMER catalogue, a new battery model was created. Parameters entered into the model are summarised in Table 3.12 and based on the product data sheet in Appendix E.1.

Table 3.12. LG Chem battery parameters for HOMER

Parameter	Value
Voltage	51.8 V
Capacity	6.4 kWh
Capacity	126 Ah
Maximum discharge current	110 A
Maximum state of charge (arbitrary)	100%
Minimum state of charge (arbitrary)	15%
Roundtrip efficiency	95%
Lifetime throughput	35 000 kWh
Expected life	3 years

3.7.13 Battery charge controller economic model

HOMER does not have a battery charge controller that can be entered as a separate piece of hardware. To apply the battery controller in HOMER, cost and control considerations must be made separately.

First, the financial cost of the controller needed to be integrated with the cost of the BESS or of the inverter. Although charge controllers have been around for some time for the off-grid market, different requirements are necessary for grid interfacing. Several controllers exist, but it was difficult to find the cost for a separate component. Normally, controllers are included as part of a package. One such controller is the Storedge battery interface. The lowest price that could be inferred for this hardware is $1500. This price will be added to the price of the LG battery in the HOMER optimisation engine.

Second, actual "control" of the battery in HOMER is implemented in the grid tariff regime model. Battery control regimes were introduced in a recent version of HOMER. The level of control that may be applied is straight-forward, and is applied on a "per tariff price" basis. Noting the fact that this project uses a TOU tariff in the modelling, the

following basic controls were employed (further noting that these control regimes are simpler than those proposed for the final power flow controller detailed in section 3.4.17):

- BESS discharging to the grid was prohibited at all times.
- All BESS discharging, to grid and to load, was prohibited during the off-peak period.
- BESS charging by the grid was permitted only during the overnight off-peak period.
- BESS charging by any means was prohibited during the peak period.
- Logical extensions of the first two points meant that BESS discharging only occurred to the load, and only during shoulder and peak periods.
- Logical extensions of the third and fourth points meant that BESS charging by the grid could only occur during the off-peak times. However, charging can occur outside of peak periods by excess wind and PV.

Because of the limitations of HOMER, the charge and discharge schedule followed the TOU tariff schedule. The schedules are summarised in Table 3.13. Note that charging and discharging is subject to other constraints, particularly C, P_{bCmax} and P_{bDmax} as described earlier in Table 3.2 in section 3.4.6.

Table 3.13. BESS discharging and charging schedules.

BESS discharge schedule

time (hrs)	0	1	2	3	4	5	6	7	8	9	10	11	12	13	14	15	16	17	18	19	20	21	22	23
Mon	nil							residence only									residence only						nil	
Tues																								
Wed																								
Thurs																								
Fri																								
Sat																								
Sun																								

BESS charge schedule

time (hrs)	0	1	2	3	4	5	6	7	8	9	10	11	12	13	14	15	16	17	18	19	20	21	22	23
Mon	Grid, wind							solar PV or wind									nil						Grid, wind	
Tues																								
Wed																								
Thurs																								
Fri																								
Sat																								
Sun																								

3.7.14 Inverter economic model

Although the transient model was designed to accommodate a single-phase connection, only three-phase models are available in the capacity required. Further complicating matters was the fact that inverters often are only capable of two DC input strings, each rated to a maximum power that is less than the total inverter power rating. A decision was made to develop the model with an SMA Tripower 17 kW inverter, as it has the capacity to deliver two MC-4 paired DC inputs, both with MPPT. The inverter can be configured to accommodate two MPPT inputs with up to 5 strings on one input and a single string on the other input. This would enable three PV strings on one input and the wind on the other. However, the minimum input voltage is 150 V on each string which means that the 48 V rectified output of the wind turbine would need additional boosting to achieve 150 V, likely by a DC boost inverter, which will cost additional money. Indeed, it is questionable as to why a single inverter would be used in this system design, because

the small size of the wind specification and the large size of the PV specification suggests that the two different production media are optimal at different DC voltages, i.e. the wind at a voltage below 240 V and the solar PV above 240 V. This would suggest a two-string inverter with different conversion topologies on each string, particularly their DC input voltage specification. This further suggests the specialized nature of the co-gen topology specified by the current project. A grid-connected wind rectifier/inverter at the rated project specification can obtained at a lower cost than that for the additional boost converter stage required to bring the wind power to minimum input voltages specified by most grid-tied converters today. If a co-gen inverter is to truly be designed as a single unit, then it is appropriate to suggest at this point that the unit really be designed as two individual, parallel inverters housed in the same box. This then leads to the technical definition of an inverter, i.e., does the design of two inverters in one module qualify as a "co-gen" inverter?

Other rationale for the choice of the SMA inverter was its price. This inverter can be obtained on ebay for the (low) price of $2500 (Supercheapsolaroz2016 2016). Installation of just the inverter is extra and is estimated as $400, approximately a half-day of work for an electrician. As noted in section 3.7.10, a typical PV installation includes inverters and inverter installation, and is included in the total package price. It was estimated that $400 of a typical PV installation should be deferred to the inverter, so the overall cost of the inverter was estimated at $2900. Operating and maintenance expenses were estimated as $50 per annum, which is approximately equivalent to an hour's work for an electrician once every two years.

The inverter lifetime is estimated as 15 years; efficiency as specified is 97.2%. The search space was modified to include proportionally priced inverters of 12 to 18 kW, rather than the 6 to 12 that would cover the wind and solar PV maximum outputs. This is because HOMER does not adjust the inverter size based on the optimally sized wind and PV components; for example, it returned an optimal system that included a 7 kW inverter with 10 kW of panels in one run of the program.

3.8 Methodology summary

A number of economic and technical models required development prior to implementation and analysis. These included:

- Power flow modelling
  - Power flow summary
  - Power flow control

- Context modelling
  - Solar energy resource
  - Wind energy resource
  - Temperature resource
  - Load
  - Grid tariff regime
  - Economic framework

- Transient modelling
  - Solar PV and MPPT
  - Wind turbine
  - BESS
  - Inverter
  - Battery charge controller
  - Load model
  - Solar and wind resources

- Hardware economic modelling
  - Solar PV
  - Wind turbine
  - BESS
  - Inverter
  - Battery charge controller

A summary of the capital and operating expenditures can be found in Appendix I.

Chapter 4: Transient model results and analysis

4.1 Implementation of solar PV and boost converter model

Simulink Sim Power Systems provides a pre-designed solar PV function block. This function block was a primary feature of the final model described in section 3.5.9. Inputs to the solar PV function block include irradiance, in W/m^2, and temperature. The transient design for this project used the irradiance block only.

4.1.1 Response to maximum fixed insolation

The first test was at fixed maximum insolation, with a duty ratio to vary between 0.02 and 0.02948, on a fixed resistive load as specified in sections 3.5.6 to 3.5.9. The results for the PV characteristics and load characteristics are shown in Figure 4-1 and Figure 4-2, respectively.

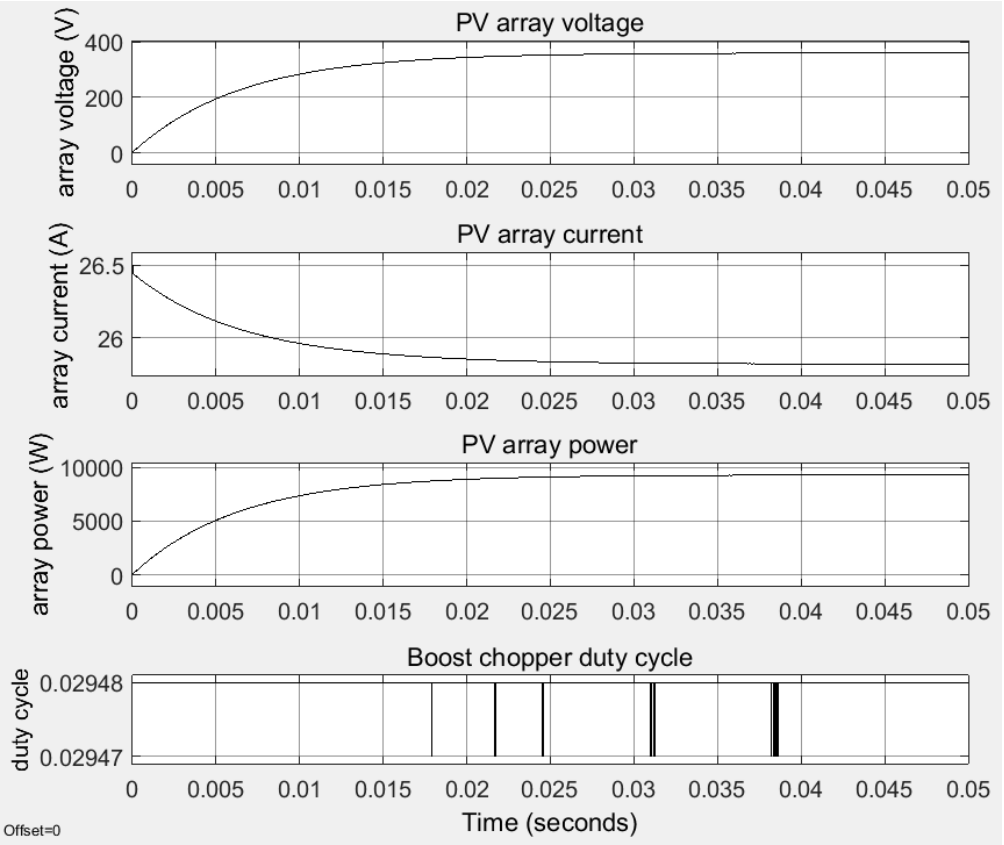

Figure 4-1. PV array output, maximum insolation, 2.948% chopper duty cycle.

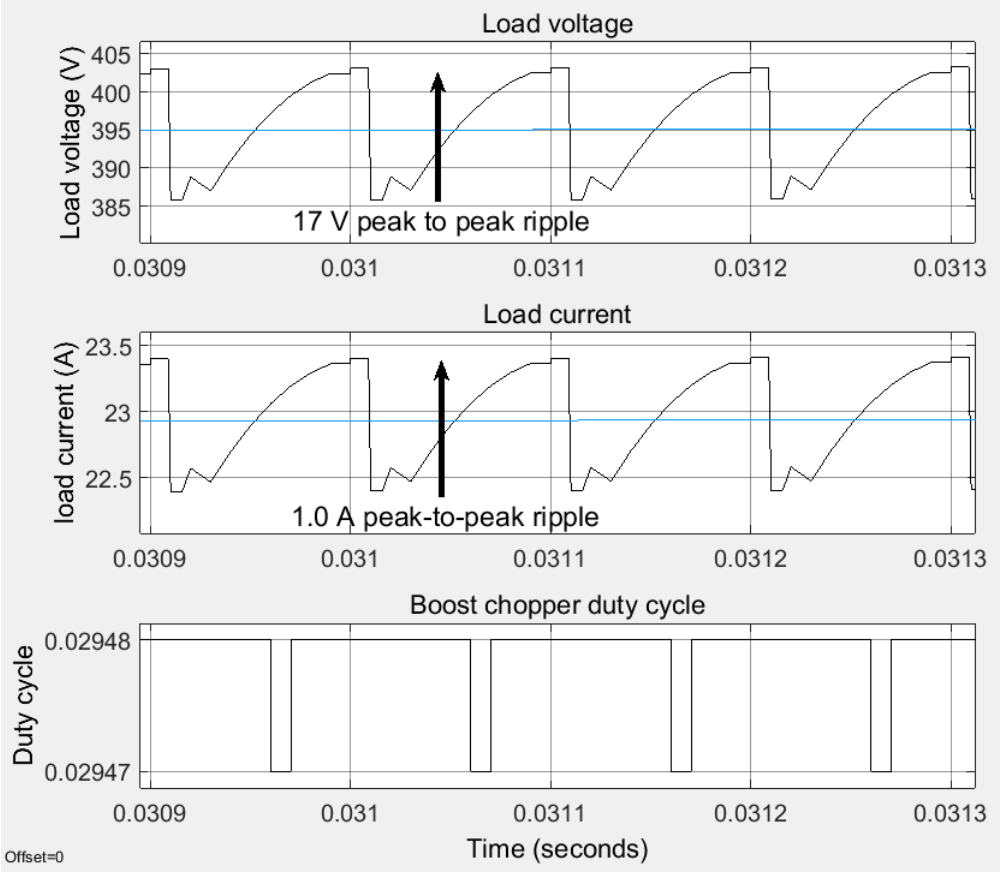

Figure 4-2. Steady state load current and voltage ripple, maximum insolation, 17.2 ohm load.

The load voltage and current ripples, $\%V_{ripple}$ and $\%I_{ripple}$ in Figure 4-2 can be determined as followed:

$$\%V_{ripple} = \frac{V_{ripple}}{V_{rms}} \qquad [4.1]$$

$$\%V_{ripple} = \frac{17\ V}{395\ V} = 4.30\%$$

$$\%I_{ripple} = \frac{I_{ripple}}{I_{rms}} \qquad [4.2]$$

$$\%I_{ripple} = \frac{1\ A}{22.9\ A} = 4.37\%$$

These ripple values demonstrate the possible need for additional or upgraded filtering circuitry for the load, (what was to have been the grid inverter input), but this is deferred to future work.

The other result from Figure 4-2 is that the voltage across the load, about 395 VRMS did not quite reach the designed value of 413.9 V, as per sections 3.5.4 and 3.5.5.

4.1.2 Cloud transients

The second test was conducted to simulate the effect of cloud transients. To simulate a clouding transient of 200 W/m^2/s, two additional tests were conducted at this rate, both for clouding, as seen in Figure 4-3, and for de-clouding, as seen in Figure 4-4. The MPPT block response to the clouding transients, in order to vary the chopper duty cycle, is clearly seen in both cases.

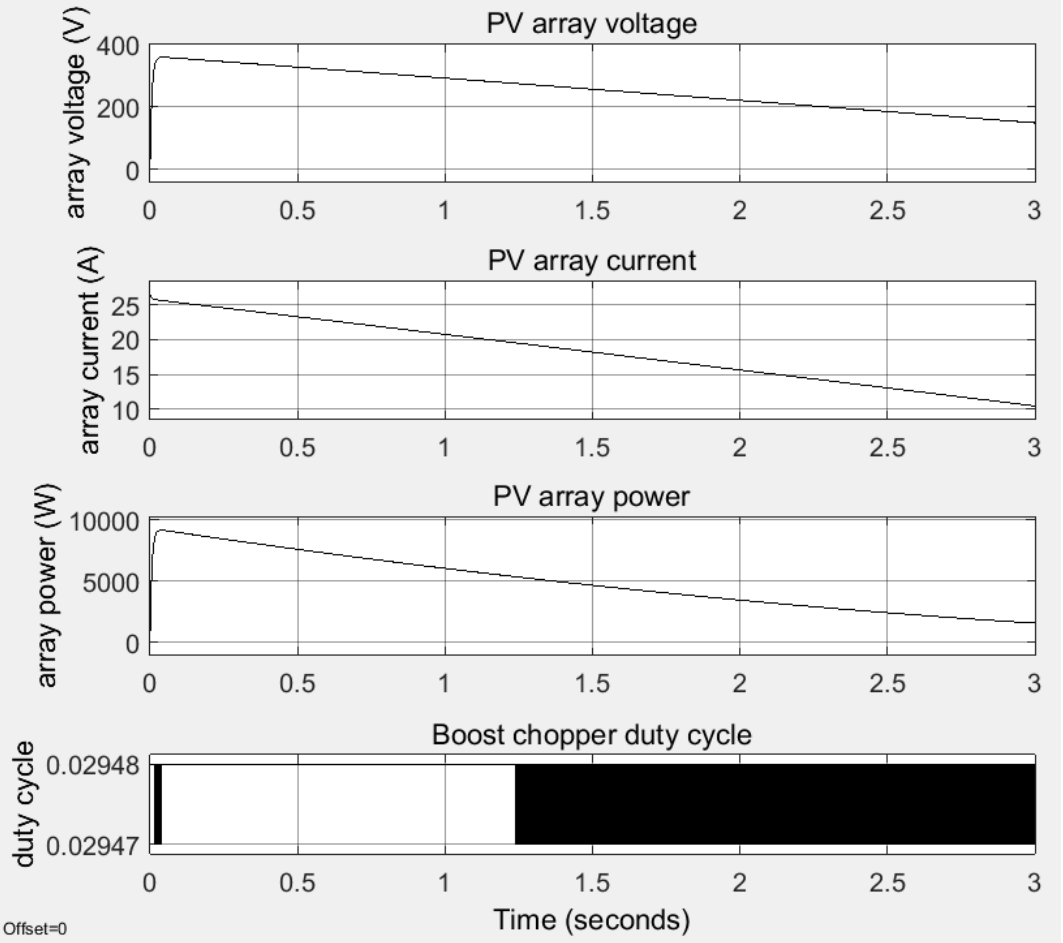

Figure 4-3. PV response to clouding transient of 600 W/m2 in 3 s.

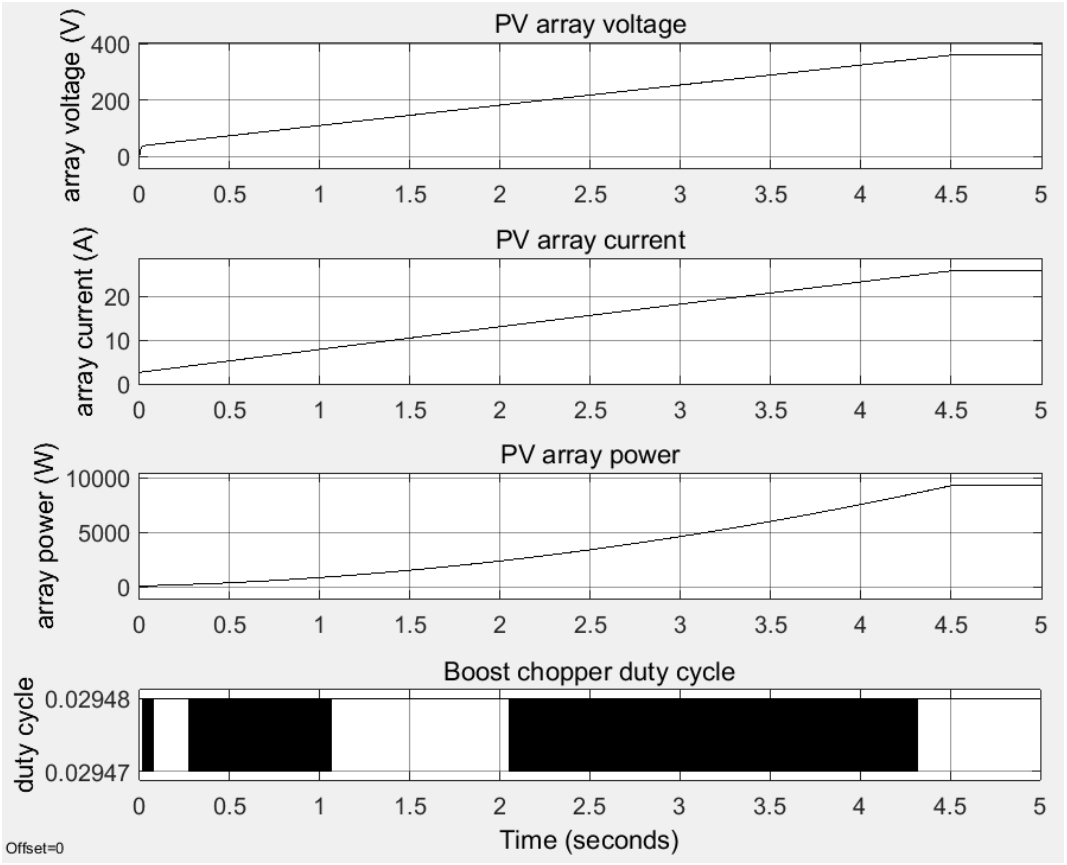

Figure 4-4. PV array response to de-clouding transient of 600 W/m2 in 5 s.

4.2 BESS controller simulation - charging

Unless otherwise noted, the initial SOC for all simulations was 50%.

4.2.1 Charging step response

The first simulation aimed to conduct a simple assessment of the tracking of the controller, using a small step change in power reference, from -50 to -150 W, indicating an increase in current sunk by the battery to charge it. The results are viewed in Figure 4-5, Figure 4-6, and Figure 4-7.

The top plot of Figure 4-5 displays the response of the pulse gate period length to the change in power reference. The second plot displays the 'actual' current sunk by the battery as measured by Simulink. From the graph it can be interpreted that the response time for this -100 W step change is approximately 250 μs. The third plot displays the reference current; the fourth displays the control current reference.

Figure 4-6 is a close-up plot of the transient response. Note that the actual BESS current tracks towards the reference current, despite the control current being slightly less negative than the reference current as the BESS current progresses to steady-state. This is due to the influence of the inductor DC offset designed into the control current parameter that was implemented in the PID controller block to remove some of the impact of the hysteretic effect. This was designed to allow the average BESS current to track the reference current more closely. As noted in subsequent simulations, this DC offset remained constant regardless of power reference, and is reflective of the inductor current ripple.

Figure 4-7 displays the changes in current through and voltage across the charging IGBT switch as it responded to the -100 W step change to the reference power. It can be seen that the IGBT current is positive, that is, flowing from the high potential of the DC link voltage to the lower potential of the battery.

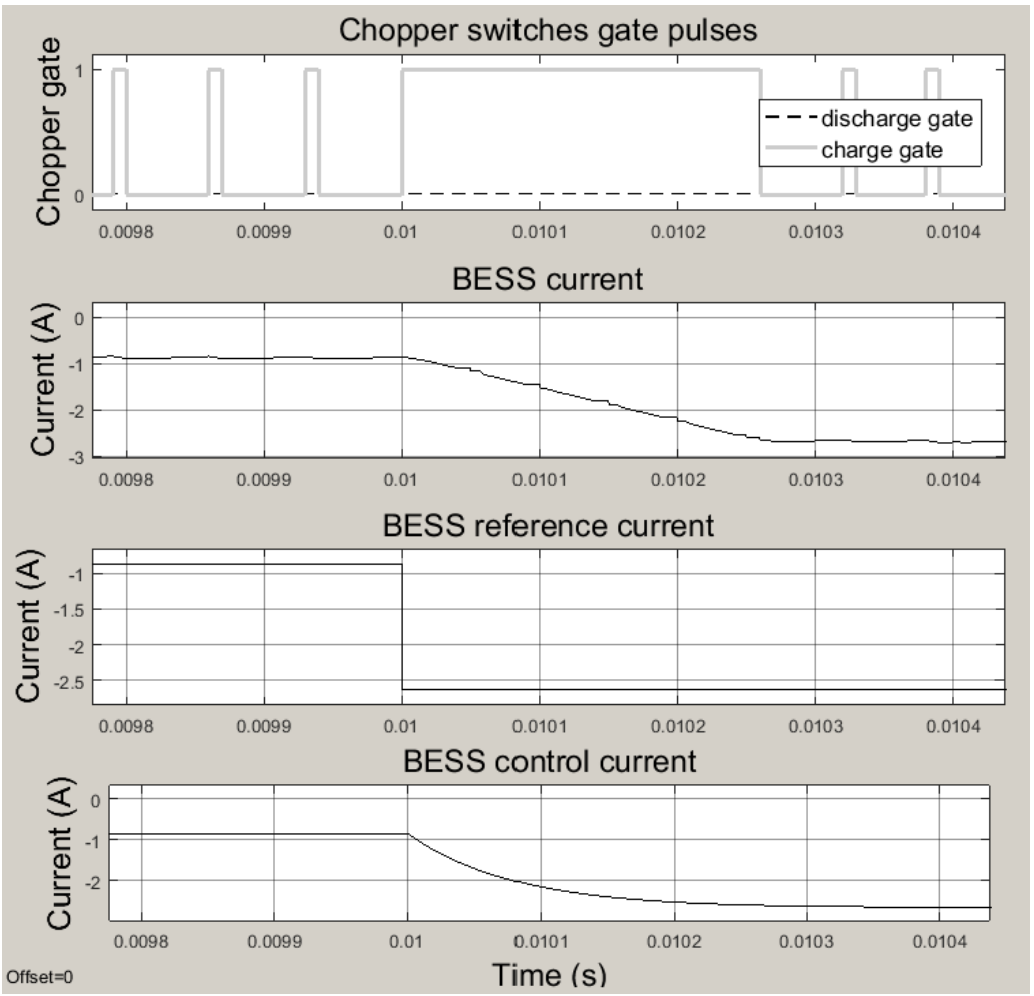

Figure 4-5. Step response for 100 W change in power reference.

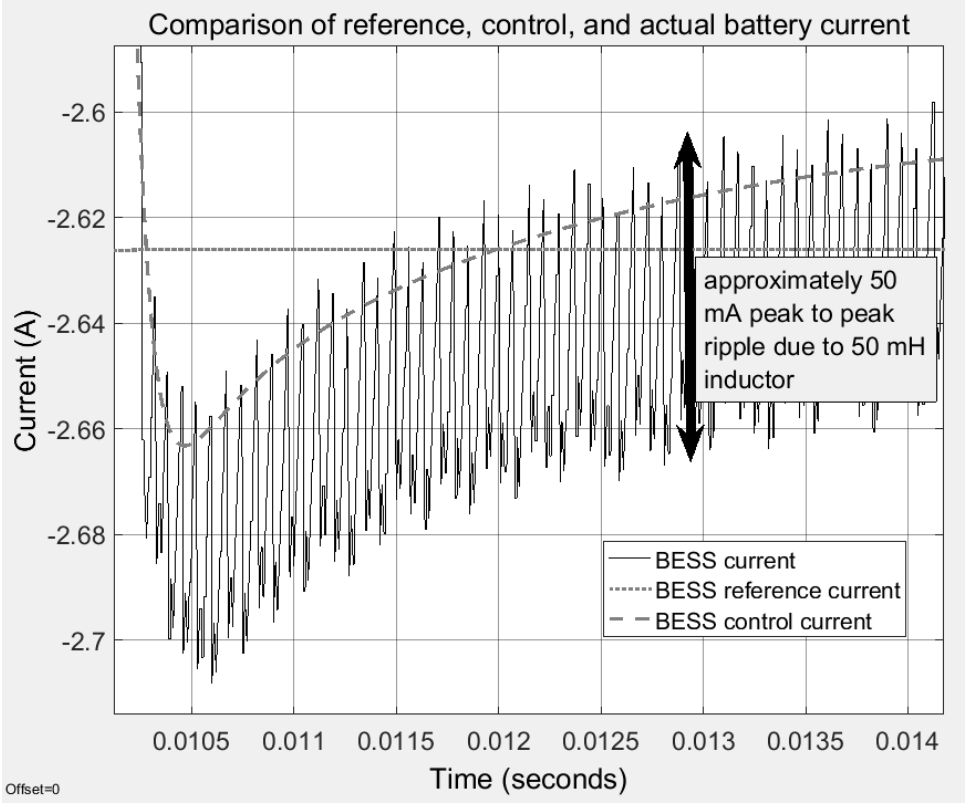

Figure 4-6. Transient response of BESS current to 100 W step change.

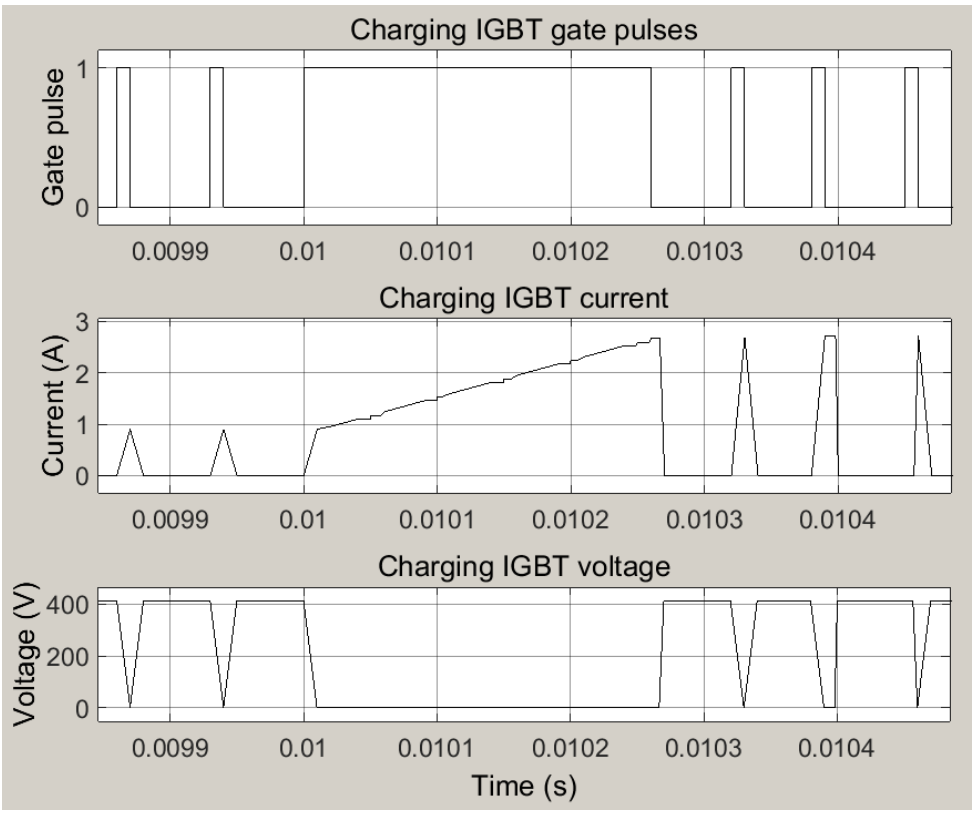

Figure 4-7. Charging IGBT switch current and voltage response to 100 W step change.

The next simulation to test the step response was to change from a small negative power reference to the nominal charging current of -42 A; at 57 V, this is a power reference of about -2400 W. The response can be viewed in Figure 4-8. Note that the response time to achieve steady-state in this case is slightly less than six (6) ms.

At this point of the analysis, it is instructive to view the inductor and IGBT current behaviour at steady state to view the response of the IGBT switch to the control current. This is described by the annotations in Figure 4-9. As the battery current passes above the control threshold, the IGBT switch is turned on, its current approaches that of the inductor. The IGBT on-state acts to recharge the inductor and to increase the charging current. When the IGBT switches off, the inductor current slowly decreases, reducing the charging current until it passes above the control threshold, and the switching cycle repeats. Not shown in Figure 4-9 is the fact that as the battery state of charge increases, its voltage also increases. This has a small impact on the transient inductor current behaviour, as noted. As the state of charge continues to increase, so does the battery voltage, which in turn reduces the reference and control current values, and hence the actual battery current.

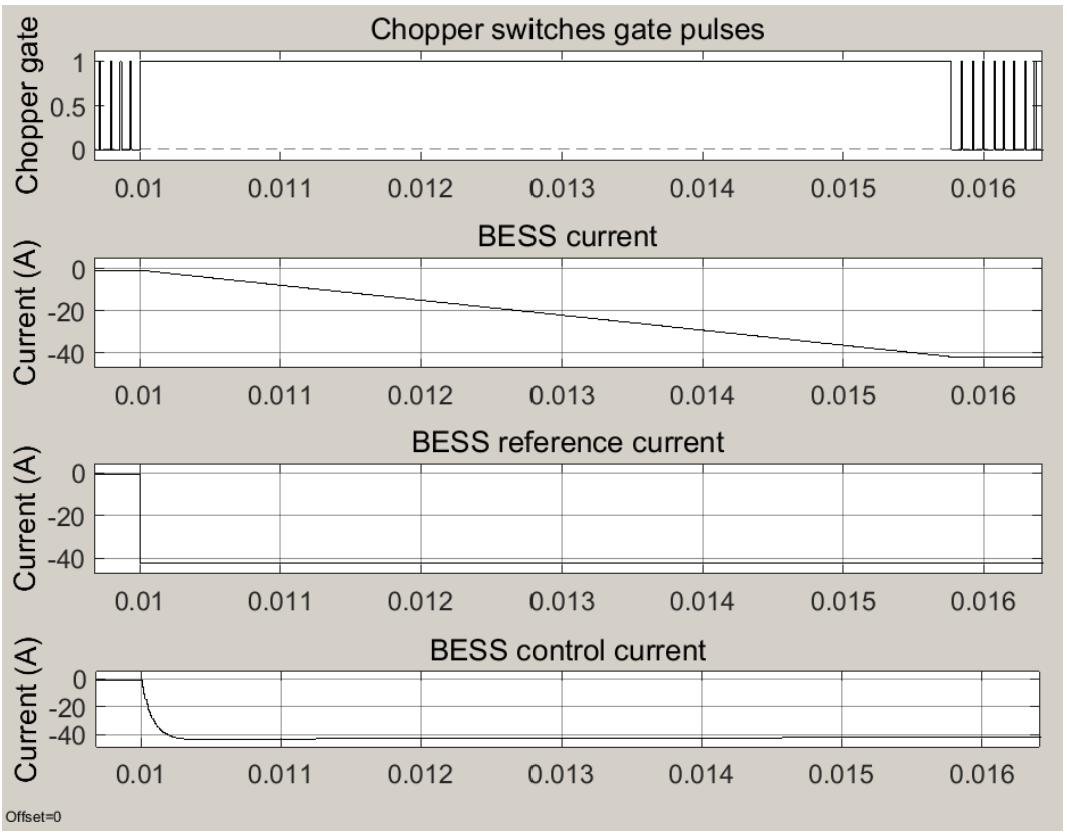

Figure 4-8. Step response to nominal charging current

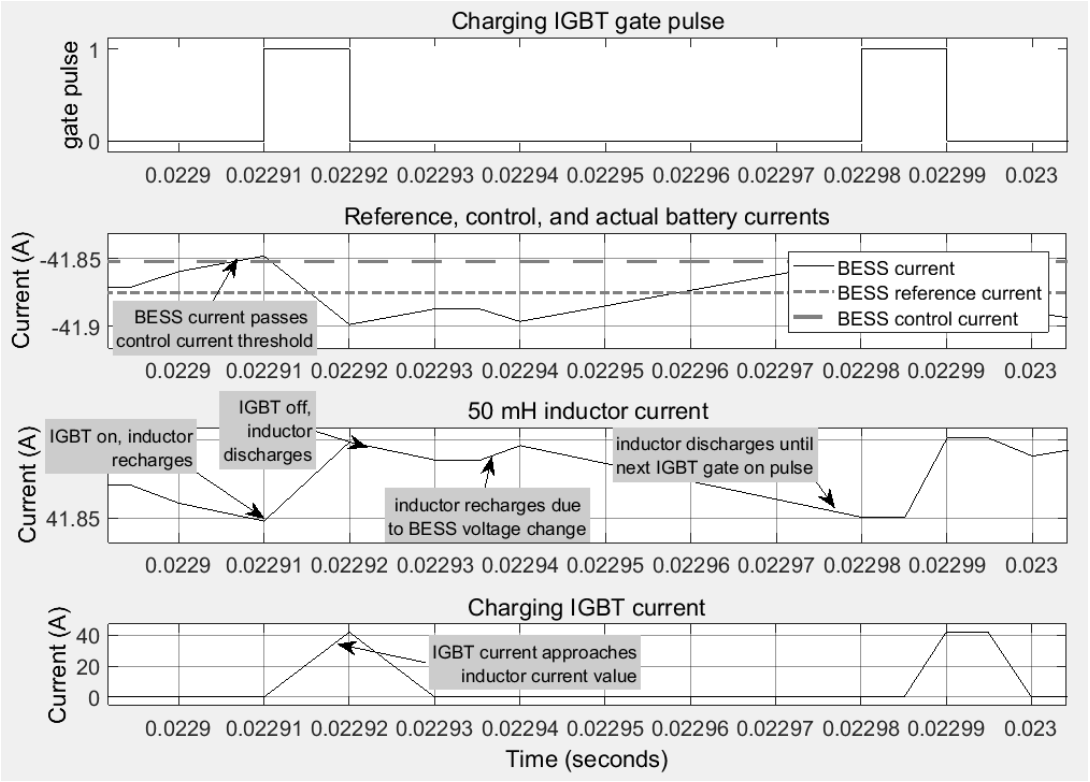

Figure 4-9. Inductor and IGBT current behaviour at steady state.

4.2.2 Charging ramp response

To evaluate the ramp response, a saturation block was added as seen in Figure 4-10. This mimiced the effect of a power limiting device. The upper (discharge) limit was set to 5000 W, as per LG battery specification; the lower (charging) limit was set to -3000 W, somewhat more than the power of 2436 W at maximum battery voltage and nominal charge current.

The ramp test was a conducted at a rate of -3000 W/ms. The results are shown in Figure 4-11. As expected, at 10 ms, the current limiter prevents the reference current from proceeding beyond a 3000 W charging rate, or approximately -53 A. It can be seen that the charging IGBT switch has longer on-times per pulse during the ramping, and shorter-on times upon reaching steady-state, after the current-limiting saturation block takes effect. In the second plot of Figure 4-11, it is difficult to view the differences among the reference, control, and actual currents, demonstrating the efficacy of the controller's ability to follow this power reference signal.

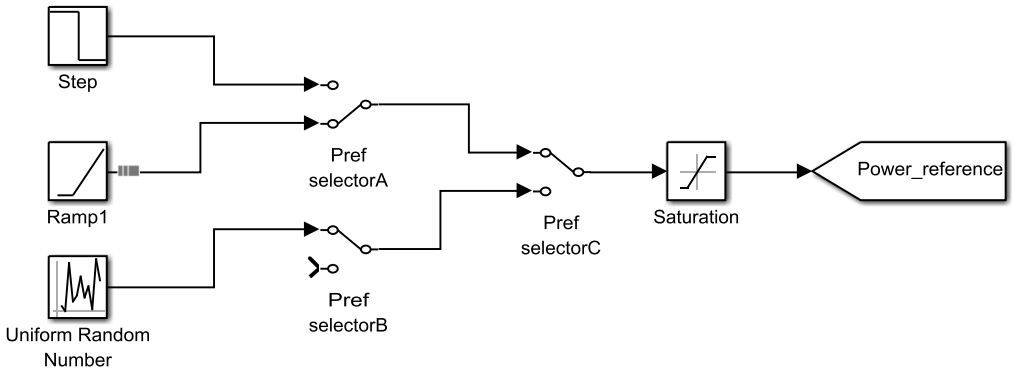

Figure 4-10. Setting the ramp response.

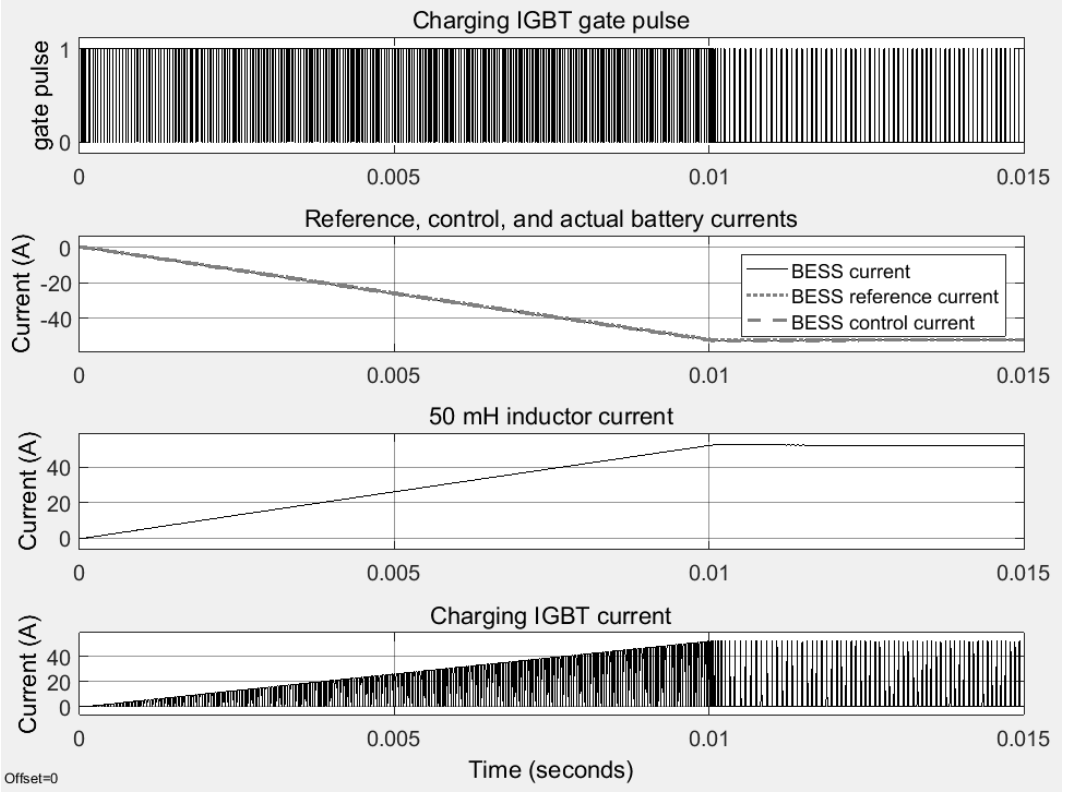

Figure 4-11. -3000 W/ms ramp response.

To provide a higher time-resolution understanding of the ramp response, refer to Figure 4-12. It can be seen that the IGBT on-time is about 0.04 ms. The actual battery current appears to track the reference current reasonably closely.

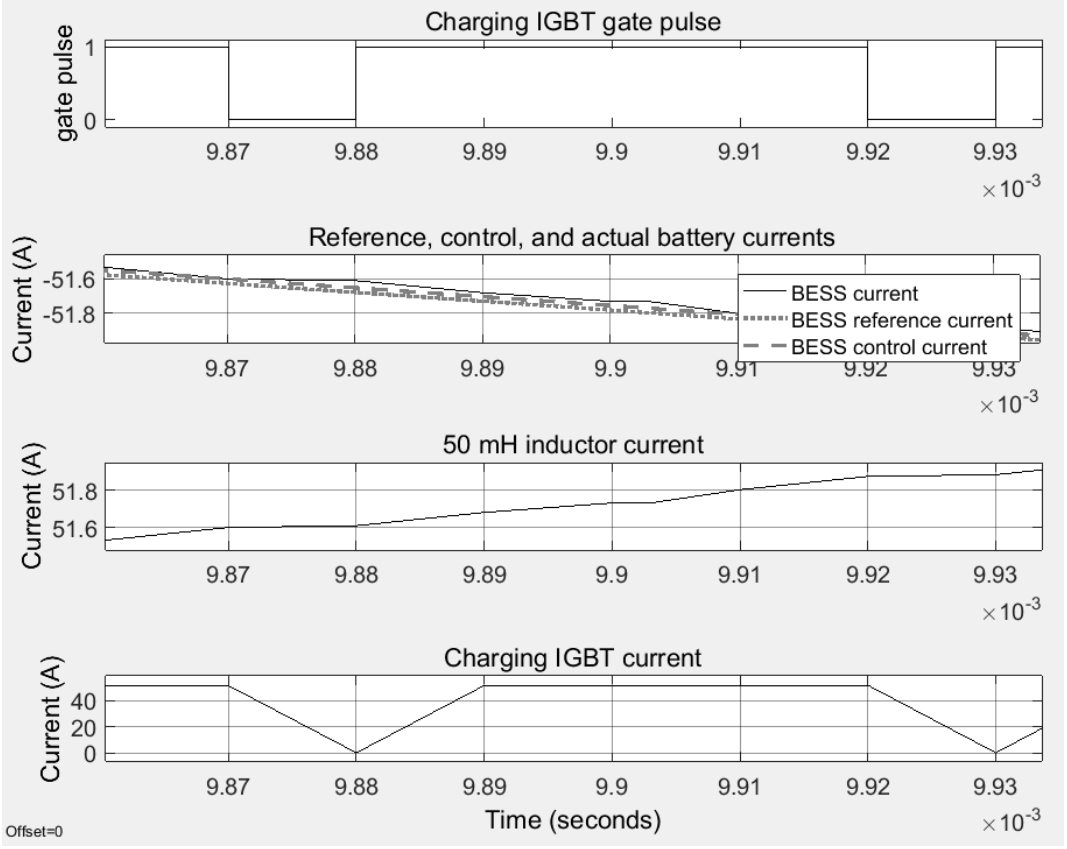

Figure 4-12. Ramp response of -3000 W/ms viewed over 70 microseconds.

4.2.3 Response to random charging reference

In this simulation, a random power reference between zero and -3000 W was applied every 10 ms. Figure 4-13 displays the controller response. The most notable piece of information to be derived is from the second plot. It can be seen that the controller has faster responses as the current reference becomes more negative, rather than less negative. That is, when a higher rate of charging is referred, the controller responds more quickly. When a lower rate of charging is referred, the controller takes longer to reach steady-state. This is reflective of the voltage change across the inductor when the charging IGBT switch changes state.

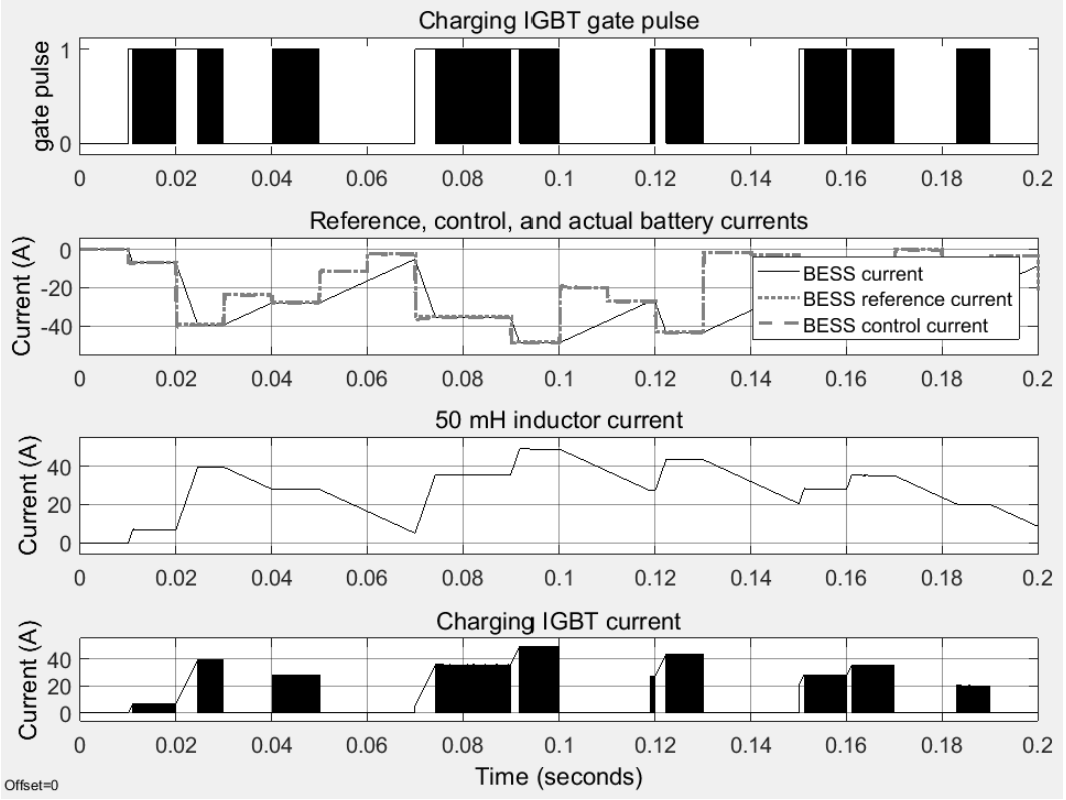

Figure 4-13. Response to random charging power reference.

Changing the inductor size to 10 mH, and the relevant term of the PID controller, results in a faster response, both for increases and decreases in power reference. This phenomenon can be viewed in Figure 4-14, using the same random power references as for the response to the system using the 50 mH inductor viewed in Figure 4-13. The trade-off for the faster response by using this smaller inductor is, of course, a significantly larger current ripple, as viewed in Figure 4-15. This can be compared to, for example, Figure 4-6, where the output ripple is explicitly denoted on the figure, or see also Figure 4-9.

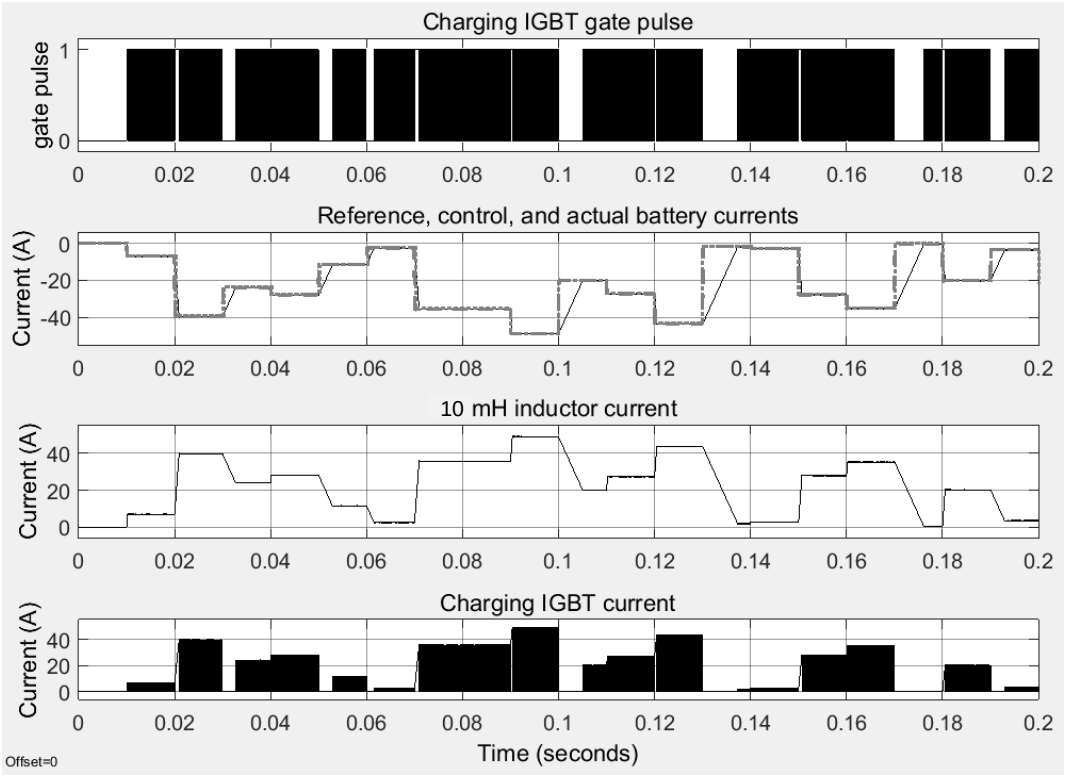

Figure 4-14. Response to randomly changing power reference, but using 10 mH inductor.

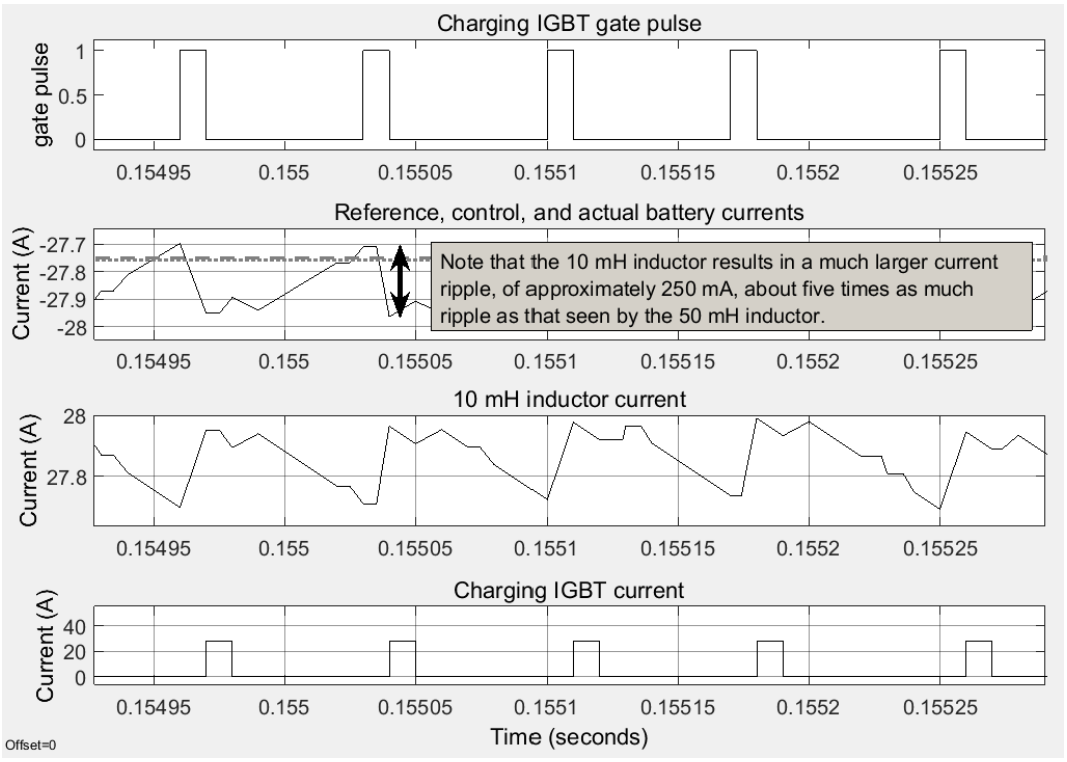

Figure 4-15. Effect of smaller inductor on charging current output ripple.

4.3 BESS controller simulation – discharging

4.3.1 Discharging step response

Figure 4-16 shows the step response to a +100 W step. The controller required just over 1.5 ms to reach the steady-state. Compare this to the 250 μs response to the -100 W step in Figure 4-5.

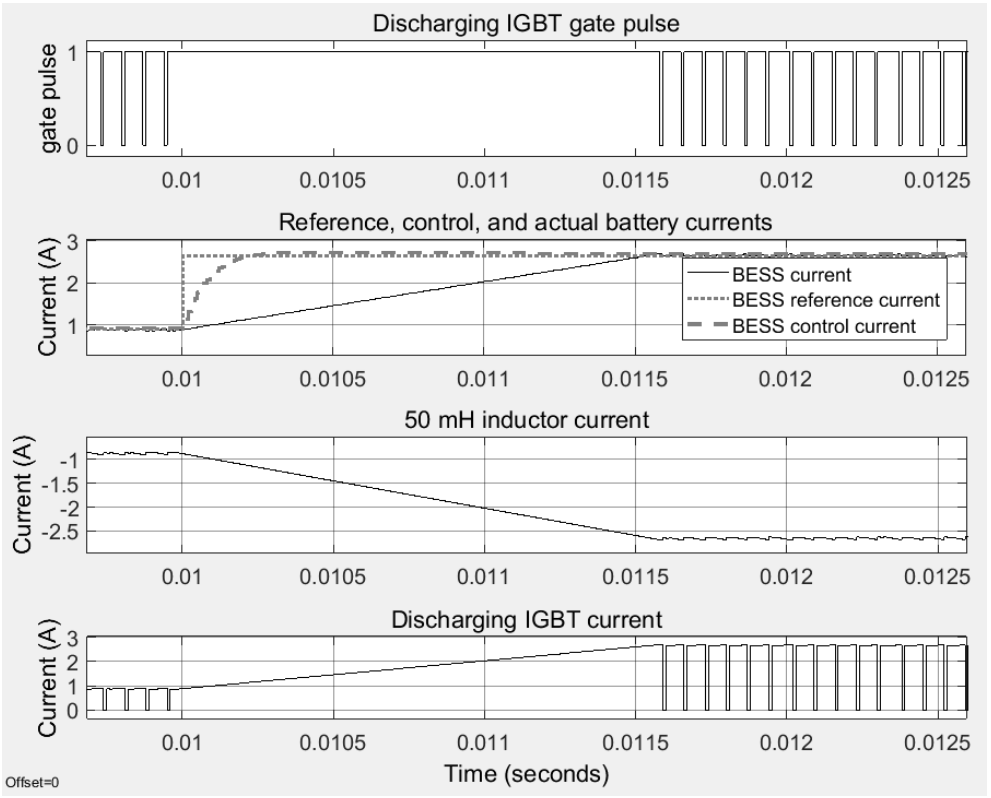

Figure 4-16. Step response to +100 W step.

The next simulation to test the step response was to change from a small positive power reference to the nominal discharging current of 42 A; at 57 V, this is a power reference of approximately 2400 W. The response can be viewed in Figure 4-17. The response time to steady state was approximately 36 ms. Compare this to a response time of about six (6) ms for the same step in the charging mode, described in section 4.2.1.

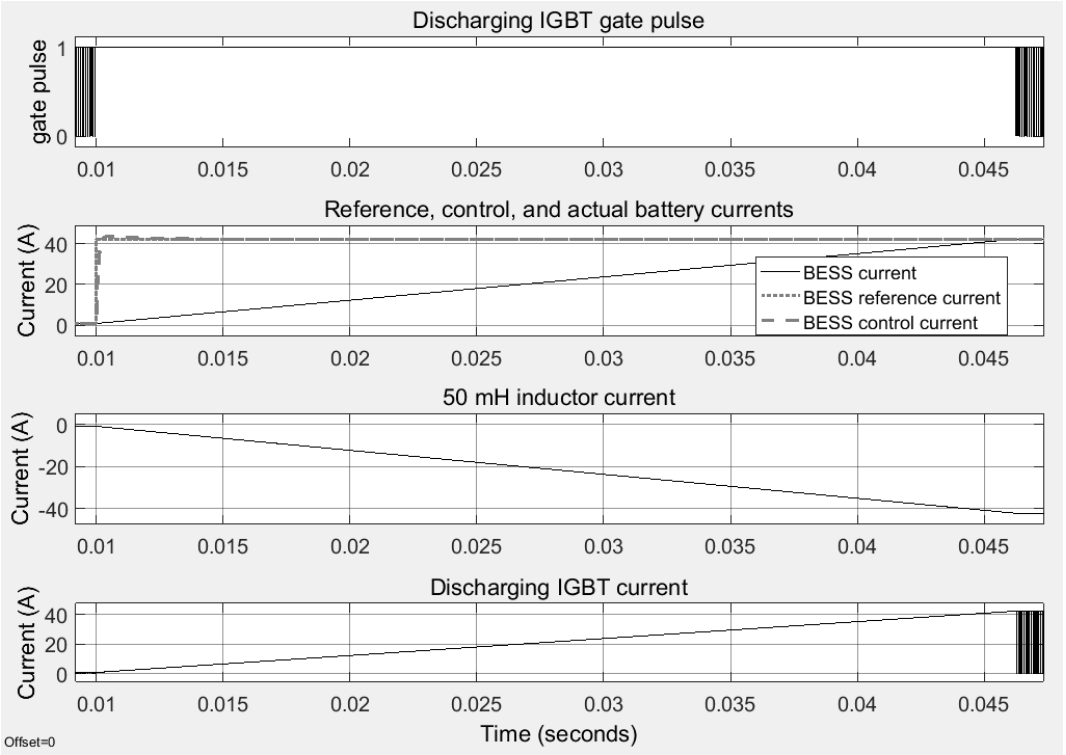

Figure 4-17. Step response to nominal discharge current rating.

4.3.2 Discharging ramp response

In the first test, the ramp response was conducted at a rate of +5000 W/ms. Because discharging can occur at a higher current than charging, according to the specifications of the battery, the current limiting (saturation) block is held at 5000 W, so the cut-off time for the reference and control currents occurred later. The response can be seen in Figure 4-18. It required 76 ms to reach the current cut-off value at steady state.

To compare to the charging scenario, the test was repeated, but the cut-off power reference was held at 3000 W. The results are not shown here, but required 46 ms to reach the current cut-off value. Note that the time to power reference ratios are nearly

identical for the two cases. This value of 46 ms compares to just over 10 ms for the ramp response to the charging scenario in Figure 4-11.

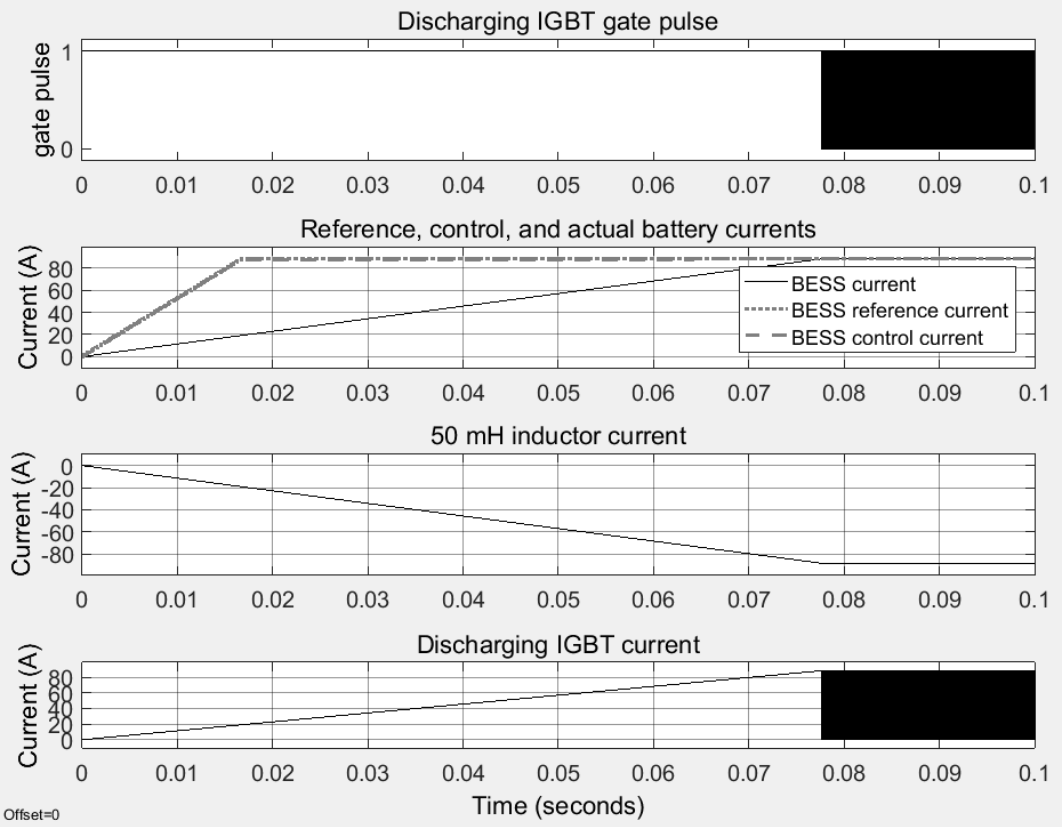

Figure 4-18. Ramp response of discharging current scenario, 3000 W/ms.

4.3.3 Discharging random response

Based on the results of the previous sections, it was expected that the controller would have a less robust response to random discharging power references than to random charging references. This was not a completely valid assumption, as it only applied to a random increase in the power reference. A decrease in the power reference was enacted more quickly. The results of the random test can be viewed in Figure 4-19.

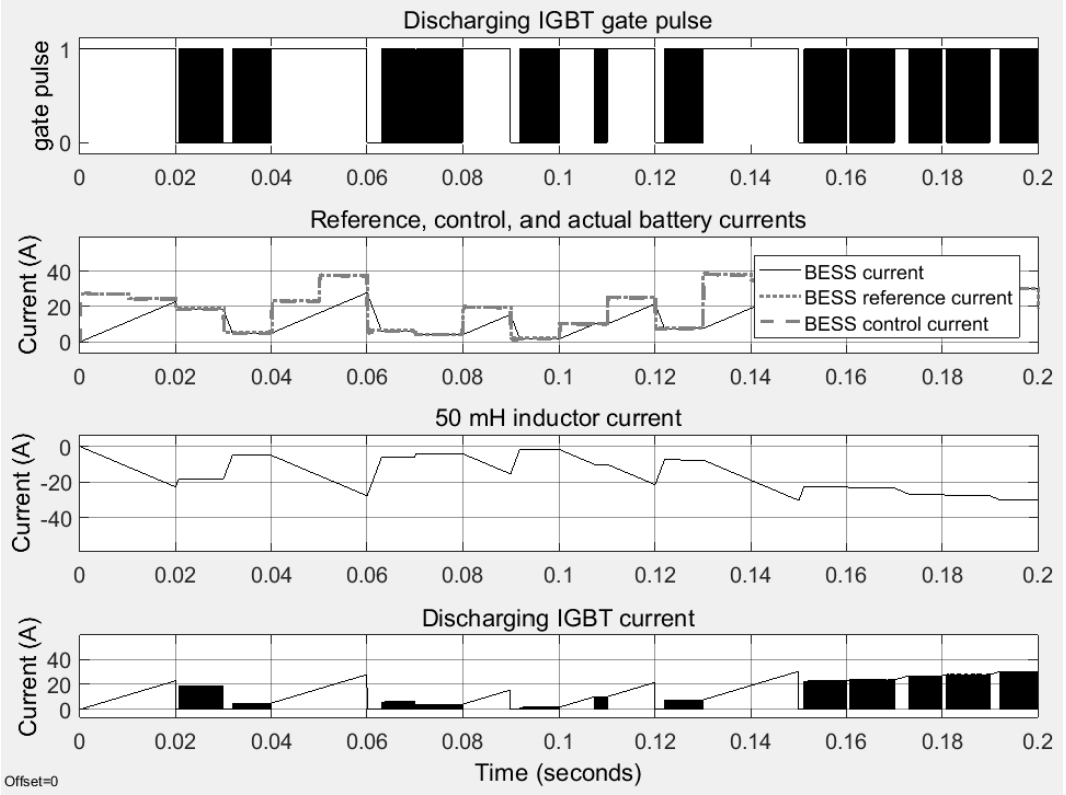

Figure 4-19. Random discharging power reference response

4.4 Discussion

The common link between the charging and discharging scenarios is the rate of response to different power references. If the direction of the change in power reference is negative, the controller response is faster than if the direction of the change is positive. That is to say, if a reduction in discharging rate, or an absolute increase in charging rate is dictated by the power reference of the system, then the response time will be faster than if the same magnitude of increase in discharging rate, or absolute decrease in charging rate was demanded, respectively.

The essence of the difference in behaviour can be attributed to the voltage across the inductor. A decrease in the power reference, i.e. lower discharge rate or greater charge rate, is associated with the switching off of the discharge IGBT or the switching on of the charging IGBT, respectively, sees a voltage of about 357 V across the inductor. Conversely, when the power reference increases, i.e. greater discharge rate or lower charge rate, is associated with the switching on of the discharge IGBT or the switching off of the charging IGBT, respectively, sees a voltage of about -57 V across the inductor.

This can be seen by viewing the inductor voltage characteristics in response to random power references in the discharging and charging modes, as displayed in Figure 4-20, and Figure 4-21, respectively.

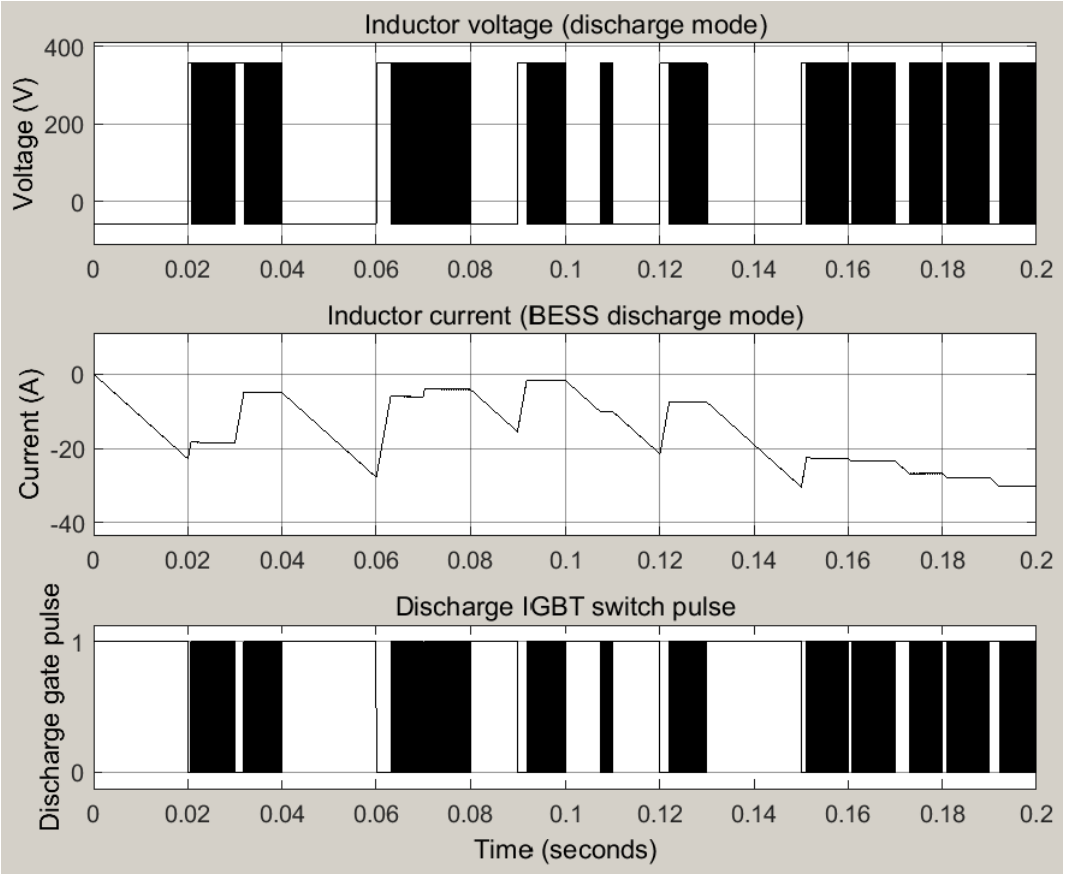

Figure 4-20. Inductor voltage and current characteristics, discharge mode.

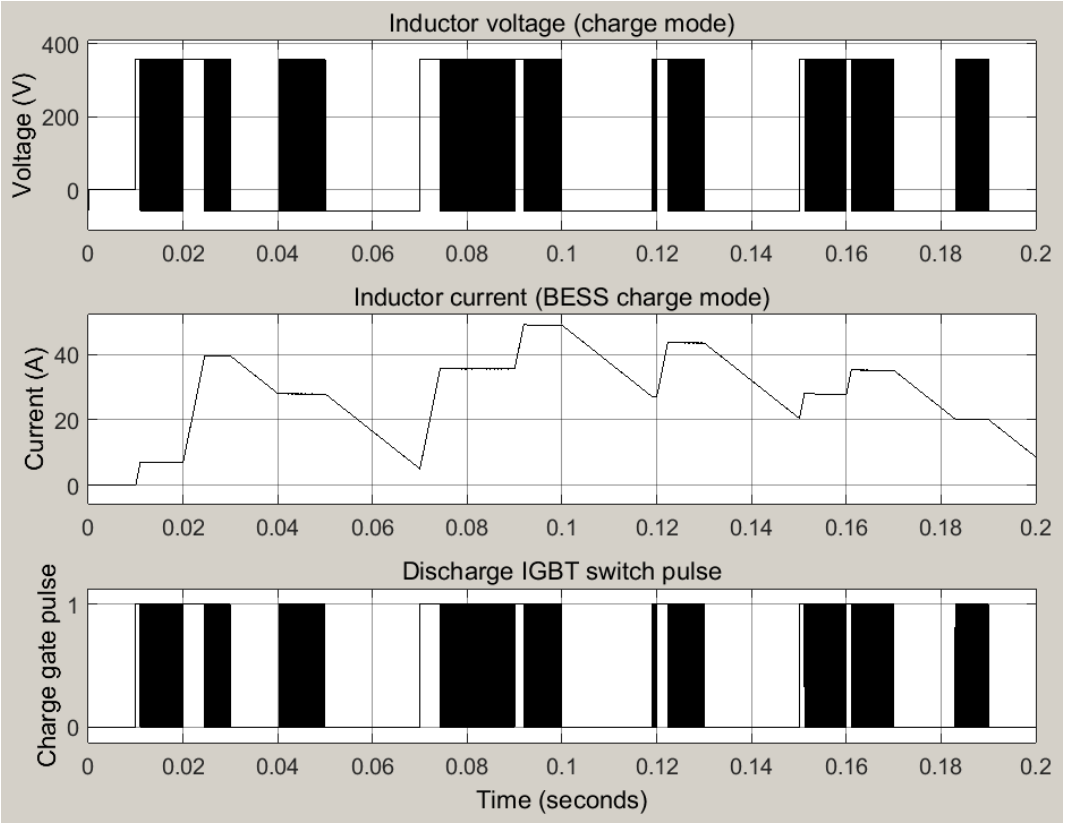

Figure 4-21. Inductor voltage and current characteristics, BESS charging mode.

Regardless of the switches' states,

$$v_L = L\frac{di}{dt} \qquad [\ 4.3]$$

where v_L is the inductor voltage

L is the inductor's inductance, in Henries (H)

$\frac{di}{dt}$ is the rate of change of inductor current with respect to time.

Rearrangement of [4.3] obtains

$$\frac{v_L}{L} = \frac{di}{dt} \qquad [\ 4.4]$$

This relationship shows that the rate of change of inductor current is in direct proportion to the voltage across the inductor, or

$$v_L \propto \frac{di}{dt} \qquad [\ 4.5]$$

Hence, as the magnitude of v_L increases, the rate of change of inductor current is greater, i.e. it requires less time to achieve a change in current. It therefore stands to reason that it takes more time for the controller to respond to an increase in the discharging rate, than to an increase in the charging rate. As described in section 4.3.1, a discharging step response was achieved in about 36 ms, compared to about 6 ms for the same magnitude of change in power reference for the charging step response, or approximately six times the difference.

It is proposed that it may be useful to consider the ratio of voltages across the inductor in the different states as an indicator of the expected performance of the controller. That is, the ratio of response times to the same magnitude of increase in charging or discharging power reference may be predicted as follows:

$$\frac{t_{con}}{t_{don}} \sim \left|\frac{V_{Ldon}}{V_{Lcon}}\right| \qquad [\ 4.6]$$

where t_{con} is expected response time to increased charging reference magnitude

t_{don} is expected response time to increased discharging reference

V_{Lcon} is inductor voltage with charging IGBT switched "on"

V_{Ldon} is inductor voltage with discharging IGBT switched "on".

To test this idea, responses to the step inputs, described in sections 4.2 and 4.3 were evaluated.

The right hand side ratio of [4.6], is first evaluated:

$$\left|\frac{V_{Ldon}}{V_{Lcon}}\right| = \left|\frac{-57}{357}\right| = 0.1597.$$

The left hand side ratio of [4.6] was then evaluated for times to respond to the 100 W step as per sections 4.2.1 and 4.3.1:

$$\frac{t_{con}}{t_{don}} = \frac{250\mu s}{1.5ms} = 0.1667.$$

The left hand side ratio of [4.6] was then evaluated for times to respond to the 2900 W step as per sections 4.2.1 and 4.3.1:

$$\frac{t_{con}}{t_{don}} = \frac{6\ ms}{36\ ms} = 0.1667.$$

The results indicate that there may be a relationship present, but more precise time evaluations of the step response would be indicated and are suggested as future work.

The evaluation of the ratio of responses to the ramp input were not evaluated, because during the charging ramp input, the charging IGBT switched rapidly between on and off states.

Chapter 5: Economic Model – Benefits and Risks

5.1 Economics

As mentioned in section 3.7.9, several economic scenarios were considered. These included inflation from 2 – 5.5% and discount rate of 3 – 6.5%, both in increments of 0.5%. Since each parameter is modelled for 8 different values, 64 different net present cost values were obtained for each scenario. Dollar values specified in the paragraphs below are average of these 64 cases, unless otherwise specified.

5.2 Scenarios and simulations modelled

To develop a coherent understanding of the system model, a number of scenarios were constructed. The scenarios are as follows:

- Residential load pattern simulated with just the grid providing the electricity
- Base system of 1 kW wind, 9.455 kW PV, plus a single BESS
- Base system of 1 kW wind, 9.455 kW PV, plus two BESS
- Base system of 1 kW wind, 9.455 kW PV, plus zero BESS
- Choose the most optimal system from a range of 0-3 wind turbines, 5-10 kW solar PV, and 0 to 2 BESS
- Choose the most optimal system within the capacity of the 17 kW inverter
- Determine if a smaller pro-rata BESS might have better economics than the larger 6.4 kWh BESS
- Determination of the peak TOU tariff price that would make a system with a single BESS more economically feasible than a system without a BESS
- Determine the influence of residential energy consumption levels on net present cost
- Determine the influence of deferrable load on net present cost
- Determine the influence of changing the maximum charge and discharge settings on NPC
- Examine the influence of bulk-buy battery discount on NPC
- Determine the discount required for a BESS to break-even with a system that does not have a BESS
- Determine the influence of changing the restrictions on the control regimes
- Examine the base case in the context of different electricity retailers' tariffs

5.3 Typical BESS charge and discharge pattern

HOMER permits a variety of views of system behaviour. As this project focuses on battery control, it is instructive to view the typical charging and discharging pattern. Although this can be displayed for an entire year, a typical day for the system configuration and battery control scheme looks like that in Figure 5-1. Because of the large size of the PV system relative to the battery, charging typically occurred during the first half of the day, mostly by the sun, as seen in the triangular plot on the left hand side of the upper graph in Figure 5-1. As the battery approached full SOC, seen as the plateau on the lower graph of Figure 5-1, the charging was stopped. Because of the size of the PV system relative to the typical load profile, daytime loads were typically served by the PV system. The gap between the two plots reflects this inactivity on the part of the BESS. As the peak TOU tariff begins at 1600 hrs, discharge to the load begins, seen as the plot on the right hand side of the upper graph in Figure 5-1, and tapers off as the BESS approaches its enforced SOC limit of 15% as seen in the lower graph.

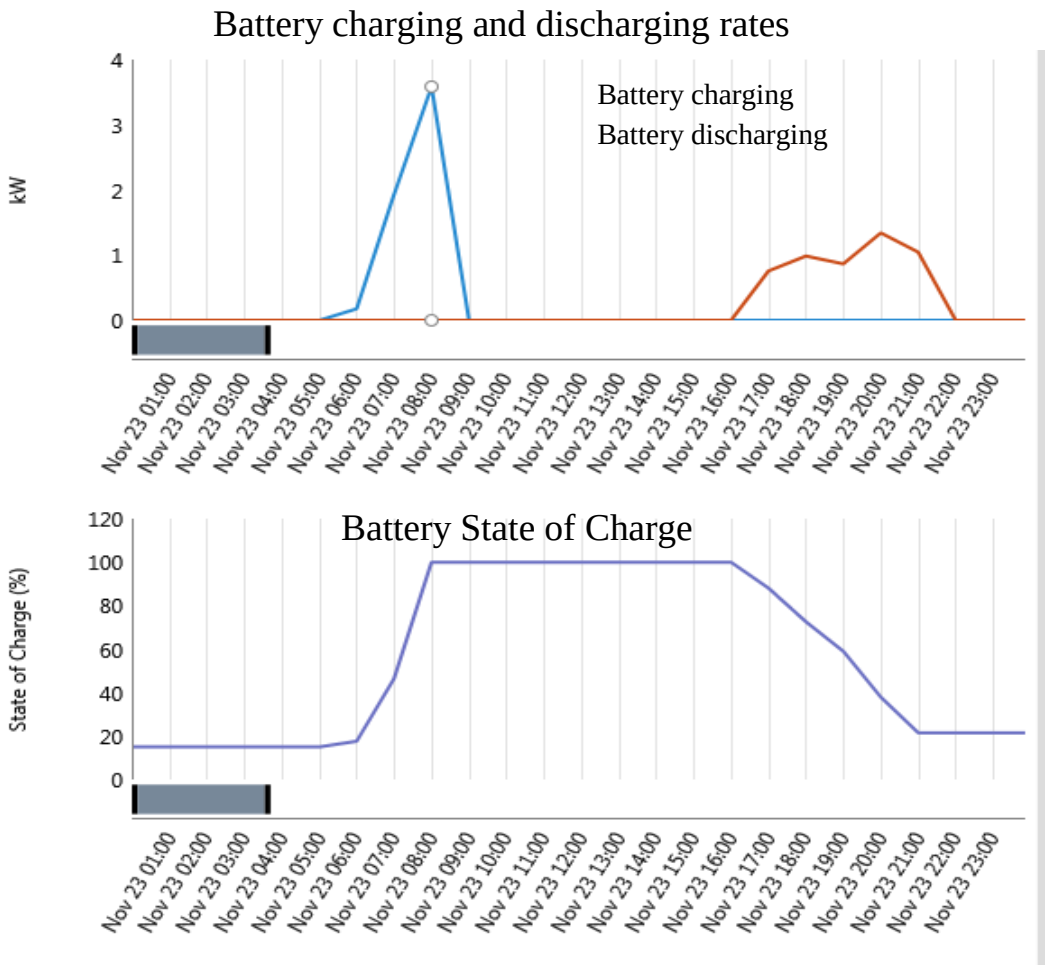

Figure 5-1. Typical BESS charging and discharging profile.

5.4 Typical power profile for a single day

To provide an example of a typical day's power profiles constructed by HOMER based on the component models constructed for input, the day of October 13th was chosen for illustration. Although graphics customisation and export from HOMER is relatively poor, Figure 5-2 displays the power plots for PV, wind, residential load, and BESS charging and discharging. It can be (only just) seen that wind power is almost negligible compared to PV, which is not surprising given Nambour's climate and the power specifications of the PV (10 kW) and wind (1 kW). Given that the up-front PV system cost is only about 3.5 times more expensive than the wind system, conclusions can be drawn about the (lack of) economic rationale for small-scale grid-tied wind turbines in Nambour.

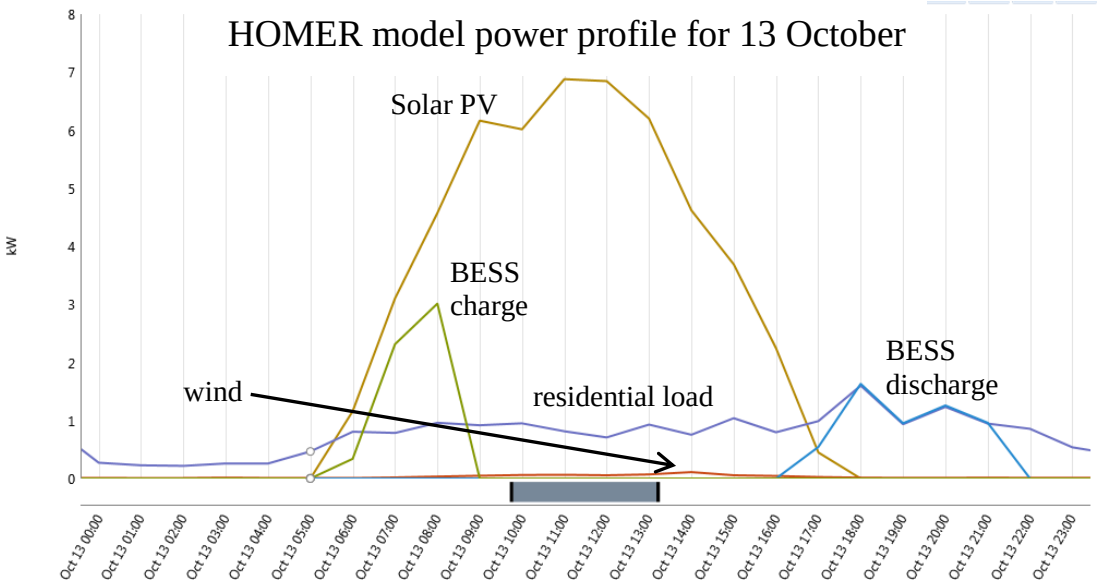

Figure 5-2. HOMER single day power profile for system components.

5.5 Grid only electricity

To provide a reference for the modelling, a base case was established, whereby it was assumed that all electricity purchases were based on the TOU tariff. The $1250 design fee was deducted from the cost, as was the annual cost of insurance. The grid only case established a net present cost (NPC) of $40 754 for the 25 years.

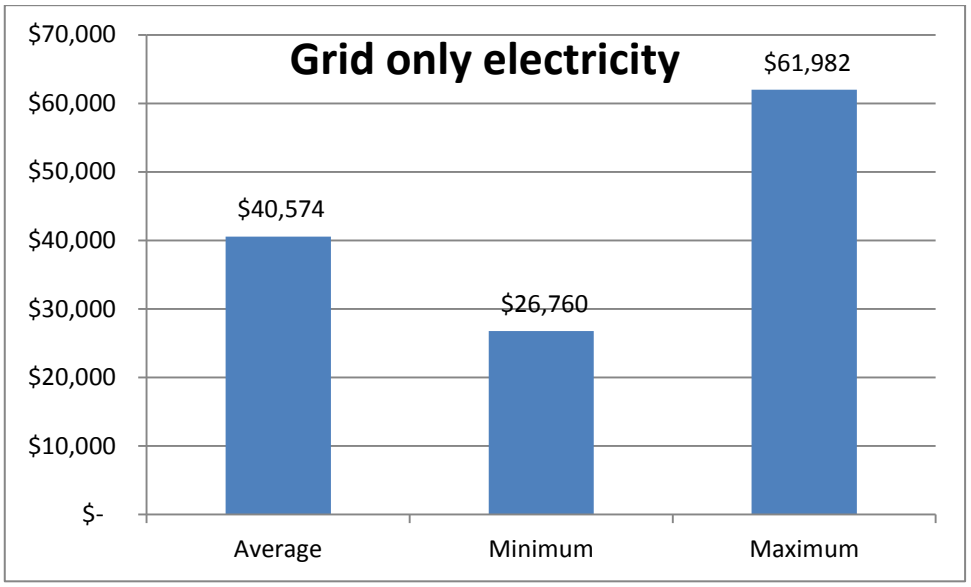

Figure 5-3. NPC for grid-only scenario.

5.6 Base system case, with varying number of BESS

The second simulation was run such that the base proposed system of 1 kW wind, 9.455 kW PV, and a single 6.4 kWh BESS could be assessed. HOMER was configured to report on the economics of the specific proposed system with zero to two BESS.

5.6.1 Base case, one BESS

The average NPC was $46 014, as seen in Figure 5-4.

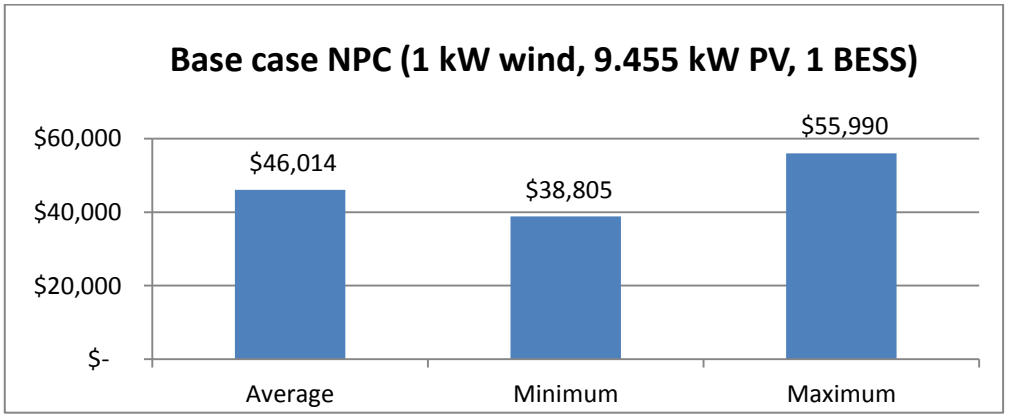

Figure 5-4. Base case scenario NPC.

5.6.2 Base case, two BESS

In this simulation, HOMER ran a sensitivity analysis on the number of BESS systems for the base case, by permitting systems with one or two BESS. In all economic cases, 1 BESS system had a lower NPC than 2 BESS systems as in Figure 5-5.

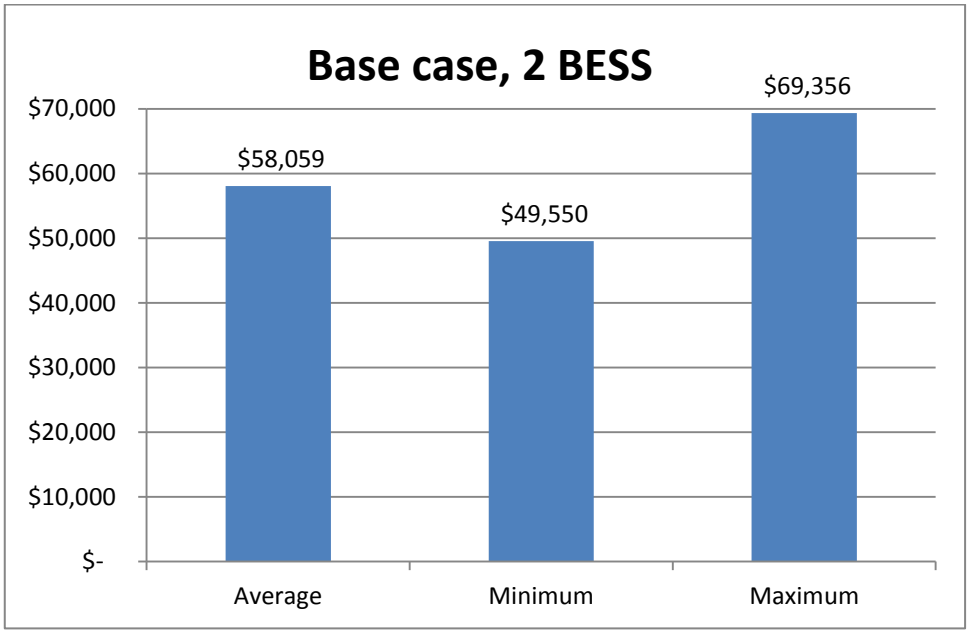

Figure 5-5. Base case NPC but with 2 BESS.

5.6.3 Base case, no BESS

The system with no BESS had a lower NPC than a system with one or two BESS, as seen in Figure 5-6.

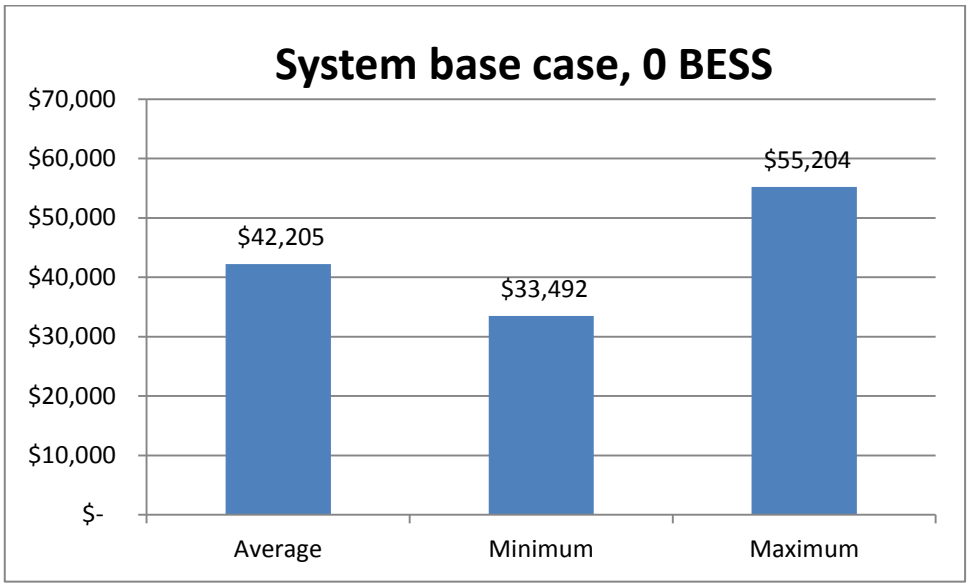

Figure 5-6. Base case NPC for system without a BESS.

5.6.4 Comparison of number of BESS assigned to base system

The simulations suggest that for the base system modelled, the lowest NPC that could be attained was one that used no BESS. It must also be considered that these values would be even less favourable towards BESS if HOMER was able to vary the inverter size – all figures reflected a 17 kW inverter. A system with no BESS would require a smaller (11 kW) and therefore less expensive inverter; a system with two BESS would require a larger (22 kW) and therefore more expensive inverter. Figure 5-7 displays the differences in NPC among the different number of BESSs per system.

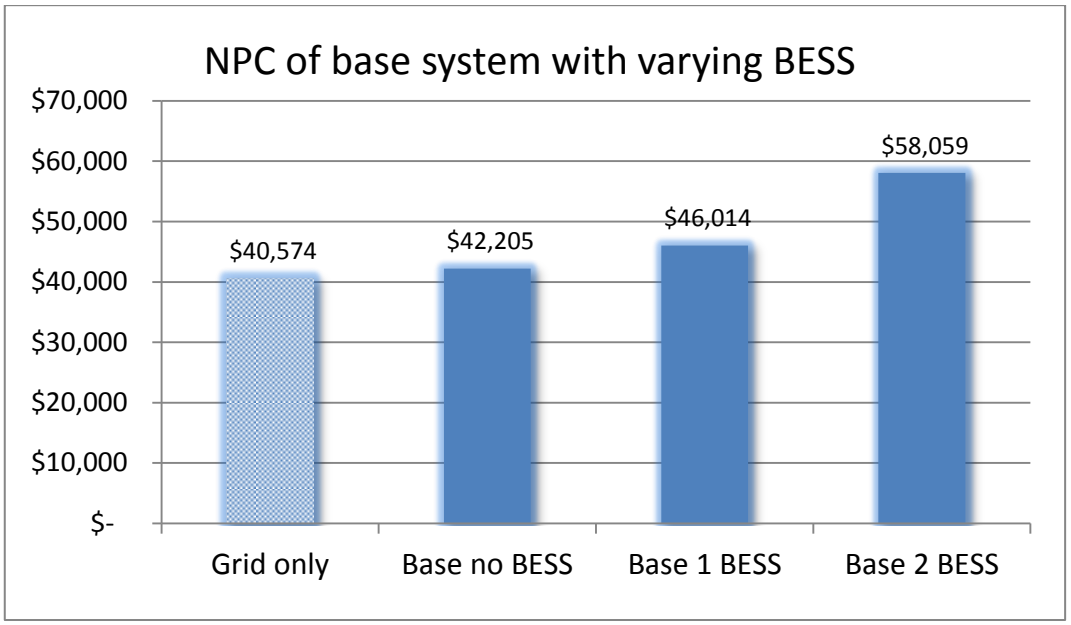

Figure 5-7. Average NPC of base system with varying BESS

5.7 Optimum system from specification search space

The third simulation allowed for a search space of 0-3 wind turbines, 5-10 kW of solar, and 0 to 2 BESS modules. From this search space, HOMER determined that the lowest NPC was found for a 10 kW PV system with no wind turbine, nor BESS. The NPC of this system was $36 838 for 25 years. Note that such a system would also only require an 11 kW inverter which would further reduce the NPC.

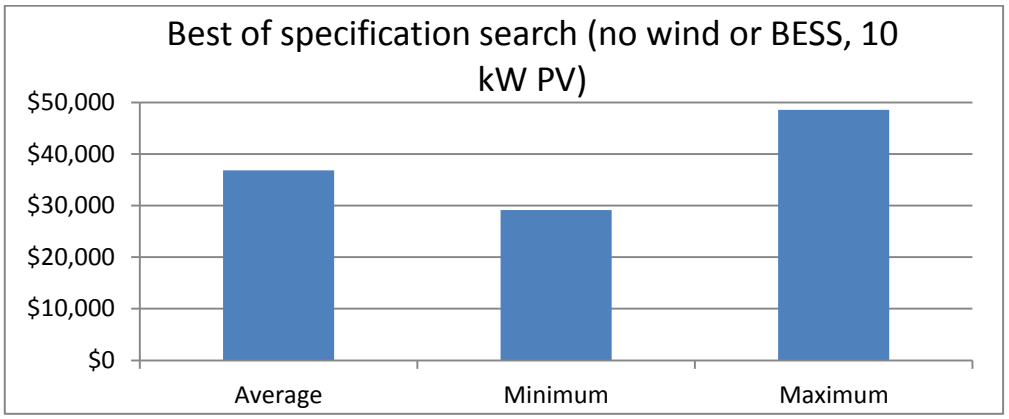

Figure 5-8. Best NPC for optimal system component quantities.

5.8 Optimum system within inverter limitations

This simulation permitted any quantity of any component starting from zero that was permissible with the limitation of the inverter (17 kW). It was found that in nearly all economic cases a 15 kW PV only system had the lowest possible NPC, with the exception of three high discount rate and low inflation, which suggested a 14.5 kW PV only system. The average NPC for this 15 kW PV only system was found to be $33 312.

5.9 Optimal system using a pro-rata battery

For this simulation, a pro-rata battery system was defined; capacity and cost of the original LG BESS were divided by 6 to obtain a pro-rata system to see if a smaller battery system might provide more benefits than a larger one. Other base case values of 1 kW wind, and 9.455 kW PV were assumed. The simulation suggested that a zero-battery system would be the most optimal in terms of NPC in all but 3 of the 64 economic models (those 3 were for a single pro-rata BESS, having low discount rate combined with high inflation). The NPC value of this wind/PV only system was $42 201, similar to that for the base system with no BESS of $42 205, the difference attributed to the 3 single pro-rata BESS models.

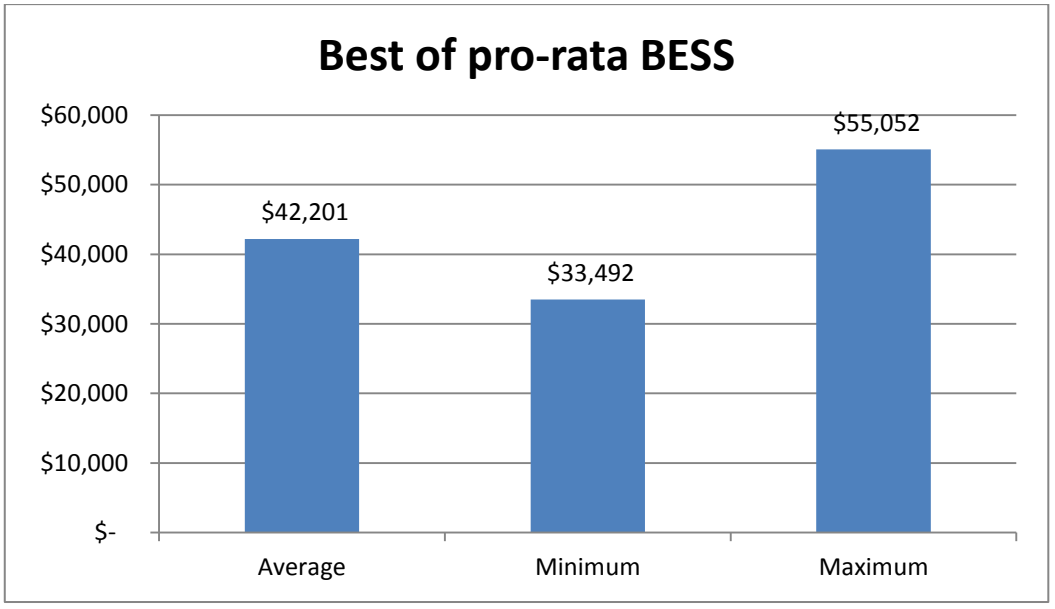

Figure 5-9. NPC for pro-rata BESS scenario.

5.10 Influence of tariff 12 peak-time price

This simulation aimed to determine the peak tariff price that would render the base case system *with a single* BESS system to be more economically feasible than the base case system *without* any BESS. In this simulation, all other values were held constant. Peak tariff price was simulated at the base AGL peak tariff of 0.35871 $/kWh, as well as 0.50, 0.60, 0.70, and 0.80 $/kWh; the BESS search space was confined to 0 and 1 BESS system (to see if 0 or 1 system resulted in lower NPC for a given tariff / inflation rate / discount rate).

In this type of comparison, it was not particularly useful to compare NPC, because the as the peak tariff increases among the models, the NPC will automatically increase. A more useful comparison that was adopted was to determine how many, and which of the 64 economic model variants determined that a BESS was more optimal than no BESS. The results are seen in Figure 5-10.

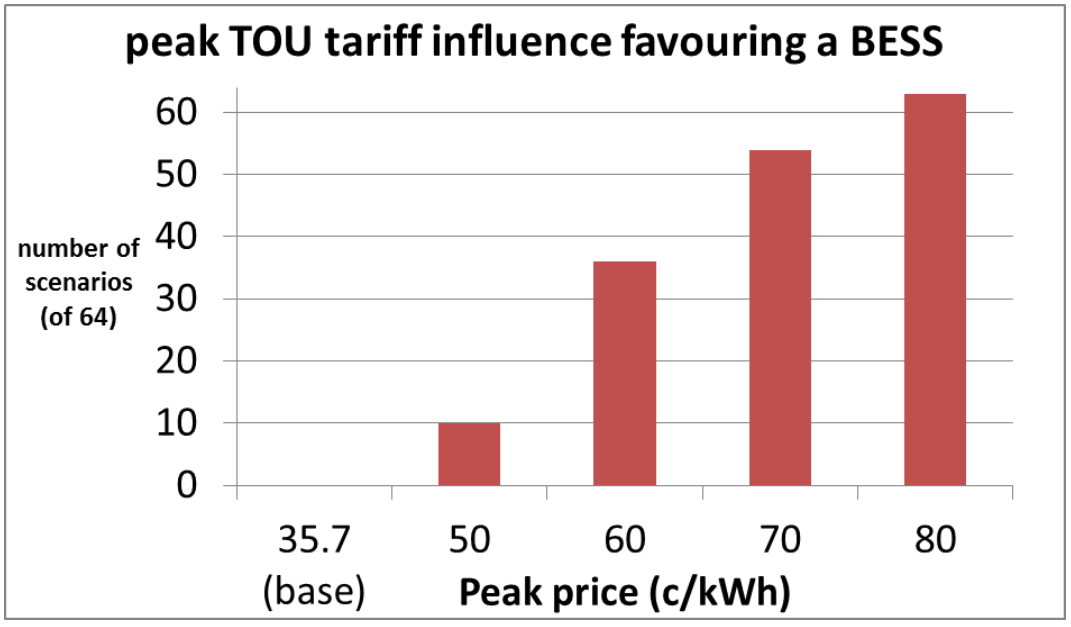

Figure 5-10. Influence of peak-time TOU tariff on NPC

At the base AGL peak-price, no economic variant was favourable to BESS. At 0.50 $/kWh, 54 of 64 economic models determined that no BESS was better. Of the 10 suggesting that a BESS was better, the common feature was high inflation and low discount rate. At 0.60 $/kWh, 36 of 64 models determined that one BESS was better. At 0.70 $/kWh, 54 of the 64 economic scenarios determined that a BESS was more feasible

than no BESS. At 0.80 $/kWh, all but one (highest discount rate, lowest inflation rate) model determined that system was more feasible with a BESS than without. The modelling revealed three key points:

- as peak tariffs increase, BESS is economically more favourable;
- as the projected rate of inflation increases, BESS is more favourable; and
- as the projected discount rate increases, BES is economically less favourable.

5.11 Influence of residential energy consumption

This simulation aimed to determine the influence of the magnitude of total energy consumption on the economic viability of installing a BESS. The residential base load scenario of average daily consumption in a year of 18.6 kWh was compared to 13.9 kWh (25% decrease), 23.4 kWh (27% increase), 26 kWh (40% increase), 30, 35, 40, 45, and 50 kWh per day. The decrease or increase was applied as a flat rate increase across the entire 8760 point hourly consumption for the year. For each consumption figure, HOMER was run to compare the base system model using one BESS and no BESS. The difference between these two figures was then obtained to determine the net present cost gap between the two system models for each level of energy consumption. In all cases, no BESS was more favourable than one BESS, but by varying amounts (Figure 5-11).

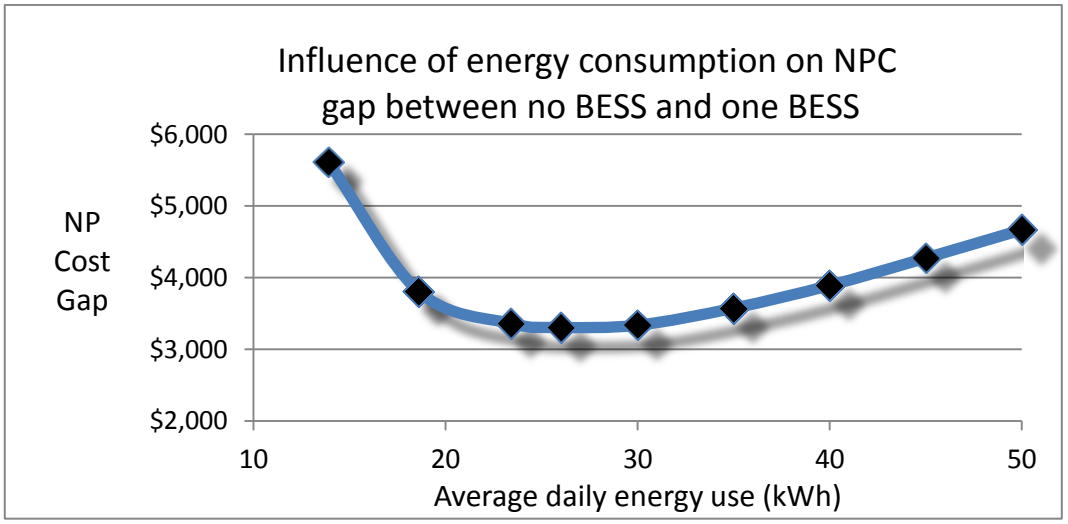

Figure 5-11. Influence of energy consumption on system NPC for no or one BESS.

The graph shows that households with somewhat larger loads are likely to see better results than the base case, but only to a point. As load continues to increase beyond about 26 kWh, BESS becomes less favourable. It may be possible that households with this level of energy consumption may find additional BESS capacity above 6.4 kWh to be advantageous, but this possibility was not considered in the modelling, and is suggested as future work. The other important limitation of the graph is that it does not consider that a zero-BESS system should have an even lower NPC because of the lower inverter capacity requirements. This would increase the NPC gap in all cases, but would not change the underlying trend displayed by Figure 5-11.

5.12 Influence of deferrable load strategy

This simulation aimed to determine the impact on the base case of transferring about 25% of the base-case load as deferrable. Deferrable loads need to be serviced at some point during the day. Examples of deferrable loads include laundry and dishwashing requirements, as well as hot water. The time of day that the load was actually energised was economically optimised by HOMER. The peak deferrable load was limited to 1 kW at any point in time. The base case configuration of a single 1 kW wind turbine, 9.455 kW of solar PV, 17 kW inverter, and single BESS configuration remained unchanged. Figure 5-12 displays the results, and includes the original figures for a system without a deferrable load strategy.

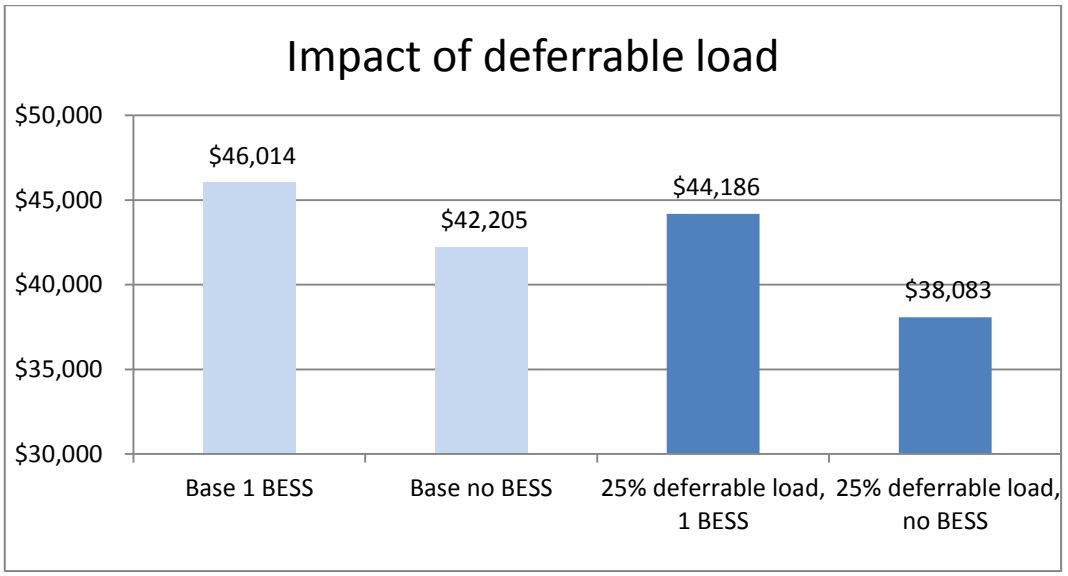

Figure 5-12. Impact of deferrable load on base system NPC.

The most important observation that can be inferred from Figure 5-12 is the NPC gap when comparing the influence of a deferrable load to the base case. Although a deferrable load reduces the NPC for systems with one BESS and with no BESS, the NP cost gap increases with the deferrable load strategy. Without a deferrable load strategy, the NP cost gap is about $3 800 in favour of a system with no BESS. The use of a deferrable load strategy increases the NP cost gap to about $6 100 in favour of a system with no BESS.

5.13 Changing the limits of state of charge and state of discharge

The tenth simulation aimed to examine the impact of changing the settings of the state of charge and discharge limits. Charging limits were varied from 90% to 100% and discharge limits from 15% to 30%, in 5% increments. To minimise simulation time, the analysis was conducted using the economic scenario most favourable to BESS, of a 6.5% discount rate, combined with 2% inflation. The original assumption of 15% discharge to 100% charge yielded the lowest NPC. In this economic scenario, the worst performer was a SOC range of 30% to 90%; NPC-wise was $44 415 vs. $43 514, about $900 more costly than the original SOC configuration (but this would also probably extend the lifetime of the battery).

5.14 Group-purchase discount

This simulation aimed to examine the impact of buying batteries in bulk, such as in a group purchase scheme. A 30% discount was applied to the original $6 100 battery only (not installation or controller costs), resulting in an up-front BESS cost of $6 170. This resulted in an NPC of $43 075, still marginally more costly than the $42 205 without BESS at all.

5.15 Break-even BESS cost

This scenario aimed to determine the 'break-even' BESS price when compared to the same base system with no BESS. Discounts of 30%, 35%, and 40% discounts were applied to the entire BESS system. The results are displayed in Figure 5-13.

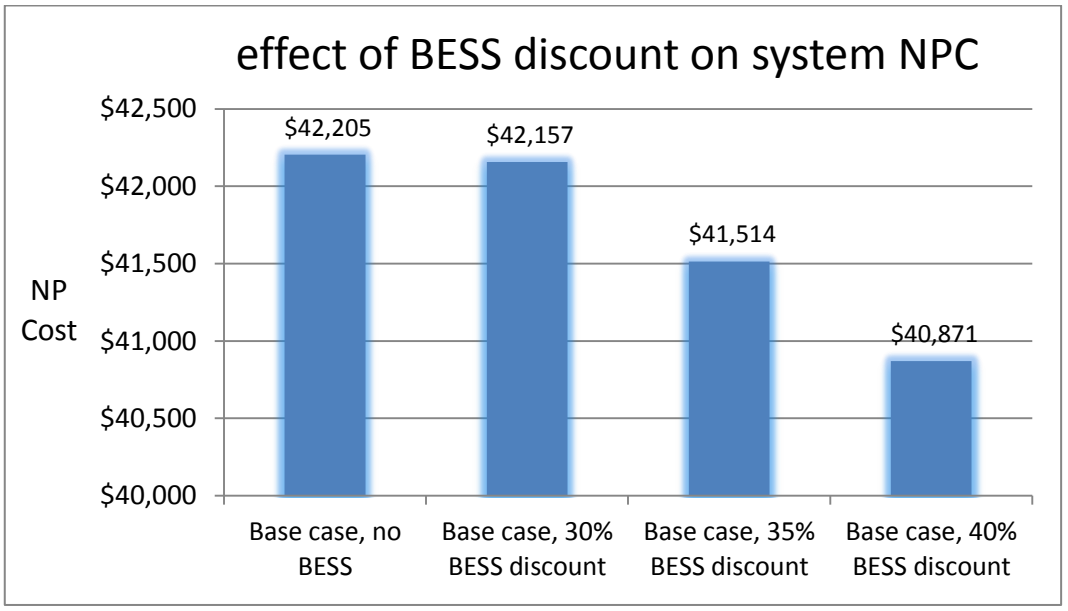

Figure 5-13. BESS break-even point: effect of BESS discounting on NPC

Compared to the base system with no BESS value of $42 205, it appears that BESS needs slightly less than a 30% price reduction to become economically feasible under the modelled system parameters. However, a system without a BESS would also require a smaller, less expensive inverter.

5.16 Impact of BESS control scheme modification

To determine the influence of the chosen control scheme, this set of simulations looked at changing the control scheme, using the same AGL tariff 12. In this case, four different modifications to the original control scheme were chosen. Table 5.1 summarises the changes made compared to the original scheme.

Table 5.1. Effect of BESS control modification on NPC.

Scheme modification	**Original parameterisation**	**NPC change**
Grid charging fine during shoulder and off-peak	Charging only permitted during off-peak hours	nil
Grid charging fine during shoulder and off-peak; Prohibit BESS discharging during off-peak hours	Charging only permitted during off-peak hours; Discharging permitted any time it was deemed economically feasible	nil
Prohibit BESS discharging during off-peak hours	Discharging permitted any time it was deemed economically feasible	nil
Prohibit BESS discharging during off-peak hours; Prohibit weekday shoulder period discharge to load.	Discharging permitted any time it was economically feasible	nil

For each of the four modifications to the original control scheme, the NPC for each economic scenario was exactly the same as the original scheme. Recall that the base control case was no battery discharging or battery grid sales during off peak, no grid charging or BESS discharge to grid during the weekday shoulder period, no battery charging at all from PV, wind, or grid during the peak (and no discharge to grid by BESS), and no battery charging from the grid during weekend shoulder period.

The fact that none of the control scheme modifications resulted in a change to the NPC, suggests that HOMER was able to easily identify the most optimal control scheme based on the TOU tariff. It also suggests that grid charging is optimal during off-peak charging only, and that BESS discharging is not economically sound during off-peak or weekend shoulder periods. Finally, the results support the original design of the BESS power flow control regime according to section 3.7.13.

5.17 Retailer scenarios

The final simulation attempted to determine the impact of existing tariff regimes offered by retailers. The tariff regimes of five retailers including the base case used in the modelling are shown in Table 5.2. The NPC of the base system for the five tariff regimes are displayed in Figure 5-14.

Table 5.2. Selected Queensland electricity retailer tariffs, (Australian Energy Regulator 2016).

Retailer	**Peak ($/kWh)**	**Shoulder ($/kWh)**	**Off-peak ($/kWh)**	**Feed-in ($/kWh)**	**Annual standby Charge ($)**
Base case (AGL)	0.35871	0.2585	0.21065	0.06	420.61
Urth “10”	0.4081	0.2827	0.2024	0.10	467.75
Dodo	0.3283	0.2324	0.1789	0.04	467.33
Energy Australia	0.3520	0.2453	0.1789	0.06	469.76
Simply Energy	0.3283	0.2324	0.1789	0.062	494.48

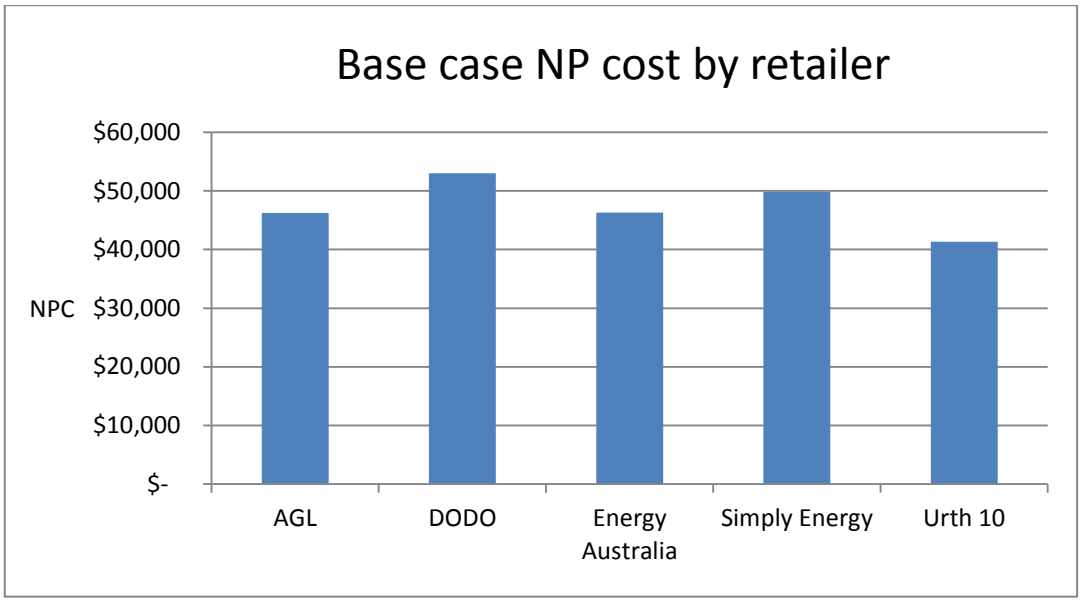

Figure 5-14. Influence of retailer choice on base case NPC.

5.18 Economic analysis

The relatively high initial cost of a BESS system, including its balance of system (BOS) costs such as charge controller and installation, as well as the forecast need for its replacement after 15 years, do not outweigh the reduction in grid energy consumption that it is projected to save. Although BESS prices continue to improve, PV panels also continue to improve in price. At this point in time, the analysis suggests that in the current context, it would be more beneficial to spend additional funds on more PV panels, rather than a BESS system, even with the modest feed-in tariff. It also suggests that the development of deferrable load strategies, which can be implemented with simple timers or more advanced technologies, will retard the uptake of BESS as they may be a more cost-effective cost-reduction strategy.

A number of factors can or will increase the viability of BESS into the future. These factors are summarised as follows.

First, the costs of BESS itself must decrease. This is anticipated to happen in the BESS market but at different rates for different technologies. It is currently possible to apply group discounts on battery purchases in some instances; this obviously favours BESS uptake.

Second, the balances of system costs (installation and controller) need to decrease. Installation costs are less likely to decrease, but wider adoption of grid-tied controllers, as well as maturity and effectiveness of software could see controller costs decline, at least relative to inflation.

Third, increases to existing tariffs favour BESS uptake. SEQ tariffs have increased significantly in the past decade; if utilities determine that widely-distributed BESS systems can have a positive impact on capital expenditures (CAPEX) (e.g. off-setting peak capacity increases) and / or operating expenditures (OPEX) (e.g. in power quality, frequency management, and load balancing), then the implementation of more aggressive TOU, economy tariff regimes, or even the adoption of an RTP tariff will encourage increased BESS penetration. Quite simply, reducing the price of storing a kWh to BESS during off-peak periods, or increasing the price of a kWh not supplied by BESS during peak periods, will improve the economic viability of BESS. However, grid-tied BESSs are still recent entrants to the electricity system. From the DNSP standpoint, it is possible that it may be less expensive (or less risky) to implement grid-level storage technologies instead. It remains to be seen how tariffs will change over time.

Fourth, BESS implementation may be more advantageous for residences with larger loads, to a point. Those with low consumption are less likely to benefit from BESS.

Other factors that will determine the economic favourability of a BESS system are the rate of inflation, generally, as well as the discount rate applied to a system model. As inflation increases, and discount rate decreases, BESS improves its economic viability.

Based on the above factors, it is possible that convergence of several of these factors could make BESS a favourable proposition in the modelled context at the current time. If one assumes a high inflation rate and low discount rate for the economic analysis, a high-consumption household that uses a group discount to purchase a BESS might just find that a BESS system is an economically feasible option. Other assumptions, such as a deflationary trend for batteries, or continued tariff increases beyond the projected rate of inflation would also favour the implementation of a BESS.

To conclude, it is important in any installation to utilise proper control methods for BESS grid integration. The specific characteristics of the battery chosen for the system, and the logic design of the battery controller must be carefully accounted for in the overall BESS design in order to optimise the system economics.

Chapter 6: Conclusion

6.1 Summary

This project linked the optimisation of economic benefits of a HRES / BESS system to the utilisation of real-time parameters stemming from that system's components. This link is the economic-mediated battery charge controller, designed to achieve real-time control of the current sourced from or sunk to the battery, in order to achieve those economic benefits.

Economic optimisation of the system began with the proper sizing and configuration of the individual components, taking into consideration the meteorological, economic, and consumer factors within which the system is to be established, as described in section 3.7 and Chapter 5. Once connected, component values and data streams from those components were used to determine the best economic course of action to take in terms of providing power to service the residential load requirements, as described in sections 3.4, 3.5, and 3.6. For the system modelled in this project, these component values included the maximum rate of charge and maximum rate of discharge for the battery. The component data streams included the power production from the system's solar PV and wind components; the residential load power requirement; the battery SOC; and the time of day as a function of electricity tariff. These variables were then processed to optimise power flows to and from both the grid and the BESS; the processing provided both grid power and BESS power references as summarised in the decision-making flow charts in 3.4.17.

In the case of the BESS power references, these were further processed with information from the system's DC link voltage to determine the optimum BESS current flow. Once this value was determined, appropriate switching control of the BESS two-quadrant DC-DC IGBTs was conducted as described in sections 3.6 and 4.2. Ultimately, this switching control logic culminated from the stream of economic information and decisions that preceded it. In its essence, the control of the switching of the DC-DC converter allows the system owner to store energy in the battery when the costs to do so are low, and to release energy from the battery when the costs to obtain it otherwise from the grid are high. Thus, delivery of optimal economic benefits could be conducted by the economically-mediated controller.

6.2 Important contributions

The two most significant contributions of the present work are (1) a case study clarification of the estimate made by Energex about the BESS cost reductions required to achieve economic viability; and (2) the design of a set of BESS controller logic decision-making procedures as described in section 3.4. Pertaining to (1), although the present work was confined to a specific case study, it did conclude that BESS cost reductions of approximately 30-35% are required to achieve economic parity to a system without a BESS. This compares to the broad estimate of a 50% cost reduction made by Energex (2015). This does not imply that the Energex estimate was incorrect; that estimate was stated over a year prior to this work; throughout which time BESS prices have continued to fall concomitant with tariff increases that exceeded the CPI. Rather, it suggests that BESS are continuing to become less expensive over time, and that their uptake is likely to increase into the mid-2020's as predicted by Energex's peak demand forecasts (Energex 2015). Pertaining to (2), although the procedures were developed for a specific system, the design procedure for the controller logic can be generally applied to other grid-tied BESS systems.

6.3 Recommendations for future work

Transient model

1. Complete the Simulink modelling of the inverter, including grid and load interactions.
2. Develop, in Simulink, the controller architecture used to maintain control of the DC link voltage and the output voltage and current of the inverter.
3. Modelling of the DNSP poles and wires.
4. Incorporate a transient wind resource model and a wind turbine physical model.
5. Incorporate a transient load block model.
6. Investigate the need for changes or additions to the filtering circuitry and switching techniques used for the DC-DC chopper output and the boost MPPT chopper output. It would be worth investigating the technical and financial trade-offs among inductor and capacitor size, circuit configuration, switching rate, switching method, and acceptable voltage and current waveforms.
7. Development of a system with the capability to undergo safe islanding, and investigate the transient response of the system in response to a grid blackout.

Battery controller

1. Because different equivalent circuit configurations exist for the two-quadrant chopper depending on the power reference provided by the system, different plant transfer functions exist at different points in time. It is worth investigating if benefits might be realised from the implementation of switching among multiple controllers, or by dynamically feeding different parameters to the plant transfer function as required by the charging or discharging situation.
2. Undertake development of the battery controller algorithms into software using a real-time systems design approach, such that simulations may be conducted with battery hardware-in-the-loop (HIL).
3. Incorporation of a near-future predictive algorithm based on meteorological forecasts and real-time weather data.
4. Exploration of the potential benefits to DNSPs of either the possible interaction of AFLC or PLC with the local BESS control scheme.

Economic modelling

1. Investigate the economic details of the system applied to different tariff schemes or configurations. For example, it was beyond the scope of the project to investigate system behaviour with Tariff 11, or in schemes using Tariff 31/33. It is also suggested that there may be value to investigate the application of the system in the beyond the scope of the project to work with the now discontinued Queensland FiT of 44c/kWh, because a significant proportion of Queensland residences can still access the tariff until 2028; these residences may be interested in how BESS might be effectively implemented in their context.
2. Testing of different load profiles for the same geographical context may be worth exploring. Rather than simply increasing or decreasing the *scale* of the load model as was done in this project, it is worth investigating different *shapes* of load profiles. Specifically, it is worth investigating what type of load profile is likely to achieve the greatest economic benefit from the application of a BESS, because these users would be more likely to have a desire to implement such strategies.
3. Test systems for commercial and/or industrial installations that use most of their electricity during the day time hours.
4. Investigation and quantification of the value of objectives that are not directly economic, such as minimum emergency energy and power capacities.
5. Development of appliance level profiles to develop a total load profile.

6. Investigate the application of other types of batteries to the BESS system, and evaluate their economic (and transient) behaviours.

Weather

1. Rather than making an arbitrary choice of location to study, as was done in the present work, it would be worth conducting a Queensland (or otherwise) geographical analysis to determine optimal wind and/or solar PV installation.
2. Conduct Monte Carlo modelling of sunshine and/or wind to estimate the probabilities that a particular location may have a string of cloudier or windier years, for example, and the influence that this might have on the economic viability of the project.
3. Investigate the impact of azimuth variation on NPC. It is possible that a westerly azimuth would increase local power production during the TOU peak period; it would be interesting to see how variations in thermal efficiencies and TOU peak period production would interplay with PV generation shortfalls in the earlier part of the day.
4. Optimisation of excess PV power utilised with the control of hot water thermostats.

DNSP benefits

1. Exploration of the potential benefits to DNSPs of tariff-mediated or enterprise-based BESS aggregation, including peak shaving, load-balancing, and power quality

6.4 Achievement of objectives, aims, and project specification

Of the three aims described in the introduction, two were met. First, this case study has contributed additional information about the estimated cost reductions required by BESS to become economically feasible. Second, the case study partially refuted and partially supported the original hypothesis, that is, "it may be cheaper in some individual customer circumstances to run a hybrid renewables / battery energy storage system (BESS) system than one that relies purely on grid power, even without subsidies". Generally, it is not cheaper at the present time to incorporate a BESS system in the context modelled by the project. However, combining the use of certain assumptions under certain conditions could result in an assessment that is favourable to BESS implementation. Third, the

project has provided a base on which to continue work in the area, albeit not to the extent originally hoped for as far as the transient model is concerned.

In the project, four of the five primary objectives specified in section 1.4 were met. First, the development of an economic supervisory battery charging control algorithm was completed. Second, a system model was developed, and suitable meteorological and load models were developed. However, , as far as the fourth objective is concerned, the system model was not fully developed to the AC side, so it is unknown if the controller and system is capable of meeting applicable regulations and standards for the transient state. Fifth, the optimal size of the selected BESS was determined for a number of different combinations and permutations of system and contextual parameters for this particular case study.

One of the two secondary objectives was met. Attainment of the first secondary objectives was not possible as AS/NZS 5139 is still under development. The second objective, building in and developing the model's capacity for sensitivity analysis, this was achieved largely because the HOMER modelling software was excellent at performing sensitivity analysis.

In terms of completing the work set in the project specification (Appendix A), items 1 and 2 were met, with the assistance of mathematical models already developed in HOMER and Simulink. Item 3 was partially met, but without the explicit development of an objective function. However, the controller algorithm was developed with an indirect objective function, that is, maximisation of economic returns to the system owner, based on the close evaluation of the context within which the controller algorithm was developed. Item 4 was met, as a sound economic mathematical model was developed for Nambour's meteorological patterns, based on historical data sets, as well as a sound transient model for transient clouding conditions. Item 5 was met, although as it turned out, this was not particularly important for either the long-term economic or short-term transient analyses. Item 6 was met, as a residential load profile was not constructed for just a single day, but actually for 24 different types of days (weekend and weekday profiles for each month of the year). Item 7 was completed in HOMER. Item 8 was only partially fulfilled, as transient modelling was conducted only for the BESS with controller on the DC side and solar PV with MPPT controller on the DC side. Item 9 was fulfilled to completion, as annual profiles were designed and implemented for meteorology, system components' power production, residential loads, and simulation results. Item 10 was fulfilled to completion in a rather straight-forward manner by HOMER, after the completion of items 4, 6, 7, and 9. Item 11 was completed for a variety of different

combinations of system components, load patterns, and tariffs. As for the discretionary elements, Item 12 was demonstrated for the HOMER modelling only. Item 13 was not attempted. Item 14 was demonstrated under the label of net present cost, rather than net present value. Item 15 was conducted in HOMER. Items 16, 17, and 18 were not attempted.

6.5 Key project learnings

The first key learning was the use of the two pieces of modelling software, Simulink, and HOMER. The author was not experienced with either before the project, but is now able to develop reasonably simple models in both applications.

The second key learning was the realisation that economic modelling is highly dependent on a number of characteristics, and that while it is possible to make general statements about BESS, its feasibility is really best assessed on a case-by-case basis.

The third key learning was the exposure to a myriad of power electronics circuits and techniques. Although only the very basic techniques were applied in the present work, it is clear that the field of power electronics offers a rather diverse set of tools that can be applied to solve a variety of problems in the renewable energy and energy storage knowledge spaces.

The final key learning is the consolidation of the concept of lifelong learning. This project made it clear that there is much to learn about many topics, ideas, and concepts; the learning journey has only just started.

List of references

Ahfock, A 2014, *Power electronics principles and applications: Study book 2*, University of Southern Queensland, Toowoomba.

Al-Saedi, W, Lachowicz, SW, Habibi, D & Bass, O 2013, 'Power flow control in grid-connected microgrid operation using particle swarm optimization under variable load conditions', *International Journal of Electrical Power & Energy Systems*, vol. 49, pp. 76-85.

Al Badwawi, R, Abusara, M & Mallick, T 2015, 'A review of hybrid solar pv and wind energy system', *Smart Science*, vol. 3, no. 3, pp. 127-138.

Alibaba.com 2016, *Trina solar panel 255w with original package and label*, viewed 03 August 2016, <https://www.alibaba.com/product-detail/Trina-solar-panel-255W-with-original_60269599853.html?spm=a2700.7724857.0.0.FnxI2s>.

Asmus, P 2010, 'Microgrids, virtual power plants and our distributed energy future', *The Electricity Journal*, vol. 23, no. 10, pp. 72-82.

Australian Broadcasting Corporation, *Battery powered homes*, Catalyst, viewed 01 April 2016, <http://iview.abc.net.au/programs/catalyst/SC1502H001S00>.

Australian Bureau of Meteorology 2016a, *Climate data online*, viewed 31 March 2016 <http://www.bom.gov.au/climate/data/>.

Australian Bureau of Meteorology 2016b, Nambour climate data, 2008-2016, *In:* Australia Bureau of Meteorology Climate Data Services (ed), Australia.

Australian Bureau of Statistics 2016a, *6401.0 - consumer price index, Australia - past releases*, viewed 08 August 2016, <http://www.abs.gov.au/AUSSTATS/abs@.nsf/second+level+view?ReadForm&prodno=6401.0&viewtitle=Consumer%20Price%20Index,%20Australia~Jun%202016~Latest~27/07/2016&&tabname=Past%20Future%20Issues&prodno=6401.0&issue=Jun%202016&num=&view=&>.

Australian Bureau of Statistics 2016b, *6401.0 - consumer price index, Australia, jun 2016*, viewed 27 July 2016, <http://www.abs.gov.au/ausstats/abs@.nsf/mf/6401.0>.

Australian Energy Regulator 2016a, *Energy made easy*, viewed 30 July 2016, <https://www.energymadeeasy.gov.au>.

Australian Energy Regulator 2016b, *Search for energy offers*, viewed 17 July 2016, <https://www.energymadeeasy.gov.au/offer-search>.

Australian Stock Exchange 2016, *Bond prices*, viewed 29 August 2016, <http://www.asx.com.au/asx/markets/interestRateSecurityPrices.do?type=GOVERNMENT_BOND>.

Australian Trade and Shipping 2016, *Quick price from prime ports to Australian ports for less than a container load of cargo*, viewed 03 August 2016, <http://australiatrade.com.au/Shipping/Price/Imports/index.htm>.

Badescu, V 1997, 'Verification of some very simple clear and cloudy sky models to evaluate global solar irradiance', *Solar Energy*, vol. 61, no. 4, pp. 251-264.

Basu, AK, Bhattacharya, A, Chowdhury, S & Chowdhury, SP 2012, 'Planned scheduling for economic power sharing in a chp-based micro-grid', *Power Systems, IEEE Transactions on*, vol. 27, no. 1, pp. 30-38.

Batarseh, I 2011, 'Chapter 4: The power MOSFET', in MH Rashid (ed), *Power electronics handbook*, 3rd ed, Butterworth-Heinemann, Oxford, UK, pp. 43-71.

Berry, A, Motlagh, O, Grozev, G, Ren, Z, Perfumo, C, Lane, B & Anticev, J 2015, *Energex customer load profile market segmentation and clustering*, Australia, CSIRO and Energex.

Blum, AF & Long Jr., RT 2016, *Hazard assessment of lithium ion battery energy storage systems: Final report*, Exponent, Inc., Maryland, USA, viewed 01 July 2015 <http://www.nfpa.org/news-and-research/fire-statistics-and-reports/research-reports/other-research-topics/hazard-assessment-of-lithium-ion-battery-energy-storage-systems>.

Bose, BK 2014, 'Energy, global warming and impact of power electronics in the present century', in H Abu-Rub, M Malinowski & K Al-Haddad (eds), *Power electronics for renewable energy systems, transportation and industrial applications*, 1st edn, John Wiley & Sons, Ltd., viewed 01 October 2015, <http://media.johnwiley.com.au/product_data/excerpt/39/11186340/1118634039-13.pdf>.

Caliao, ND & Zahedi, A 2000 'Statistical modeling of radiation and wind speed for pv/wind hybrid system', *Renewable Energy Transforming Business*, viewed 26 April 2016, <http://solar.org.au/papers/00papers/Caliao.PDF>.

Caruana, C, Sattar, A, Al-Durra, A & Muyeen, SM 2015, 'Real-time testing of energy storage systems in renewable energy applications', *Sustainable Energy Technologies and Assessments*, vol. 12, pp. 1-9.

Czarkowski, D 2011, 'Chapter 13: DC-DC converters', in MH Rashid (ed), *Power electronics handbook*, 3rd ed, Butterworth-Heinemann, Oxford, UK, pp. 249-264.

Daud, MZ, Mohamed, A & Hannan, MA 2013, 'An improved control method of battery energy storage system for hourly dispatch of photovoltaic power sources', *Energy Conversion and Management*, vol. 73, pp. 256-270.

Di Giorgio, A & Liberati, F 2014, 'Near real time load shifting control for residential electricity prosumers under designed and market indexed pricing models', *Applied Energy*, vol. 128, pp. 119-132.

Dieulot, J-Y, Colas, F, Chalal, L & Dauphin-Tanguy, G 2015, 'Economic supervisory predictive control of a hybrid power generation plant', *Electric Power Systems Research*, vol. 127, pp. 221-229.

Dufo-López, R 2015, 'Optimisation of size and control of grid-connected storage under real time electricity pricing conditions', *Applied Energy*, vol. 140, pp. 395-408.

Ecoelectric 2016, *12 kW 48 panel solar PV system | ABB and Trina*, viewed 03 August 2016, <https://www.ecoelectric.com.au/shop/12kw-48-panel-solar-pv-system-abb-and-trina.html>.

Elliston, B, Macgill, I & Diesendorf, M 2013, 'Least cost 100% renewable electricity scenarios in the australian national electricity market', *Energy Policy*, vol. 59, pp. 270-282.

Energex Limited 2015, *Energex distribution annual planning report 2015/16-2019/20*, Energex, Brisbane, viewed 05 August 2016, <https://www.energex.com.au/__data/assets/pdf_file/0006/283677/2015-DAPR-Volume-1.pdf>.

Energex Limited 2016, *Energy consumption data*, viewed 02 August 2016, <https://www.energex.com.au/about-us/our-commitment/to-our-customers/connecting-with-you/data-to-share>.

Engineers Australia 2010 *Our code of ethic*s, viewed 12 April 2016, <http://www.engineersaustralia.org.au/sites/default/files/shado/About%20Us/Overview/Governance/codeofethics2010.pdf>.

Fairchild Semiconductors 2016, *MOSFETs search parameters*, viewed 08 September 2016, <https://www.fairchildsemi.com/products/discretes/fets/mosfets/#rq=MOSFET_POLARITY=%22N%22%7CMOSFET_BVDSS%3E250>.

Fathima, AH & Palanisamy, K 2015, 'Optimization in microgrids with hybrid energy systems – a review', *Renewable and Sustainable Energy Reviews*, vol. 45, pp. 431-446.

Fei, D, Peng, L, Bibin, H, Fei, G, Chengdi, D & Chengshan, W 2010, 'Modeling and simulation of grid-connected hybrid photovoltaic/battery distributed generation system', *China International Conference on Energy Distribution 2010 Proceedings*, China, 13-16 September 2010, pp. 1-10.

Gu, W, Liu, W, Wu, Z, Zhao, B & Chen, W 2013, 'Cooperative control to enhance the frequency stability of islanded microgrids with DFIG-SMES', *Energies*, vol. 6, no. 8, p. 3951.

Guangzhou HY Energy Technology Limited Corp 2016, *HYE HY-1000L-48V 1000w/1kw power application Electricity Generator Type wind turbine*, viewed 08 August 2016, <http://www.aliexpress.com/item/HYE-HY-1000L-48V-1000w-1kw-power-application-Electricity-Generator-Type-wind-turbine/1944789484.html?spm=2114.40010508.4.39.7IJAuZ>.

HOMER 2015, 'Help chapter 5.16: generating synthetic solar data', in *Hybrid Optimisation Model for Electric Renewables (computer application)*, HOMER Energy, LLC, USA.

Infineon 2016, *Infineon solution finder*, viewed 01 September 2016, <http://www.infineon.com/cms/en/product/solutionFinder.html?channel=db3a30433cabdd35013ccebb4e4849ae&intc=0540001#!showAllParameters=false&5546d4694909da48014909dc05ad019b_false=100&5546d4694909da48014909dc0d0d0207

_false=500&sort=group&sortField=SMALLEST&5546d4694909da48014909dc081301b1_true=MAX_400.0|MAX_500.0|MAX_600.0|MAX_650.0>.

Integra Energy Group Pty Limited 2016, *Chiko 2 kW flat roof solar racking installation kit*, viewed 04 August 2016, <http://www.ebay.com.au/itm/2KW-FLAT-ROOF-SOLAR-RACKING-INSTALLATION-KIT-Suits-8-x-250W-Panels-/252461760597?hash=item3ac7e4c055:g:NQYAAOxy63FSorK2>.

IPCC 2014, *Climate change 2014: Synthesis report: Contribution of working groups i, ii and iii to the fifth assessment report of the Intergovernmental Panel on Climate Change*, RK Pachauri & LA Meyer (eds), Geneva, Switzerland.

Jargstorf, J, De Jonghe, C & Belmans, R 2015, 'Assessing the reflectivity of residential grid tariffs for a user reaction through photovoltaics and battery storage', *Sustainable Energy, Grids and Networks*, vol. 1, pp. 85-98.

Jun, Z, Junfeng, L, Jie, W & Ngan, HW 2011, 'A multi-agent solution to energy management in hybrid renewable energy generation system', *Renewable Energy*, vol. 36, no. 5, pp. 1352-1363.

Kelly-Detwiler, P 2013 'Relentless and disruptive innovation will shortly affect US electric utilities', *Forbes*,viewed 03 December 2015, <http://www.forbes.com/sites/peterdetwiler/2013/04/18/relentless-and-disruptive-innovation-will-shortly-affect-us-electric-utilities/2/#564a13973a56>.

Keyhani, A 2011, *Design of smart power grid renewable energy systems*, John Wiley & Sons, Inc., Hoboken, New Jersey, USA.

Khadem, SK, Basu, M & Conlon, MF 2011, 'Parallel operation of inverters and active power filters in distributed generation system—a review', *Renewable and Sustainable Energy Reviews*, vol. 15, no. 9, pp. 5155-5168.

Khaligh, A & Onar, OC 2010, *Energy harvesting: Solar, wind, and ocean energy conversion systems*, CRC Press, Boca Raton, FL, USA.

Khalilpour, R & Vassallo, A 2016, 'Planning and operation scheduling of PV-battery systems: A novel methodology', *Renewable and Sustainable Energy Reviews*, vol. 53, pp. 194-208.

King, C 2014, 'Transactive energy: Linking supply and demand through price signals', in FP Sioshansi (ed), *Distributed generation and its implications for the utility industry*, Academic Press, Sydney, pp. 189-204.

Kokic, P, Crimp, S & Howden, M 2014, 'A probabilistic analysis of human influence on recent record global mean temperature changes', *Climate Risk Management*, vol. 3, pp. 1-12.

Koohi-Kamali, S, Tyagi, VV, Rahim, NA, Panwar, NL & Mokhlis, H 2013, 'Emergence of energy storage technologies as the solution for reliable operation of smart power systems: A review', *Renewable and Sustainable Energy Reviews*, vol. 25, pp. 135-165.

Li, M-F, Tang, X-P, Wu, W & Liu, H-B 2013, 'General models for estimating daily global solar radiation for different solar radiation zones in mainland china', *Energy Conversion and Management*, vol. 70, pp. 139-148.

Littelfuse 2016, *Power module: 600 V 150 A IGBT module datasheet*, viewed 01 September 2016, <http://www.littelfuse.com/~/media/electronics/datasheets/power_semiconductors/littelfuse_power_semiconductor_igbt_module_mg06150s_bn4mm_datasheet.pdf.pdf>.

Lucas, A & Chondrogiannis, S 2016, 'Smart grid energy storage controller for frequency regulation and peak shaving, using a vanadium redox flow battery', *International Journal of Electrical Power & Energy Systems*, vol. 80, pp. 26-36.

Mahesh, A & Sandhu, KS 2015, 'Hybrid wind/photovoltaic energy system developments: Critical review and findings', *Renewable and Sustainable Energy Reviews*, vol. 52, pp. 1135-1147.

Mcglade, C & Ekins, P 2015, 'The geographical distribution of fossil fuels unused when limiting global warming to 2 degrees C', *Nature*, vol. 517, no. 7533, pp. 187-190.

Mégel, O, Mathieu, JL & Andersson, G 2015, 'Scheduling distributed energy storage units to provide multiple services under forecast error', *International Journal of Electrical Power & Energy Systems*, vol. 72, pp. 48-57.

Meng, L, Sanseverino, ER, Luna, A, Dragicevic, T, Vasquez, JC & Guerrero, JM 2016, 'Microgrid supervisory controllers and energy management systems: A literature review', *Renewable and Sustainable Energy Reviews*, vol. 60, pp. 1263-1273.

Mulder, G, Six, D, Claessens, B, Broes, T, Omar, N & Mierlo, JV 2013, 'The dimensioning of PV-battery systems depending on the incentive and selling price conditions', *Applied Energy*, vol. 111, pp. 1126-1135.

Nelder, C 2013, *Behind closed doors, utilities grapple with new strategies*, viewed 05 December 2015, <http://www.greentechmedia.com/articles/read/behind-closed-doors-utilities-grapple-with-new-strategies>.

Olson, C, Veltkamp, A & Sinke, W 2014, 'The external costs of electricity generation: A comparison of environmental damage of silicon photovoltaic electricity, produced with different electricity mixes, vs natural gas and coal', *Solar Energy*, vol. 2013, p. 2012.

Oz Wind Engineering 2016, *Masts / towers*, viewed 08 August 2016, <http://www.ozwindengineering.com/Products.php?Cat=Masts>.

Pandey, SK, Mohanty, SR & Kishor, N 2013, 'A literature survey on load–frequency control for conventional and distribution generation power systems', *Renewable and Sustainable Energy Reviews*, vol. 25, pp. 318-334.

Parkinson, G 2016, *Tesla model 3 orders jump to $A18.5 billion – biggest product launch ever*, viewed 17 May 2016, <http://reneweconomy.com.au/2016/tesla-model-3-orders-jump-to-a18-5-billion-biggest-product-launch-ever-11558>.

Patel, MR 2006, *Wind and solar power systems: Design, analysis, and operation*, Taylor & Francis, New York.

Pecan Street Inc. 2015, *The world's largest energy data resource*, The University of Texas at Austin, USA, viewed 03 November 2015, <https://dataport.pecanstreet.org>.

Prime Solar Power Systems 2016, *LG Chem 6.4 kWh lithium battery works with SMA and Sungrow hybrid solar inverters*, viewed 07 August 2016, <http://www.ebay.com.au/itm/LG-CHEM-6-4kwh-Lithium-Battery-works-with-SMA-and-Sungrow-Hybrid-solar-inverters-/122104574468?hash=item1c6dfff204:g:uJcAAOSwWnFWA2SS>.

Quesada, J, Sebastián, R, Castro, M & Sainz, JA 2014, 'Control of inverters in a low voltage microgrid with distributed battery energy storage. Part I: Primary control', *Electric Power Systems Research*, vol. 114, pp. 126-135.

Rahman, HA, Majid, MS, Rezaee Jordehi, A, Chin Kim, G, Hassan, MY & O. Fadhl, S 2015, 'Operation and control strategies of integrated distributed energy resources: A review', *Renewable and Sustainable Energy Reviews*, vol. 51, pp. 1412-1420.

Ratnam, EL, Weller, SR & Kellett, CM 2015, 'Scheduling residential battery storage with solar PV: Assessing the benefits of net metering', *Applied Energy*, vol. 155, pp. 881-891.

Saharia, BJ, Manas, M & Talukdar, BK 2016, 'Comparative evaluation of photovoltaic MPP trackers: A simulated approach', *Cogent Engineering*, vol. 3, no. 1, viewed 01 May 2016, <http://www.tandfonline.com/doi/full/10.1080/23311916.2015.1137206>.

Saib, S & Gherbi, A 2015, 'Simulation and control of hybrid renewable energy system connected to the grid', *5th International Youth Conference on Energy 2015*, 27-30 May 2015, Pisa, Italy, pp 1-6.

Sedić, A, Pavković, D & Firak, M 2015, 'A methodology for normal distribution-based statistical characterization of long-term insolation by means of historical data', *Solar Energy*, vol. 122, pp. 440-454.

Shivarama Krishna, K & Sathish Kumar, K 2015, 'A review on hybrid renewable energy systems', *Renewable and Sustainable Energy Reviews*, vol. 52, pp. 907-916.

Sichilalu, SM & Xia, X 2015, 'Optimal power dispatch of a grid tied-battery-photovoltaic system supplying heat pump water heaters', *Energy Conversion and Management*, vol. 102, pp. 81-91.

Simpson, C 2016, *Australia's first powerwall batteries are already installed in NSW*, viewed 05 March 2016, <http://www.gizmodo.com.au/2016/01/australias-first-powerwall-home-batteries-are-already-installed-in-western-sydney/>.

Soubdhan, T, Emilion, R & Calif, R 2008, 'Classification of daily solar radiation distributions using a mixture of dirichlet distributions', *Aricle soumis `a Solar Energy*, no. <hal-00289567>, viewed 20 April 2016, < https://hal.archives-ouvertes.fr/hal-00289567/document>.

Standards Australia 2005, *Grid connection of energy systems via inverters - installation requirements*: 4777.1-2005, Standards Australia, Australia.

Standards Australia 2013, *Smart grid vocabulary*: AS 5711-2013, Standards Australia, Australia.

Standards Australia 2014, *Installation and safety requirements for photovoltaic (PV) arrays* AS/NZS 5033:2014, Standards Australia, Australia.

Standards Australia 2015a, *El-042 - renewable energy power supply systems - published standards*, viewed 12 April 2016, <http://sdpp.standards.org.au/ActiveProjects.aspx?SectorName=Electrotechnology%20and%20Energy&CommitteeNumber=EL-042&CommitteeName=Renewable%20Energy%20Power%20Supply%20Systems%20&%20Equipment#simple4>.

Standards Australia 2015b, *Standards development public portal: El-048 - wind turbine systems*, viewed 12 April 2016, <http://sdpp.standards.org.au/ActiveProjects.aspx?SectorName=Electrotechnology%20and%20Energy&CommitteeNumber=EL-048&CommitteeName=Wind%20Turbine%20Systems#simple4>.

Standards Australia 2016a, *Energy storage standards consultation paper 1*, viewed 02 June 2016, <http://www.standards.org.au/OurOrganisation/News/Documents/Standards%20Australia%20Energy%20Storage%20Consultation%20Paper.pdf>.

Standards Australia 2016b, *Search "batteries"*, viewed 15 May 2016, <https://www-saiglobal-com.ezproxy.usq.edu.au/online/autologin.asp>.

Standards Australia 2016c, *World first on demand response of electrical energy storage*, viewed 27 September 2016, <http://www.standards.org.au/OurOrganisation/News/Documents/World%20First%20on%20Demand%20Response%20of%20Electrical%20Energy%20Storage.pdf>.

Subburaj, AS, Pushpakaran, BN & Bayne, SB 2015, 'Overview of grid connected renewable energy based battery projects in USA', *Renewable and Sustainable Energy Reviews*, vol. 45, pp. 219-234.

Sulthan, SM & Devaraj, D 2014, 'Simulation and analysis of stand-alone photovoltaic system with boost converter using Matlab/Simulink', *Proceedings of the IEEE International Conference on Circuit, Power and Computing Technologies - ICCPCT-2014*, 2014 Tamilnadu, India, DOI: 10.1109/ICCPCT.2014.7054991.

Sungwoo, B & Kwasinski, A 2012, 'Dynamic modeling and operation strategy for a microgrid with wind and photovoltaic resources', *Smart Grid, IEEE Transactions on*, vol. 3, no. 4, pp. 1867-1876.

Supercheapsolaroz2016 2016, *17kw grid tied solar inverter sma sunny boy tripower 17000tl-10 three phase*, viewed 05 August 2016, <http://www.ebay.com.au/itm/17kW-Grid-Tied-Solar-Inverter-SMA-SUNNY-BOY-TRIPOWER-17000TL-10-THREE-PHASE-/252344324537?hash=item3ac0e4d1b9:g:JygAAOSw5VZXA5zf>.

The Treasury New Zealand 2002, *Determining the discount rate for government projects*, viewed <http://www.treasury.govt.nz/publications/research-policy/wp/2002/02-21/07.htm>.

Tyagi, AK 2012, *MATLAB and Simulink for engineers*, Oxford University Press, New Delhi, India.

Upadhyay, S & Sharma, MP 2014, 'A review on configurations, control and sizing methodologies of hybrid energy systems', *Renewable and Sustainable Energy Reviews*, vol. 38, pp. 47-63.

Walton, R 2015, *Stem, PG&E bid aggregated energy storage into CAISO real-time market*, viewed 30 September 2015, <http://www.utilitydive.com/news/stem-pge-bid-aggregated-energy-storage-into-caiso-real-time-market/405218/>.

Wang, X, Palazoglu, A & El-Farra, NH 2015, 'Operational optimization and demand response of hybrid renewable energy systems', *Applied Energy*, vol. 143, pp. 324-335.

Wang, Y, Tan, KT & So, PL, 'Coordinated control of battery energy storage system in a microgrid', *Proceedings of the 2013 Power and Energy Engineering Conference (APPEEC)*, Kowloon, Hong Kong, pp. 1-6.

Wollny, M & Hermes, M 2007, 'AC coupled hybrid systems and mini grids', *Proceedings of the 45th Australia New Zealand Solar Energy Society*,Alice Springs NT, Australia.

Yarhands, DA 2013, 'Probability distributional analysis of hourly solar irradiation in Kumasi-Ghana', *International Journal of Business and Social Research,* vol. 3, no. 3, pp. 63-75.

Yoon, Y & Kim, Y-H 2016, 'Effective scheduling of residential energy storage systems under dynamic pricing', *Renewable Energy,* vol. 87, March 2016, pp. 936-945.

Zeng, Z, Yang, H, Zhao, R & Cheng, C 2013, 'Topologies and control strategies of multi-functional grid-connected inverters for power quality enhancement: A comprehensive review', *Renewable and Sustainable Energy Reviews,* vol. 24, pp. 223-270.

Zheng, M, Meinrenken, CJ & Lackner, KS 2014, 'Agent-based model for electricity consumption and storage to evaluate economic viability of tariff arbitrage for residential sector demand response', *Applied Energy,* vol. 126, pp. 297-306.

Zhou, H 2016, ELE3307 *Real-time systems study book*, University of Southern Queensland, Toowoomba, Australia.

Appendix A: Project Specification

For: C. Morgan Smith

Title: "Battery SMART charge controller / combined co-gen grid connected inverter design and simulation design confirmation for domestic sustainable energy production 5 - 10 kW PV and 0.5 - 1 kW wind generator."

Major: Power engineering

Supervisors: Dr. Narottam Das
Mr. Andreas Helwig

Enrolment: ENG4111 – EXT S1, 2016 ENG4112 – EXT S2, 2016

Project Aim: Design of a battery charging control algorithm that maximises economic benefit of a grid-tied hybrid renewable energy system; demonstration of its efficacy in simulation

Programme: Issue A – for initial consideration, 05/03/2016

1. Design of, and component selection for, the proposed physical system
2. Evaluate and specify mathematical models of system components
3. Specify and design an economic controller algorithm including control technique, objective function, constraints, and mathematical models of system parameters
4. Mathematically model a specific, local meteorological pattern for simulation purposes
5. Derive system power production profile, based on steps 2 and 4, for *a single day*
6. Specify and derive a typical residential load profile for *a single day*
7. Conduct steady-state simulation modelling in HOMER
8. Model and test the transient state of system behaviour in SIMULINK
9. Repeat steps 4 to 7 for *annual* profiles
10. Repeat steps 4 to 7 for expected BESS lifetime
11. Economically optimise BESS capacity for the system, location, and profiles specified in steps 1 to 6 and 10, considering charge and discharge rates and depths, expected life, and cost.

Time and resources permitting

12. Demonstrate algorithm's flexibility to adapt to ranges of system size specified in the title, as well as other control logic components; for example, location/tariff
13. Repeat steps 1 to 11, changing only the BESS technology type
14. Conduct NPV analysis of system
15. Conduct economic analysis of HRES with / without BESS and controller
16. Test the controller algorithm using hardware-in-the-loop techniques
17. Repeat steps 4 to 6 using Monte Carlo technique
18. Repeat Step 3 with an alternative control technique.

Appendix B: Consequential effects and ethical responsibility

B.1 Sustainability issues

Sustainability is at the core of the author's rationale for making a career change to electrical engineering. Based on the author's experience as a science and mathematics teacher and other background knowledge, it is the opinion of the author that climate change is the issue of our times. The earth provides the physical framework and resource base for society's agricultural, economic, political, and sociological frameworks. Distortion of the physical parameters of the atmosphere such as temperature, hydrosphere such as pH, and of the land such as moisture levels can already be seen in examples as significant declines in Artic sea ice volume and areal extent, bleaching of the Great Barrier Reef, and the Russian and Canadian boreal forest fires of recent years, and three straight months of the global average monthly temperatures at unprecedented, i.e. record, values.

As mentioned in the introduction, there is an exceedingly high probability that human fossil fuel burning is causing global warming. It is hoped that the present dissertation will provide a small contribution to the solution of the issue. It is proposed that it will do so by adding to the case for increasing the penetration of renewable energy sources on the distribution grid, which will have the flow-on effect of reducing coal and gas as energy sources for electricity production. Coal and gas, of course, emit carbon dioxide, which is a greenhouse gas, which exacerbate global warming.

B.2 Ethical issues

The ethical issues outlines in this section are based on Engineers Australia's Code of Ethics (Engineers Australia 2010).

The first section of the Code, "Demonstrate Integrity" includes "Act on the basis of a well-informed conscience". Section 5.1 describes how this dissertation seeks act on the author's conscience. It also includes "respect the dignity of all persons"; acting to stem climate change does this because some of the complications of climate change, i.e. weather-related disasters, have the capacity to remove a person's dignity by removing the capacity to provide for oneself and their family.

The second section of the Code, "Practise Competently" includes "Maintain and develop knowledge and skills". Development of this dissertation has already expanded and deepened the candidate's knowledge and skills in a number of areas including: systems design; proficiency with computer-based applications; mathematical modelling involved

with power converters, solar, wind, and battery power production; control schemes; and simulation modelling of meteorological and load parameters. This section also includes "Act on the basis of adequate knowledge". This quality will be tested in the synthesis of this dissertation.

The third section of the Code, "Exercise Leadership", includes "Communicate honestly and effectively, taking into account the reliance of others on engineering expertise". For the current work to act as a starting point for future work by others and the candidate, honest and effective communication means that this dissertation needs to be both objective and succinct.

The fourth section of the Code, "Promote Sustainability" includes "Practice engineering to foster the health, safety and wellbeing of the community and the environment" and "Balance the needs of the present with the needs of future generations". These two points are covered in the context of climate change in section 5.1.

Appendix C: Safety and Standards

C.1 Standards applicable to batteries and battery charging

AS 2676.1-1992: Guide to the installation, maintenance, testing and replacement of secondary batteries in buildings - Vented cells

AS 2676.2-1992: Guide to the installation, maintenance, testing and replacement of secondary batteries in buildings - Sealed cells

AS 3011.1-1992: Electrical installations - Secondary batteries installed in buildings - Vented cells

AS 3011.2-1992: Electrical installations - Secondary batteries installed in buildings - Sealed cells

AS 4044-1992: Battery chargers for stationary batteries

AS 4086.1-1993: Secondary batteries for use with stand-alone power systems - General requirements

AS 4086.2-1997: Secondary batteries for use with stand-alone power systems - Installation and maintenance

AS/NZS 3017:2007: Electrical installations - Verification guidelines

AS/NZS 4755.3.5:2016: Demand response capabilities and supporting technologies for electrical products - Interaction of demand response enabling devices and electrical products - Operational instructions and connections for grid-connected electrical energy storage (EES) systems

C.2 Lithium-ion battery storage risk and mitigation strategies

As summarised by Blum and Long Jr. (2016), much is not understood about the hazards of Li-ion ESS and related risk mitigation strategies. Work is needed to resolve gaps, conflicting statements, and contradictions within existing fire codes and regulations in the USA. A few existing international standards provide limited guidance, and development is underway on a number of others. No AS/NZS standards exist, although there is probably scope for their inclusion in AS/NZS 5319, which was still in the consultation and development phase as of October 2016. The gaps in the fire and safety knowledge is reflected by Li-ion technology's "high energy density coupled with a flammable organic, rather than aqueous, electrolyte (which) has created a number of new challenges with regard to the design of batteries containing Li-ion cells, and with regard to fire suppression" (Blum & Jr 2016 p. 8). Under abnormal heating conditions, it is possible that hydrocarbon-based electrolytes within the Li-ion cell will evaporate and escape the cell. Materials that may escape the cell include volatile organic compounds (VOCs), hydrogen gas, carbon monoxide (CO) and carbon dioxide (CO_2), metal oxide particulates, and gaseous fluoride compounds, at temperatures that may exceed 600 degrees Celsius at the point of exit.

Blum and Long Jr. (2016) observed outdoor tests of internal and external ignition of single units of the commercial sized 100 kWh Tesla Powerpack. Temperatures observed at the external surface of the Powerpack cabinet during the external ignition test would not cause ignition of combustibles if the manufacturer's clearance limits were adhered to. However, it experienced large flames at the top surface, and although manufacturer's recommendations are for five feet of vertical clearance, Blum and Long Jr. (2016) suggested that this may not be adequate in some circumstances, and that vertical clearance be evaluated during system installations. Hydrogen fluoride (HF) gas was detected in concentrations that exceed recommended exposure limits; it was recommended that the use of standard breathing equipment be used by firefighters battling outdoor blazes involving Li-ion ESS. It was also suggested that indoor systems be augmented with ventilation equipment.

A summary of the hazards, and control measures if identified or suggested, are summarised in Table C.1. Blum and Long Jr. (2016) recommended that further research be conducted in the areas of fire suppression techniques, fire and toxic gas behaviour within enclosures, and the influence of additional proximal units on fire spread.

Table C.1. Li-ion BESS hazards and controls, adapted from Blum and Long Jr. (2016).

Hazard	**Controls**
Heat emissions during a fire	Use manufacturer's recommendations for clearances to combustible materials Consider additional vertical clearance - evaluate during system design / installation
Hydrogen fluoride gas emission beyond exposure limits	Standard firefighting breathing equipment Ventilation of indoor systems
Other hot toxic gas expulsion (VOCs, hydrogen, CO, CO2, fluoride compounds)	Not tested
Hot particulate matter expulsion (metal oxides)	Not tested
Flammable gas emission into existing fire (hydrogen gas, VOCs)	Not tested

C.3 Solar PV risk and mitigation strategies

Section 3 of AS/NZS 5033:2014 (Standards Australia 2014) makes specific reference to safety issues of solar PV installations. These include electric shock, earth faults, overcurrent, and lightning/overvoltage risks.

Section 5.4 specifically refers to, and is titled as, "fire emergency information". Section 5.4.1 specifies the installation of a sign installed on the building's main switchboard, visible when the door is open, stating the array location, short circuit current and open circuit voltage. Section 5.4.2 specifies the installation of a prominent green reflective circular sign on or very close to the meter box and main switchboard with the two letters "PV".

Table C.2 Solar PV hazards and risk controls.

Hazard	**Controls**	**Reference to AS/NZS 5033:2014**
Short circuit current	For protection against electric shock, "Components and cable in PV arrays shall be protected by double or reinforced insulation between any live conductor and any earthed or exposed conductive part".	3.2
	Note that detection may be difficult because such faults may approach "normal full load currents".	2.1.8
Earth fault	"Earth fault protection and alarm, or shutdown, or both could be required…to reduce the risk of fire".	2.1.8
	Earth fault protection depends on "the type of system earthing" and "power converter equipment (PCE)". "PCE charge controllers…shall also provide fault detection and alarm functions".	3.4.1
	An external earth fault alarm must also be installed for LV PV systems.	3.4.3

Overcurrent	Properly specified CBs or fuses in accordance with sections 4.3.4 or 4.3.8, respectively. Individual PV strings should use fuses for string overcurrent protection, not CBs. Subarray overcurrent protection may be required but this depends on the size of the array.	3.3.2 3.3.5.2
Additional overcurrent protection for integrated BESS systems	**Additional protection is required for hybrid BESS/PV systems:** In PV systems using BESS, BESS are a 'source of high prospective fault currents and shall have fault current protection installed…generally between the battery and charge controller', and for all active conductors. If CBs are used, they must be appropriately rated and non-polarized. "PV array cable overcurrent protection is only required for systems connected to batteries".	2.1.7 3.3.3 3.3.5.3
Lightning	Only required if the array changes the local physical profile significantly	3.5.1
Overvoltage	Avoidance of wiring loops, surge protector installation, and shielding of long cables.	3.5.2

C.4 Personal project safety

As this dissertation is to be carried out entirely in the realm of simulation, no safety issues are proposed for this dissertation beyond the normal risk mitigation of injuries related to computer work at stationary desktop and chair.

Appendix D: Simulink BESS controller model

Simulink BESS controller logic block

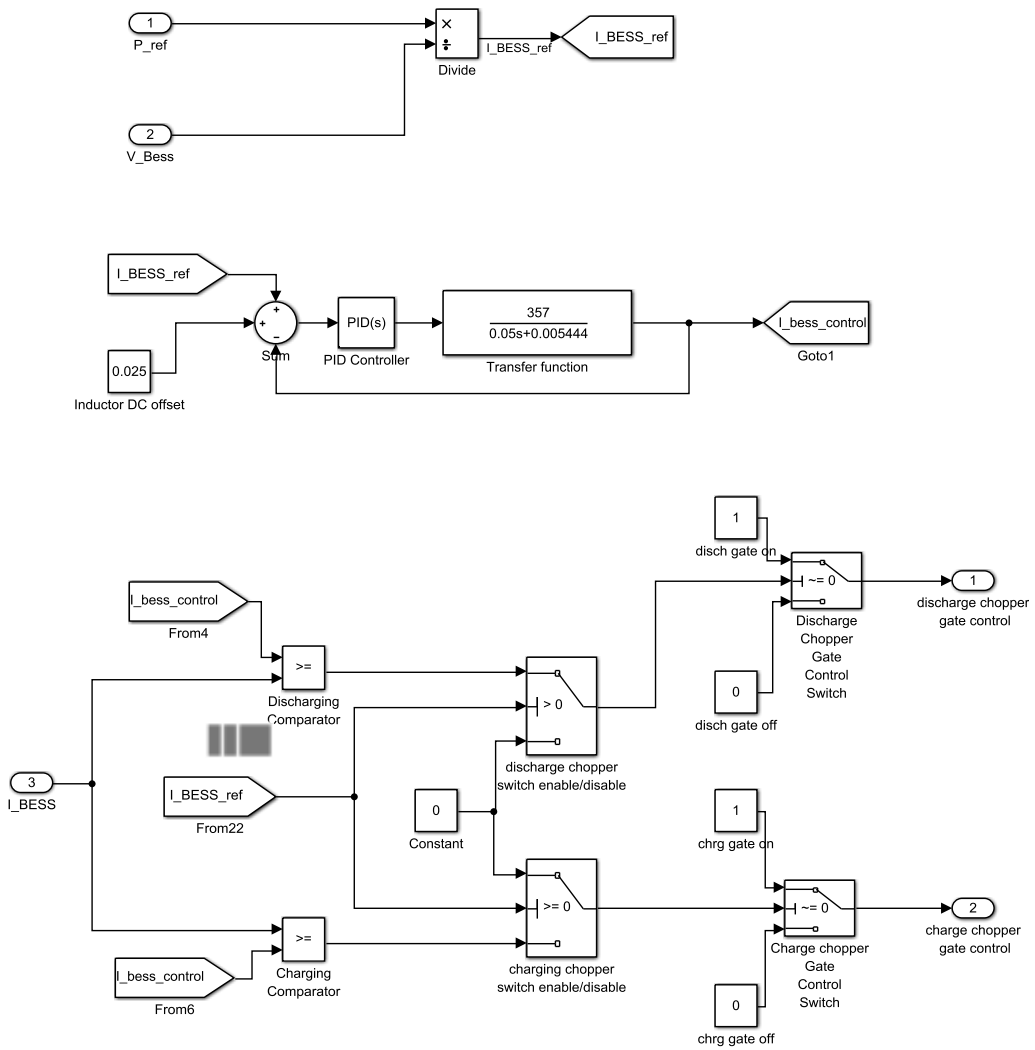

Figure D-1. Battery controller for IGBTs' gate pulses.

Appendix E: Data sheets

E.1 LG Chem RESU 6.4 EX Battery pack specifications

Nominal voltage	51.8 V
Operating voltage	45.2 V to 58.1 V
Nominal capacity	126 A·h
Nominal Energy	6.4 kW·h
Nominal charge current	42 A
Nominal discharge current	42 A
Maximum discharge current[a]	110 A
Peak power	5 kW
Faradic charge efficiency (25°C/77°F)	99%
Battery round-trip efficiency (C/3, 25°C/77°F)	95%
Expected lifetime at 25°C/77°F	More than 10 years
Cycle life (90% DOD, 25°C/77°F)	6000 cycles (EOL 60%)
Cycle life (80% DOD, 25°C/77°F)	10000 cycles (EOL 60%)
Communication interface	CAN 2.0B
Dimensions	406 mm × 165 mm × 664 mm
Weight	60 kg
Available operating temperature[b]	0°C to 40°C
Optimal operating temperature	15°C to 30°C
Storage temperature	–30°C to 50°C
Cooling	Natural convection
Battery pack safety	CE, (IEC 62619 in May, 2015)
Battery cell safety	IEC 62133
UN number	UN 3481
Hazardous materials classification	Class 9
UN transportation testing requirements	UN 38.3
International protection marking	IP21

[a]If the temperature inside the battery pack rises, the charging and discharging current may be derated to keep the battery safety and lifetime.

[b]As the degradation of battery products is accelerated in high temperatures, it is not recommended to place the battery pack in an area above 40°C.

E.2 Littelfuse IGBT Module specifications

Littelfuse®
Expertise Applied | Answers Delivered

Power Module
600V 200A IGBT Module

MG06200S-BN4MM

RoHS

Features

- High short circuit capability, self limiting short circuit current
- $V_{CE(sat)}$ with positive temperature coefficient
- Fast switching and short tail current
- Free wheeling diodes with fast and soft reverse recovery
- Low switching losses

Agency Approvals

AGENCY	AGENCY FILE NUMBER
	E71639

Applications

- High frequency switching application
- Medical applications
- Motion/servo control
- UPS systems

Module Characteristics (T_c = 25°C, unless otherwise specified)

Symbol	Parameters	Test Conditions	Min	Typ	Max	Unit
T_J max	Max. Junction Temperature				175	°C
$T_{J\,op}$	Operating Temperature		-40		150	°C
T_{stg}	Storage Temperature		-40		125	°C
V_{isol}	Insulation Test Voltage	AC, t=1min		3000		V
CTI	Comparative Tracking Index		350			
Torque	Module-to-Sink	Recommended (M6)	3		5	N·m
Torque	Module Electrodes	Recommended (M5)	2.5		5	N·m
Weight				160		g

Absolute Maximum Ratings (T_c = 25°C, unless otherwise specified)

Symbol	Parameters	Test Conditions	Values	Unit
IGBT				
V_{CES}	Collector - Emitter Voltage	T_J=25°C	600	V
V_{GES}	Gate - Emitter Voltage		±20	V
I_C	DC Collector Current	T_C=25°C	300	A
		T_C=60°C	200	A
I_{CM}	Repetitive Peak Collector Current	t_p=1ms	400	A
P_{tot}	Power Dissipation Per IGBT		600	W
Diode				
V_{RRM}	Repetitive Reverse Voltage	T_J=25°C	600	V
$I_{F(AV)}$	Average Forward Current	T_C=25°C	300	A
		T_C=60°C	200	A
I_{FRM}	Repetitive Peak Forward Current	t_p=1ms	400	A
I^2t		T_J =125°C, t=10ms, V_R=0V	3500	A^2s

Life Support Note:
Not Intended for Use in Life Support or Life Saving Applications
The products shown herein are not designed for use in life sustaining or life saving applications unless otherwise expressly indicated.

Electrical and Thermal Specifications (T_C = 25°C, unless otherwise specified)

Symbol	Parameters	Test Conditions		Min	Typ	Max	Unit
IGBT							
$V_{GE(th)}$	Gate - Emitter Threshold Voltage	$V_{CE}=V_{GE}$, I_C=3.2mA		4.9	5.8	6.5	V
$V_{CE(sat)}$	Collector - Emitter Saturation Voltage	I_C=200A, V_{GE}=15V, T_J=25°C			1.45		V
		I_C=200A, V_{GE}=15V, T_J=125°C			1.6		V
I_{CES}	Collector Leakage Current	V_{CE}=600V, V_{GE}=0V, T_J=25°C				1	mA
		V_{CE}=600V, V_{GE}=0V, T_J=125°C				5	mA
I_{GES}	Gate Leakage Current	V_{CE}=0V,V_{GE}=±15V, T_J=125°C		-400		400	nA
R_{Gint}	Integrated Gate Resistor				2		Ω
Q_{ge}	Gate Charge	V_{CC}=300V, I_C=200A , V_{GE}=±15V			2.15		µC
C_{ies}	Input Capacitance	V_{CE}=25V, V_{GE}=0V, f =1MHz			13		nF
C_{res}	Reverse Transfer Capacitance				0.38		nF
$t_{d(on)}$	Turn - on Delay Time	V_{CC}=300V I_C=200A R_G =2.0Ω V_{GE}=±15V Inductive Load	T_J=25°C		150		ns
			T_J =125°C		160		ns
t_r	Rise Time		T_J=25°C		30		ns
			T_J =125°C		40		ns
$t_{d(off)}$	Turn - off Delay Time		T_J=25°C		340		ns
			T_J =125°C		370		ns
t_f	Fall Time		T_J=25°C		60		ns
			T_J =125°C		70		ns
E_{on}	Turn - on Energy		T_J=25°C		1		mJ
			T_J =125°C		1.55		mJ
E_{off}	Turn - off Energy		T_J=25°C		5.65		mJ
			T_J =125°C		6.9		mJ
I_{SC}	Short Circuit Current	t_{psc}≤6µS , V_{GE}=15V; T_J=125°C,V_{CC}=360V			1000		A
R_{thJC}	Junction-to-Case Thermal Resistance **(Per IGBT)**					0.25	K/W
Diode							
V_F	Forward Voltage	I_F=200A , V_{GE}=0V, T_J =25°C			1.55		V
		I_F=200A , V_{GE}=0V, T_J =125°C			1.5		V
I_{RRM}	Max. Reverse Recovery Current	I_F=200A , V_R=300V di_F/dt=-5700A/µs T_J =125°C			230		A
Q_{rr}	Reverse Recovery Charge				17		µC
E_{rec}	Reverse Recovery Energy				5.2		mJ
R_{thJCD}	Junction-to-Case Thermal Resistance **(Per Diode)**					0.45	K/W

Figure 1: Typical Output Characteristics

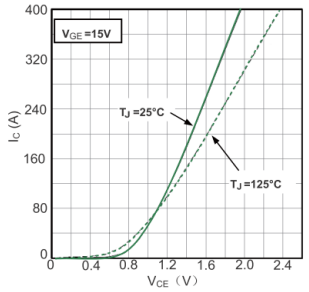

Figure 2: Typical Output characteristics

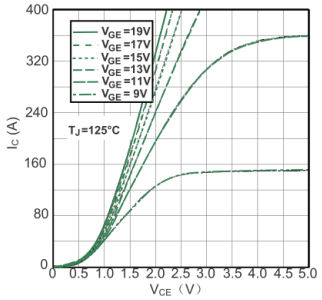

Figure 3: Typical Transfer characteristics

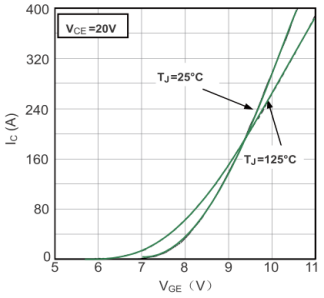

Figure 4: Switching Energy vs. Gate Resistor

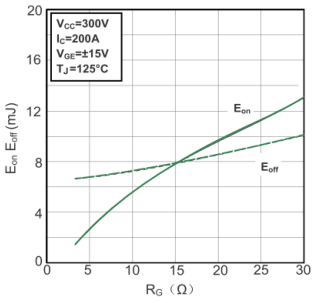

Figure 5: Switching Energy vs. Collector Current

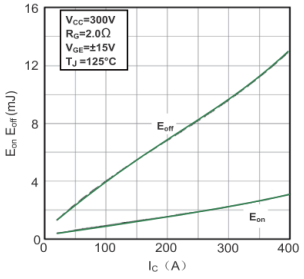

Figure 6: Reverse Biased Safe Operating Area

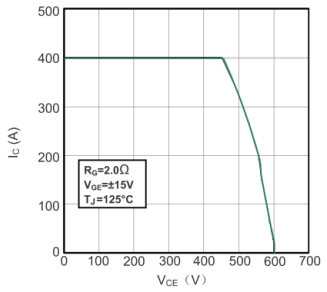

Figure 7: Diode Forward Characteristics

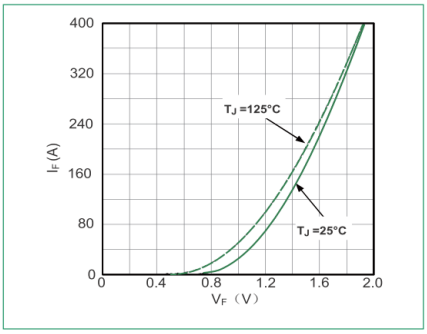

Figure 8: Switching Energy vs. Gate Resistor

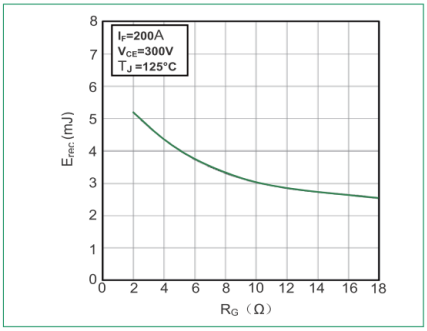

Figure 9: Switching Energy vs. Forward Current

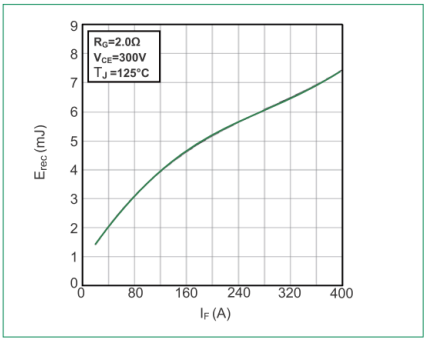

Figure 10: Transient Thermal Impedance

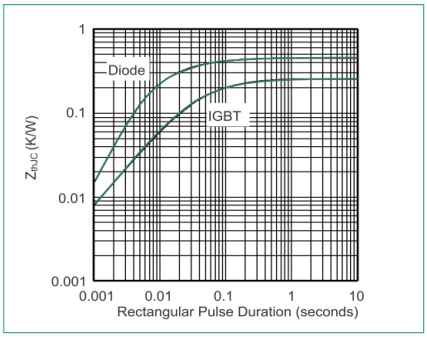

Power Module
600V 200A IGBT Module

Dimensions-Package S

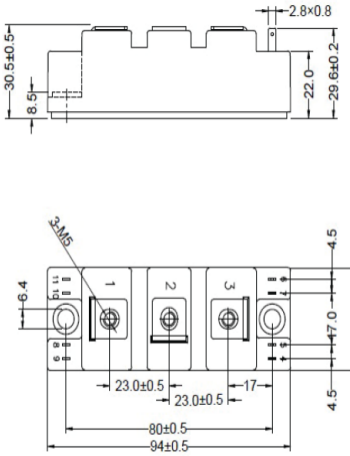

Circuit Diagram

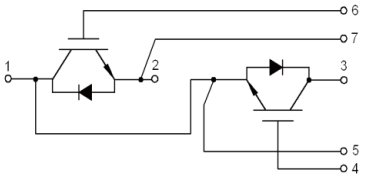

Packing Options

Part Number	Marking	Weight	Packing Mode	M.O.Q
MG06200S-BN4MM	MG06200S-BN4MM	160g	Bulk Pack	100

Part Numbering System

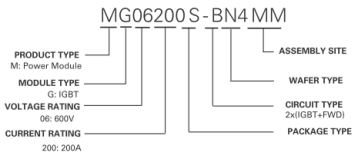

Part Marking System

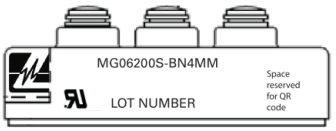

E.3 SMA Sunny Tripower 17000 TL

SUNNY TRIPOWER
10000TL / 12000TL / 15000TL / 17000TL

Efficient
- Maximum efficiency of 98.1%
- OptiTrac™ Global Peak for best tracking efficiency
- *Bluetooth*® communication

Safe
- Electronic string fuse and failure detection
- Optional DC overvoltage protector (Type II)
- String current monitoring

Flexible
- DC input voltage up to 1000 V
- Integrated grid management functions
- Custom plant design with Optiflex

Simple
- Three-phase feed-in
- Cable connection without tools
- SUNCLIX® DC plug system
- Easily accessible connection area

SUNNY TRIPOWER
10000TL / 12000TL / 15000TL / 17000TL

The three-phase inverter for easy system design

The Sunny Tripower is packed full of innovation. Thanks to the new SMA Optiflex technology, which features two MPP inputs and a very broad input voltage range, the three-phase Sunny Tripower is suited to almost any module configuration. This flexibility simplifies plant design and is perfect for systems up to the megawatt range. The Sunny Tripower also assists grid managers. It meets all the requirements for reactive power supply, utility interaction management and grid support. The Optiprotect safety concept, with its self-learning string failure detection, electronic string fuse and available DC overvoltage protector (Type II), ensures maximum uptime.

Technical data	Sunny Tripower 10000TL	Sunny Tripower 12000TL
Input (DC)		
Max. DC power (@ cos φ = 1)	10200 W	12250 W
Max. input voltage	1000 V	1000 V
MPP voltage range / rated input voltage	320 V – 800 V / 600 V	380 V – 800 V / 600 V
Min. input voltage / initial input voltage	150 V / 188 V	150 V / 188 V
Max. input current input A / input B	22 A / 11 A	22 A / 11 A
Max. input current per string input A[2] / input B[2]	33 A / 12.5 A	33 A / 12.5 A
Number of independent MPP inputs / strings per MPP input	2 / A:4, B:1	2 / A:4, B:1
Output (AC)		
Rated power (@ 230 V, 50 Hz)	10000 W	12000 W
Max. apparent AC power	10000 VA	12000 VA
Nominal AC voltage	3 / N / PE; 220 / 380 V, 3 / N / PE; 230 / 400 V, 3 / N / PE; 240 / 415 V	3 / N / PE; 220 / 380 V, 3 / N / PE; 230 / 400 V, 3 / N / PE; 240 / 415 V
Nominal AC voltage range	160 V – 280 V	160 V – 280 V
AC power frequency / range	50 Hz, 60 Hz / -6 Hz ... +5 Hz	50 Hz, 60 Hz / -6 Hz ... +5 Hz
Rated power frequency / rated grid voltage	50 Hz / 230 V	50 Hz / 230 V
Max. output current	16 A	19.2 A
Power factor at rated power	1	1
Adjustable displacement power factor	0.8 overexcited ... 0.8 underexcited	0.8 overexcited ... 0.8 underexcited
Feed-in phases / connection phases	3 / 3	3 / 3
Efficiency		
Max. efficiency / European weighted efficiency	98.1 % / 97.7 %	98.1 % / 97.7 %
Protective devices		
DC disconnect device	●	●
Ground fault monitoring / grid monitoring	● / ●	● / ●
DC surge arrester type II	○	○
DC reverse polarity protection / AC short-circuit current capability / galvanically isolated	● / ● / –	● / ● / –
All-pole-sensitive residual-current monitoring unit	●	●
Protection class (according to IEC 62103) / overvoltage category	I / III	I / III
General data		
Dimensions (W / H / D)	665 / 690 / 265 mm (26.2 / 27.2 / 10.4 inch)	665 / 690 / 265 mm (26.2 / 27.2 / 10.4 inch)
Weight	59 kg / 130.07 lb	59 kg / 130.07 lb
Operating temperature range	-25 °C ... +60 °C / -13 °F ... +140 °F	-25 °C ... +60 °C / -13 °F ... +140 °F
Noise emission (typical)	51 dB(A)	51 dB(A)
Self-consumption (night)	1 W	1 W
Topology / cooling concept	Transformerless / OptiCool	Transformerless / OptiCool
Degree of protection / connection area degree of protection	IP65 / IP54	IP65 / IP54
Climatic category (according to IEC 60721-3-4)	4K4H	4K4H
Max. permissible value for relative humidity (non-condensing)	100 %	100 %
Features		
DC coupling	SUNCLIX	SUNCLIX
AC coupling	Spring clamp terminal	Spring clamp terminal
Display	Graphic	Graphic
Interface: RS485 / Bluetooth / multi-function relay	○ / ● / ●	○ / ● / ●
Warranty: 5 / 10 / 15 / 20 / 25 years	● / ○ / ○ / ○ / ○	● / ○ / ○ / ○ / ○
Certificates and approvals (more available on request)	CE, VDE0126-1-1, RD661/2007, PPC, AS4777, EN50438[1], C10/11, PPDS, IEC61727, ENEL-Guida, UTEC15-712-1, G59/2, VDE-AR-N4105, BDEW 2008, RD1699	
Certificates and approvals (planned)	CEI 0-21	
Type designation	STP 10000TL-10	STP 12000TL-10

Sunny Tripower 15000TL	Sunny Tripower 17000TL		
15340 W	17410 W		
1000 V	1000 V		
360 V – 800 V / 600 V	400 V – 800 V / 600 V		
150 V / 188 V	150 V / 188 V		
33 A / 11 A	33 A / 11 A		
40 A / 12.5 A	40 A / 12.5 A		
2 / A:5; B:1	2 / A:5; B:1		
15000 W	17000 W		
15000 VA	17000 VA		
3 / N / PE; 220 / 380 V, 3 / N / PE; 230 / 400 V, 3 / N / PE; 240 / 415 V	3 / N / PE; 220 / 380 V, 3 / N / PE; 230 / 400 V, 3 / N / PE; 240 / 415 V		
160 V – 280 V	160 V – 280 V		
50 Hz, 60 Hz / -6 Hz ... +5 Hz	50 Hz, 60 Hz / -6 Hz ... +5 Hz		
50 Hz / 230 V	50 Hz / 230 V		
24 A	24.6 A		
1	1		
0.8 overexcited ... 0.8 underexcited	0.8 overexcited ... 0.8 underexcited		
3 / 3	3 / 3		
98.2 % / 97.8 %	98.2 % / 97.8 %		
●	●		
● / ●	● / ●		
○	○		
● / ● / –	● / ● / –		
●	●		
I / III	I / III		
665 / 690 / 265 mm (26.2 / 27.2 / 10.4 inch)	665 / 690 / 265 mm (26.2 / 27.2 / 10.4 inch)		
59 kg / 130.07 lb	59 kg / 130.07 lb		
-25 °C ... +60 °C / -13 °F ... +140 °F	-25 °C ... +60 °C / -13 °F ... +140 °F		
51 dB(A)	51 dB(A)		
1 W	1 W		
Transformerless / OptiCool	Transformerless / OptiCool		
IP65 / IP54	IP65 / IP54		
4K4H	4K4H		
100 %	100 %		
SUNCLIX	SUNCLIX		
Spring clamp terminal	Spring clamp terminal		
Graphic	Graphic		
○ / ● / ●	○ / ● / ●		
● / ○ / ○ / ○ / ○	● / ○ / ○ / ○ / ○		
CE, VDE0126-1-1, RD661/2007, PPC, AS4777, EN50438[1], C10/11, PPDS, IEC61727, ENEL-Guida, UTEC15-712-1, G59/2, VDE-AR-N4105, BDEW 2008, RD1699			
CEI 0-21			
STP 15000TL-10	STP 17000TL-10		

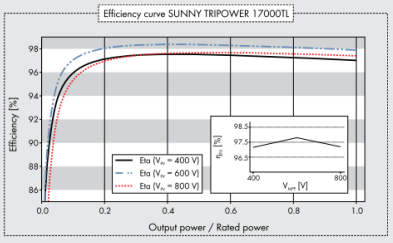

Accessories

RS485 interface
DM-485CB-10

DC surge arrester
(Type II), input A
DCSPD KIT1-10

DC surge arrester
(Type II), inputs A and B
DCSPD KIT2-10

* Does not apply to all national deviations of EN 50438

** To be observed in case of a short circuit in the electronic string fuse

● Standard features ○ Optional features – Not available

Data at nominal conditions

E.4 Trina TSM-255 PC/PA05A solar PV panel

Mono Multi Solutions

TSM-PC05A
TSM-PA05A
THE Honey MODULE

by Trinasolar

15.9%
MAX EFFICIENCY

260W
MAX POWER OUTPUT

10 YEAR
PRODUCT WARRANTY

25 YEAR
LINEAR POWER WARRANTY

Module can bear snow loads up to **5400Pa** and wind loads up to **2400Pa**

Guaranteed power output
0~+3%

High performance under low light conditions
Cloudy days, mornings and evenings

Independently certified by **international certification bodies**

Manufactured according to International Quality and Environment Management System Standards
ISO9001, ISO14001

Founded in 1997, Trina Solar is a vertically integrated PV manufacturer, involved in the production of ingots, wafers and cells to the assembly of high quality modules, using both mono and multicrystalline technologies. As of July 2011, the Company has already achieved an annualized nameplate module capacity of approximately 1.9GW. Trina Solar's wide range of products are used in residential, commercial, industrial and public utility applications throughout the world.

Only by matching an efficient cost-structure with proven performance will we as an industry achieve grid parity. And at Trina Solar, we have both.

Trina Solar Limited
www.trinasolar.com

Trinasolar
The power behind the panel

NEW

LINEAR PERFORMANCE WARRANTY

10 Year Prduct Warranty • 25 Year Linear Power Warranty

TSM-PC05A / TSM-PA05A THE Honey MODULE

DIMENSIONS OF PV MODULE TSM-PC/PA 05A

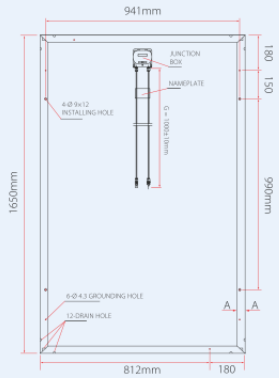

Back View

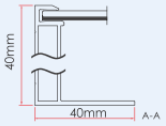

I-V CURVES OF PV MODULE TSM-250 PC/PA 05A

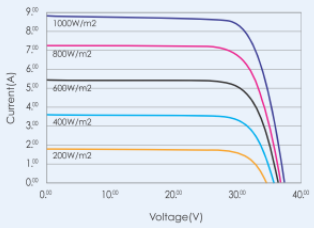

Average efficiency reduction of 4.5% at 200W/m² according to EN 60904-1.

CERTIFICATION

(on-going)

ELECTRICAL DATA @ STC	TSM-245 PC/PA05A	TSM-250 PC/PA05A	TSM-255 PC/PA05A	TSM-260 PC/PA05A
Peak Power Watts-P_{MAX} (Wp)	245	250	255	260
Power Output Tolerance-P_{MAX} (%)	0/+3	0/+3	0/+3	0/+3
Maximum Power Voltage-V_{MP} (V)	30.2	30.5	30.9	31.3
Maximum Power Current-I_{MPP} (A)	8.12	8.20	8.26	8.31
Open Circuit Voltage-V_{OC} (V)	37.7	37.8	38.0	38.2
Short Circuit Current-I_{SC} (A)	8.83	8.90	8.95	9.02
Module Efficiency η_m (%)	15.0	15.3	15.6	15.9

Values at Standard Test Conditions STC (Air Mass AM1.5, Irradiance 1000W/m², Cell Temperature 25°C).

ELECTRICAL DATA @ NOCT	TSM-245 PC/PA05A	TSM-250 PC/PA05A	TSM-255 PC/PA05A	TSM-260 PC/PA05A
Maximum Power (W)	180	183	187	191
Maximum Power Voltage (V)	27.4	27.7	28.0	28.2
Maximum Power Current (A)	6.56	6.62	6.68	6.76
Open Circuit Voltage (V)	34.6	34.8	34.9	35.1
Short Circuit Current (A)	7.14	7.20	7.24	7.30

NOCT: Irradiance at 800W/m², Ambient Temperature 20°C, Wind Speed 1M/s.

MECHANICAL DATA	
Solar cells	Multicrystalline 156 × 156mm (6 inches)
Cell orientation	60 cells (6 × 10)
Module dimension	1650 × 992 × 40mm (64.95 × 39.05 × 1.57 inches)
Weight	19.5kg (43.0 lb)
Glass	High transparancy solar glass 3.2mm (0.13 inches)
Frame	Anodized aluminium alloy
J-Box	IP 65 rated
Cables / Connector	Photovoltaic Technology cable 4.0mm² (0.006 inches²), 1000mm (39.4 inches), MC4

TEMPERATURE RATINGS	
Nominal Operating Cell Temperature (NOCT)	46°C (±2°C)
Temperature Coefficient of P_{MAX}	-0.41%/°C
Temperature Coefficient of V_{OC}	-0.32%/°C
Temperature Coefficient of I_{SC}	0.053%/°C

MAXIMUM RATINGS	
Operational Temperature	-40~+85°C
Maximum System Voltage	1000V DC(IEC)/ 600V DC(UL)
Max Series Fuse Rating	15A

WARRANTY
10 year workmanship warranty
25 year linear performance warranty

(Please refer to product warranty for details)

PACKAGING CONFIGURATION
Modules per box: 25 pcs
Modules per 40' container: 650 pcs

TSM_EN_Oct_2011

Trinasolar
The power behind the panel

E.5 HYE HY-1000L 48 V 1 kW wind turbine

Technical Specifications

Model	HY-1000
Rated Output	1000W
Peak Output	1200W
Rated Voltage(V)	off-grid DC48
Start-up Speed	2 m/s or 4.5mph
Cut-in Speed	2.5m/s or 5.6mph
Rated Wind speed	12m/s or 26.8mph
System average Cp.	>0.36
Rate Charging Current (A)	DC10.4
Noise level	<30dB (@50 feet distance from hub center)
KWH/month (Annual avg. V 5.5m)	Approx. 1049
Working Temp. range	from -40°C to 60°C
Survival Max. wind	50m/s or 110mph
Overspeed control	Electromagnetic brake & blade aerodynamic speed control
Number of Blades	5
Rotor Diameter(m)	1.96
Swept Area (m2)	3
Blade Material	Nylon and glass-fiber
Generator Type	Brushless 3-phase PMA with high performance Neodymium Magnets
Tower-top Weight	22kg
Tower Type	self-supporting, guyed, Tilt-up tower or rooftop mounting etc.
Controller Type	MPPT or PWM
Applications	solar & wind hybrid lighting,
Product Life (years)	15
Warranty (years)	3 years (optional 5 years)
Certificate	Certified by ISO9001:2000, CE, RoHS, ETL

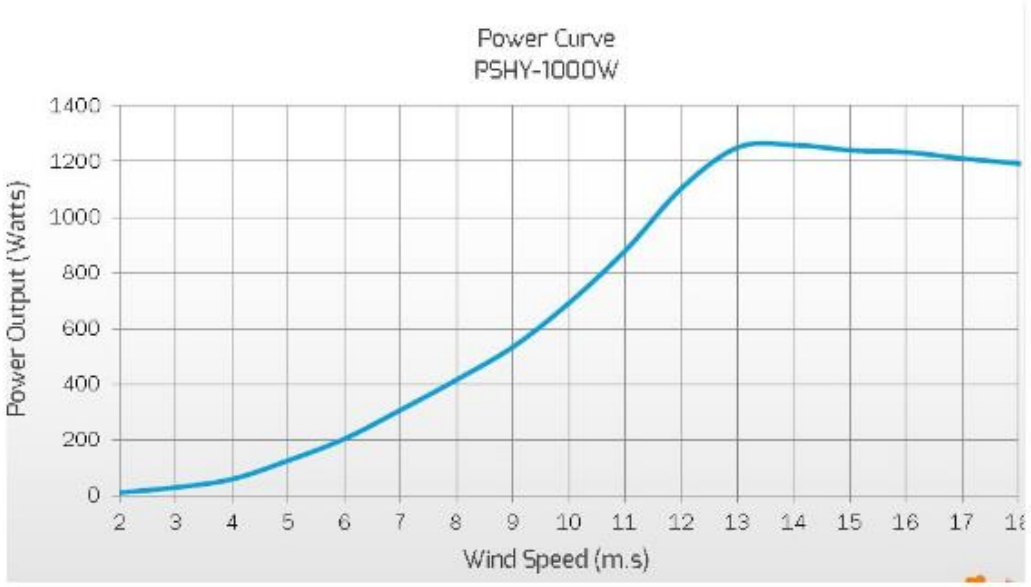

Appendix F: Average daily Nambour irradiance

Table F.1. Average daily insolation in Nambour.

average daily insolation, kWh/m^2			
Month	**HOMER 1993-2005**	**BOM 2004-2016**	**difference**
January	6.51	5.868	0.64
February	5.67	5.586	0.08
March	5.26	4.902	0.36
April	4.28	4.541	-0.26
May	3.61	3.806	-0.20
June	3.4	3.175	0.23
July	3.64	3.607	0.03
August	4.46	4.463	0.00
September	5.55	5.272	0.28
October	6.02	5.846	0.17
November	6.47	5.745	0.73
December	6.66	5.488	1.17

Appendix G: Load modelling data

G.1 Derivation of Energex-wide weekday and weekday demand

Table G.1. Derivation of Energex-wide weekday and weekend demand, adapted from Berry et al. (2015).

Time (hrs)	Weekday demand (MW)	Weekend demand (MW)	Difference
0	850	875	2.9%
0.5	750	800	6.7%
1	675	725	7.4%
1.5	625	675	8.0%
2	600	650	8.3%
2.5	525	600	14.3%
3	525	550	4.8%
3.5	525	550	4.8%
4	575	550	-4.3%
4.5	600	575	-4.2%
5	625	575	-8.0%
5.5	700	600	-14.3%
6	825	625	-24.2%
6.5	950	740	-22.1%
7	1050	800	-23.8%
7.5	1000	900	-10.0%
8	900	925	2.8%
8.5	825	975	18.2%
9	760	975	28.3%
9.5	700	925	32.1%
10	625	875	40.0%
10.5	600	800	33.3%
11	550	775	40.9%
11.5	550	760	38.2%
12	550	750	36.4%
12.5	550	750	36.4%
13	550	775	40.9%
13.5	600	800	33.3%
14	625	825	32.0%
14.5	650	850	30.8%

Time (hrs)	Weekday demand (MW)	Weekend demand (MW)	Difference
15	740	900	21.6%
15.5	800	980	22.5%
16	900	1100	22.2%
16.5	1050	1200	14.3%
17	1200	1300	8.3%
17.5	1350	1400	3.7%
18	1450	1480	2.1%
18.5	1500	1500	0.0%
19	1450	1400	-3.4%
19.5	1425	1375	-3.5%
20	1425	1375	-3.5%
20.5	1350	1325	-1.9%
21	1350	1350	0.0%
21.5	1300	1275	-1.9%
22	1200	1200	0.0%
22.5	1075	1100	2.3%
23	1025	1050	2.4%
23.5	900	975	8.3%
TOTAL	41925	44835	6.9%

G.2 Weekday hourly load profile

Table G.2. Weekday hourly modelled load profile by month.

Weekday hourly load profile, kWh consumption												
time	**Jan**	**Feb**	**Mar**	**Apr**	**May**	**Jun**	**Jul**	**Aug**	**Sep**	**Oct**	**Nov**	**Dec**
00:00	0.36	0.34	0.35	0.33	0.35	0.36	0.39	0.38	0.33	0.36	0.32	0.37
01:00	0.29	0.28	0.28	0.27	0.29	0.29	0.32	0.31	0.27	0.30	0.26	0.30
02:00	0.26	0.24	0.24	0.23	0.25	0.25	0.28	0.27	0.23	0.26	0.22	0.26
03:00	0.24	0.22	0.23	0.22	0.23	0.23	0.26	0.25	0.22	0.24	0.21	0.25
04:00	0.27	0.25	0.25	0.24	0.26	0.26	0.29	0.28	0.24	0.27	0.23	0.28
05:00	0.46	0.43	0.44	0.42	0.44	0.45	0.50	0.48	0.42	0.46	0.40	0.47
06:00	0.81	0.75	0.77	0.73	0.78	0.79	0.88	0.85	0.73	0.81	0.71	0.83
07:00	0.93	0.87	0.89	0.84	0.90	0.91	1.01	0.98	0.85	0.93	0.82	0.96
08:00	0.88	0.82	0.84	0.79	0.85	0.86	0.95	0.92	0.80	0.88	0.77	0.90
09:00	0.91	0.85	0.87	0.82	0.88	0.89	0.99	0.95	0.83	0.91	0.80	0.94
10:00	0.83	0.78	0.80	0.75	0.81	0.82	0.91	0.88	0.76	0.83	0.73	0.86
11:00	0.75	0.70	0.72	0.68	0.72	0.73	0.81	0.79	0.68	0.75	0.66	0.77
12:00	0.75	0.70	0.72	0.68	0.72	0.73	0.81	0.79	0.68	0.75	0.66	0.77
13:00	0.78	0.73	0.75	0.71	0.76	0.77	0.85	0.82	0.71	0.78	0.69	0.81
14:00	0.79	0.74	0.76	0.72	0.77	0.78	0.86	0.83	0.72	0.79	0.70	0.82
15:00	0.87	0.82	0.83	0.79	0.84	0.85	0.95	0.92	0.80	0.87	0.77	0.90
16:00	0.88	0.83	0.85	0.80	0.86	0.87	0.96	0.93	0.81	0.89	0.78	0.91
17:00	1.16	1.08	1.11	1.05	1.12	1.13	1.26	1.22	1.05	1.16	1.01	1.19
18:00	1.34	1.25	1.28	1.21	1.29	1.31	1.46	1.41	1.22	1.34	1.17	1.38
19:00	1.30	1.22	1.25	1.18	1.26	1.28	1.42	1.37	1.19	1.31	1.14	1.35
20:00	1.26	1.18	1.20	1.14	1.22	1.23	1.37	1.32	1.15	1.26	1.10	1.30
21:00	1.20	1.12	1.15	1.09	1.16	1.18	1.31	1.26	1.10	1.20	1.05	1.24
22:00	1.03	0.96	0.99	0.93	1.00	1.01	1.12	1.08	0.94	1.03	0.90	1.07
23:00	0.655	0.612	0.6256	0.593	0.634	0.641	0.712	0.688	0.597	0.656	0.574	0.676

G.3 Weekend hourly load profile

Table G.3. Weekend hourly modelled load profile by month.

Weekday hourly load profile, kWh consumption												
time	**Jan**	**Feb**	**Mar**	**Apr**	**May**	**Jun**	**Jul**	**Aug**	**Sep**	**Oct**	**Nov**	**Dec**
00:00	0.36	0.33	0.34	0.32	0.34	0.35	0.39	0.37	0.32	0.36	0.31	0.37
01:00	0.30	0.28	0.28	0.27	0.29	0.29	0.32	0.31	0.27	0.30	0.26	0.31
02:00	0.27	0.25	0.25	0.24	0.26	0.26	0.29	0.28	0.24	0.27	0.23	0.27
03:00	0.23	0.22	0.22	0.21	0.23	0.23	0.25	0.25	0.21	0.23	0.20	0.24
04:00	0.24	0.22	0.23	0.22	0.23	0.23	0.26	0.25	0.22	0.24	0.21	0.25
05:00	0.25	0.23	0.24	0.23	0.24	0.24	0.27	0.26	0.23	0.25	0.22	0.26
06:00	0.29	0.27	0.28	0.26	0.28	0.28	0.31	0.30	0.26	0.29	0.25	0.30
07:00	0.72	0.67	0.69	0.65	0.70	0.71	0.78	0.76	0.66	0.72	0.63	0.74
08:00	0.91	0.85	0.87	0.82	0.88	0.89	0.99	0.96	0.83	0.91	0.80	0.94
09:00	1.11	1.03	1.06	1.00	1.07	1.08	1.20	1.16	1.01	1.11	0.97	1.14
10:00	1.07	1.00	1.02	0.97	1.03	1.04	1.16	1.12	0.97	1.07	0.93	1.10
11:00	0.98	0.91	0.93	0.88	0.95	0.96	1.06	1.03	0.89	0.98	0.86	1.01
12:00	0.95	0.89	0.91	0.86	0.92	0.93	1.04	1.00	0.87	0.96	0.84	0.99
13:00	1.00	0.94	0.96	0.91	0.97	0.98	1.09	1.05	0.91	1.00	0.88	1.04
14:00	0.98	0.91	0.93	0.88	0.94	0.95	1.06	1.02	0.89	0.98	0.86	1.01
15:00	1.00	0.93	0.95	0.90	0.96	0.98	1.08	1.05	0.91	1.00	0.87	1.03
16:00	0.98	0.91	0.93	0.88	0.94	0.95	1.06	1.02	0.89	0.98	0.86	1.01
17:00	1.15	1.07	1.09	1.04	1.11	1.12	1.25	1.20	1.04	1.15	1.00	1.18
18:00	1.26	1.18	1.21	1.14	1.22	1.24	1.37	1.33	1.15	1.27	1.11	1.31
19:00	1.18	1.10	1.12	1.07	1.14	1.15	1.28	1.24	1.07	1.18	1.03	1.22
20:00	1.15	1.07	1.09	1.04	1.11	1.12	1.25	1.20	1.04	1.15	1.00	1.18
21:00	1.11	1.04	1.06	1.01	1.08	1.09	1.21	1.17	1.01	1.11	0.98	1.15
22:00	0.98	0.91	0.93	0.88	0.94	0.95	1.06	1.02	0.89	0.98	0.86	1.01
23:00	0.64	0.602	0.615	0.583	0.623	0.631	0.701	0.677	0.587	0.645	0.565	0.665

Appendix H: HOMER economic models summary

Note to reader: The following figures are derived from 64 economic variations run for each scenario. Variations were inflation between 2 to 5.5% and discount rate between 3 to 6.5%, each in 0.5% increments. The full data set is included in the DVD submitted with the dissertation.

Table H.1. Economic modelling summary A

Scenario (Base case refers to 9.455 kW PV, 1 kW wind, 1 BESS unless otherwise specified)	**Net Present Cost $AUD (based on 64 economic scenarios)**		
Hardware optimisation	**Average**	**Minimum**	**Maximum**
Energy supplied by grid only	40,574	26,760	61,982
Base case	46,014	38,805	55,990
Base case, 2 BESS	58,059	49,550	69,356
Base case, no BESS	42,205	33,492	55,204
Specification optimisation (10 kW PV, no BESS, no wind)	36,838	29,122	48,545
17 kW inverter optimisation (15 kW PV, no wind, no BESS)	33,312	28,462	40,536
Base case but optimise 0-6 prorata BESS - 0 BESS is best in all but 3 scenarios	42,201	33,492	55,052

Peak time of use (TOU) tariff ($/kWh)	**Average**	**Minimum**	**Maximum**
Base case, peak 0.328295	42,205	33,492	55,204
Peak, 0.5	44,724	35,296	56,326
Peak, 0.6	45,893	36,573	56,564
Peak, 0.7	46,456	37,850	56,802
Peak 0.8	46,699	39,127	57,040

Deferrable load scenario	**Average**	**Minimum**	**Maximum**
Base case, 25% deferrable load	44,186	37,599	53,197
Base case without BESS, 25% deferrable load	38,083	30,774	48,908

Table H.2. Economic modelling summary B

Scenario (Base case refers to 9.455 kW PV, 1 kW wind, 1 BESS unless otherwise specified)	Net Present Cost $AUD (based on 64 economic scenarios)		
Customer energy consumption variation, no BESS	**Average**	**Minimum**	**Maximum**
13.9 kWh	35,389	28,997	44,793
Base consumption (18.6 kWh)	42,205	33,492	55,204
23.4 kWh	49,792	38,496	66,795
26 kWh	53,503	40,944	72,463
30 kWh	59,765	45,074	82,030
35 kWh	67,813	50,382	94,325
40 kWh	76,072	55,829	106,941
45 kWh	84,524	61,404	119,853
50 kWh	93,145	67,089	133,021

Customer energy consumption variation, one BESS	**Average**	**Minimum**	**Maximum**
13.9 kWh	41,005	35,501	48,338
BASE (18.6 kWh)	46,014	38,805	55,990
23.4 kWh	53,154	43,514	66,897
26 kWh	56,810	45,926	72,482
30 kWh	63,102	50,076	82,094
35 kWh	71,388	55,541	94,752
40 kWh	79,964	61,197	107,853
45 kWh	88,799	67,024	121,349
50 kWh	97,814	72,970	135,120

Table H.3. Economic modelling summary C

Scenario (Base case refers to 9.455 kW PV, 1 kW wind, 1 BESS unless otherwise specified)	Net Present Cost $AUD (based on 64 economic scenarios)		
control scheme variation	**Average**	**Minimum**	**Maximum**
BASE CASE	46,014	38,805	55,990
discharge to load any time	46,014	38,805	55,990
control no off peak discharging	46,014	38,805	55,990
control off peak charging only	46,014	38,805	55,990
control no weekday shoulder discharging	46,014	38,805	55,990

discounts and break-even modelling	**Average**	**Minimum**	**Maximum**
Base case, no BESS, no discount	42,205	33,492	55,204
Base case, 30% battery bulk buy discount	43,073	36,225	52,649
Base case, 30% BESS discount	42,157	35,421	51,608
Base case, 35% BESS discount	41,514	34,857	50,878
Base case, 40% BESS discount	40,871	34,293	50,147

Retailer tariff modelling	**Average**	**Minimum**	**Maximum**
AGL (base)	46,014	38,805	55,990
DODO base	52,693	43,210	66,193
Energy Australia	46,077	38,847	56,086
Simple Energy	49,553	41,139	61,396
Lumo basic	50,547	41,795	62,914
Urth 10	41,131	35,584	48,530

Appendix I: Economic model cost summary

Capital expenditures summary

Solar system		cost
PV panels	$	4,500
shipping	$	1,000
system installation	$	1,700
per panel installation	$	1,200
tilt and rail kit	$	1,400
inverter installation deferred	-$	400
Solar system total	$	9,400

Wind system		cost
turbine	$	1,650
mast	$	800
installation	$	450
Wind system total	$	2,900

BESS		cost
battery	$	6,100
installation	$	400
controller	$	1,500
BESS total	$	8,000

Grid inverter system		cost
Inverter	$	2,500
Installation	$	400
Grid inverter total	$	2,900

System design fee	$	1,250

Total capital expenditures	$	24,450

Operating expenses summary

item	cost p.a.
Solar PV cleaning and inspection	$ 20
wind system inspection	$ 25
BESS inspection	$ 20
Inverter inspection	$ 50
insurance	$ 55
annual operating expenses	$ 170

Appendix J: Secondary work

J.1 Script for determination of solar insolation at Nambour, Queensland

```
% minute by minute solar exposure for clear sky on 25 September (Julian calendar day 267)
clc; close all; clear all;
I_sc = 1376; % W*m^2; solar constant
day=355; % Julian calendar day, Jan 1 = 1; Feb 1 = 32, etc.
h = 2*pi()*(day-1)/365; % day angle, in radians
I_o = I_sc*(1.00011+0.034221*cos(h)+0.0128*sin(h)-0.000719*cos(2*h)+0.000077*sin(2*h)); % intensity of extraterresterial solar radiation on Julian day h
EOT = 0.000075+0.01868*cos(h)-0.032077*sin(h)-0.14615*cos(2*h)-0.04084*sin(2*h); % equation of time difference, in minutes
LSM = 150; % Local standard meridian for Nambour
LS= 152.94; % Nambour geographical longitude
LST = 0:(1/3600):24; % VECTOR; hour of day, in minute intervals; go 1/3600 for per second intervals
TST = LST + EOT/60 + (LSM-LS)/15; % VECTOR; true solar time
v = 15*abs(12-TST)*pi()/180; % VECTOR; solar hour angle in radians
d = 0.006918 - 0.399912*cos(h) + 0.070257*sin(h) - 0.006759*cos(2*h) + 0.000907*sin(2*h) - 0.002697*cos(3*h) + 0.00148*sin(3*h); % solar declination, in radians
w = -26.64*pi()/180; % Nambour geographical latitude in radians
cosine_of_zenith = sin(w)*sin(d) + cos(w)*cos(d)*cos(v); % VECTOR; cosine of zenith
G_inst = I_o*cosine_of_zenith; % VECTOR; instantaneous extraterresterial solar irradiance, W*m^-2
for n=1:numel(G_inst)
   if G_inst(n) < 0
      G_inst(n)=0;
   else G_inst(n)=G_inst(n);
   end
end
G_ga = 1098*cosine_of_zenith;
G_gb = 1*exp(-0.057./cosine_of_zenith);
G_g = G_ga.*G_gb; % VECTOR; Instantaneous solar irradiance reaching earth's surface, W*m^-2
for n=1:numel(G_g)
   if G_g(n) < 0
      G_g(n)=0;
   else G_g(n)=G_g(n);
   end
end
figure(2)
plot(LST, G_inst, LST,G_g);
```

J.2 Initial design of BESS DC-DC converter

The BESS system was designed in isolation, consisting of a battery model, a two-quadrant converter capable of providing bi-directional current flow under positive voltage conditions, a converter controller, and a pure DC voltage source to simulate the DC link voltage in the complete system.

A conventional two-quadrant, two-switch buck-boost converter was chosen for interfacing with the DC link. The two-quadrant converter was modelled after the design described in section 5.6 of Ahfock (2014). The inverter is designed to operate in the first and second quadrants, allowing for current sourcing from or sinking to the BESS. Ideally this current can be sourced from wind, PV, or grid sources as required and mandated by the control system.

The switches were modelled with the Simulink IGBT switch with anti-parallel diode. The BESS system was connected to the two- quadrant DC-DC converter. To test the basic circuit in charging and discharging conditions, a DC voltage source was placed in parallel with the converter output terminals. This DC voltage source was meant to model the DC link voltage and was intended to be replaced by the DC link voltage once all system components were modelled. However, the complexity of the modelling and time constraints of the project meant that this task was deferred to future work.

Proper operation of the DC-DC converter would result in the state (on/off) and gate pulse width and frequency of the IGBT switches to properly respond to the battery reference power that is supplied by the power flow monitoring system (see section 3.4.17). To provide a power reference in the modelling, a manual selector block consisting of the choice among a step, ramp, or random input was designed.

First, only one of the charging switches should only operate if the battery reference power is negative, that is, the battery is to charge, by sinking power. The discharging switch should only operate if the battery reference power is positive, i.e. the battery is to discharge, by supplying power. If the battery reference power is zero, then both switches should be held off. Under no circumstance should both switches be active. This must be considered in cases where the battery is to switch states between charging and discharging. To prevent simultaneous switching, it is necessary to hold both switches off for a certain dead-time period. Additional considerations for changing from discharging to charging mode, or vice-versa, should also be made for the physical chemistry dynamics of the battery, but this is deferred as future work.

In the first instance of the switch control design, DC-DC PWM controllers were used to control the on-time pulse width of each IGBT switch. These PWM controllers receive a duty cycle signal as an input and deliver a gate pulse at specified frequency and width to the switch gate. To be able to maintain control, the converter should operate in continuous current mode.

The duty cycle of the circuit in battery charging mode was generated as a function derived from section 5.6 of Ahfock (2014):

$$V_o = D_1 * V_{DCl}$$

$$I_o = \frac{V_o - V_b}{R}$$

$$D_1 = \frac{I_o * R + V_b}{V_{DCl}}$$

where:

$D_1$is the duty cycle of the 1st quadrant IGBT switch,

V_o is the output voltage,

I_o is the reference battery current derived from the battery power reference that is derived from the overall system state as per section 3.4.17,

V_b is the instantaneous battery voltage value as provided from the Simulink battery model,

V_{DCl} is the DC link voltage, and

R is the circuit series resistance, composed of the internal battery resistance.

Specifications for the design are:

DC link voltage = 413.9 V

Nominal charge/discharge current = 42 A

Maximum discharge current = 110 A

Nominal battery voltage = 51.8 V

The design of this system includes:

Size of capacitor across battery terminals to hold battery output voltage for a switching cycle; size of inductor to store charge current; minimum discharge current; switching frequency of IGBTs, and series resistance.

To simulate incorporation with the entire system, a power reference block was created, as well as a logic block to ensure the switches remain inactive when the power reference is zero.

The Simulink block used to provide the duty cycle reference for the charging block is in Figure J-1.

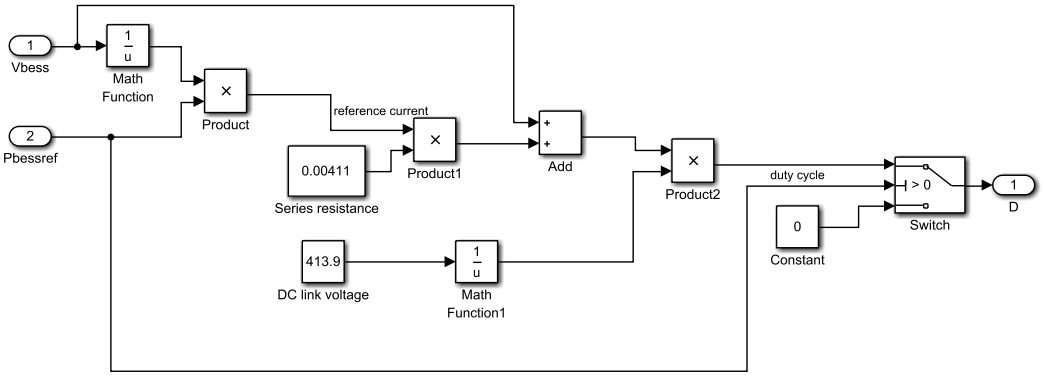

Figure J-1. Duty cycle setting for charging IGBT switch block

The duty cycle for discharging mode was also derived from section 5.6 of Ahfock (2014).

$$V_o = V_d - D_2 * V_d$$

$$I_o = \frac{V_o - V_b}{R}$$

$$D_2 = 1 - \frac{I_o * R - V_b}{V_d}$$

A discharging duty cycle block was derived from these equations similar to that for the charging block.

The final battery controller block for this first design, before implementation with the overall system can be seen in Figure J-2.

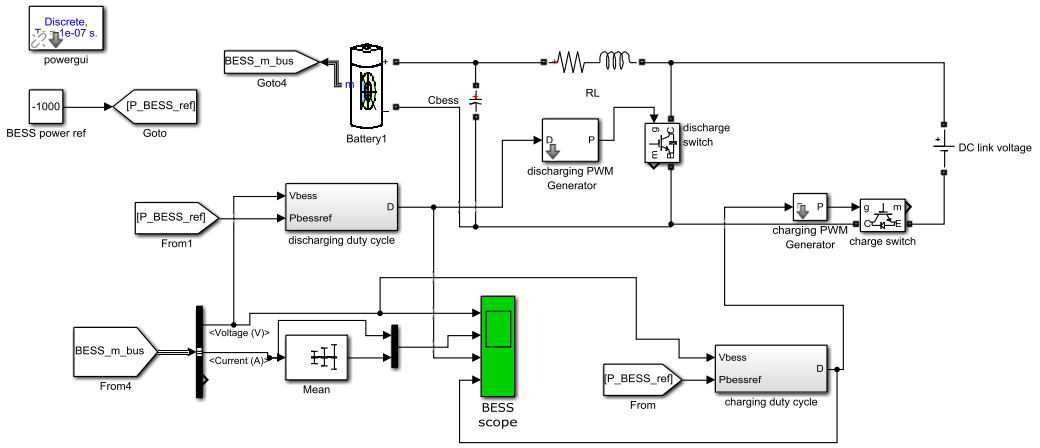

Figure J-2. Isolated battery controller block.

Unfortunately, this design was unable to have the desired result. Although this was explored to some extent, no solution could be found to the problem. The decision was made to abandon this design and instead focus on the hysteresis controller modelled in the main paper.